WDM of Solitons in Dispersion Managed Transmission Systems

John Fraser Laird Devaney

Doctor of Philosophy

Aston University

July, 1998

Aston University

WDM of Solitons in Dispersion Managed Transmission Systems

John Fraser Laird Devaney

Doctor of Philosophy

1998

This thesis investigates the physical behaviour of solitons in wavelength division multiplexed (WDM) systems with dispersion management in a wide range of dispersion regimes. Background material is presented to show how solitons propagate in optical fibres and key problems associated with real systems are outlined. Problems due to collision induced frequency shifts are calculated using numerical simulation and these results compared with analytical techniques where possible.

Different two-step dispersion regimes, as well as the special cases of uniform and exponentially profiled systems, are identified and investigated. In shallow profiles, the constituent second-order dispersions in the system are always close to the average soliton value. It is shown that collision-induced frequency shifts in WDM soliton transmission systems are reduced with increasing dispersion management. New resonances in the collision dynamics are illustrated, due to the relative motion induced by the dispersion map. Consideration of third-order dispersion is shown to modify the effects of collision-induced timing jitter and third-order compensation investigated. In all cases pseudo-phase-matched four-wave mixing was found to be insignificant compared to collision induced frequency shift in causing deterioration of data. It is also demonstrated that all these effects are additive with that of Gordon-Haus jitter.

Keywords

Solitons, wavelength division multiplexing, optical communications, dispersion management.

Acknowledgements

I would like to thank Professor Nick Doran for his supervision and Wladek Forysiak and Anne Niculae for discussions, ideas and technical assistance. I am also grateful to GPT Ltd for CASE sponsorship.

Contents

List of Tables

List of Figures

Chapter 1

Introduction

1.1 Background

Described, variously, as the Information Age, Storytelling Age and the Space Age, we are living in a time characterised by continuous technological revolution. Telecommunications in particular has grown exponentially [1] in its total data content without any sign of slowing, indicating a seemingly endless demand for bandwidth.

As each new communication medium has developed, from written word to Internet, it has been exploited to the full. For example, there has been rapid progress from the ticker-tape and telephone being the communication system for information-hungry newspaper offices covering the assassination of JFK in 1963 to small-medium sized businesses communicating to their suppliers and customers over ISDN lines carrying multi-media information today.

This introduction, no matter what is chosen as an example of 'communications today', will be out-dated within months. Suffice to say, any feasible method of exploiting more of the existing telecommunications network will be seized upon rapidly. It is the purpose of this thesis to investigate one aspect of exploiting further the bandwidth of

fibre optic communication links (wavelength division multiplexing of solitons) and the improvements that may be afforded by dispersion management.

Comparisons will be made with optical time division multiplexing (OTDM) as a method of increasing the data-rate. Alternative methods of improving data transmission, such as filtering and phase or amplitude modulation are also examined, and their applicability to WDM assessed.

1.1.1 Optical Communications

The world is already covered by a net of optical fibres (for example, Fig 1.1). All continents have a telecommunications network carrying their telephone calls, along with computer data (email, video conferencing, etc.) and the bulk of this is optical in Europe, the U.S.A. and Japan. The oceans are crossed by several point-to-point links, also comprised of optical fibres. At present, the majority of these fibre links and networks use standard fibre with a dispersion of $17ps/(nm.km)$ which is too high for soliton propagation over any significant distance. Proposals have been made to partially exploit the opposite signs of non-linearity and dispersion by using return-to-zero (RZ) pulses, but no systems of this nature have been deployed as yet. Only the most recent trans-Atlantic links (TAT-12 and TAT-13) and a small number of land-networks use dispersion-shifted fibre. The pulses on all but some highly experimental Japanese networks are in NRZ format. Because of dispersion and loss, the signals are regenerated (converted from optical to electrical and back to optical) as often as every $30km$ in most land networks, but typically every $60km$ in the UK. TAT-12 and TAT-13 are the first trans-Atlantic links to use passive amplification and no undersea regenerators.

There are several disadvantages in this situation. As data rates increase, the cost

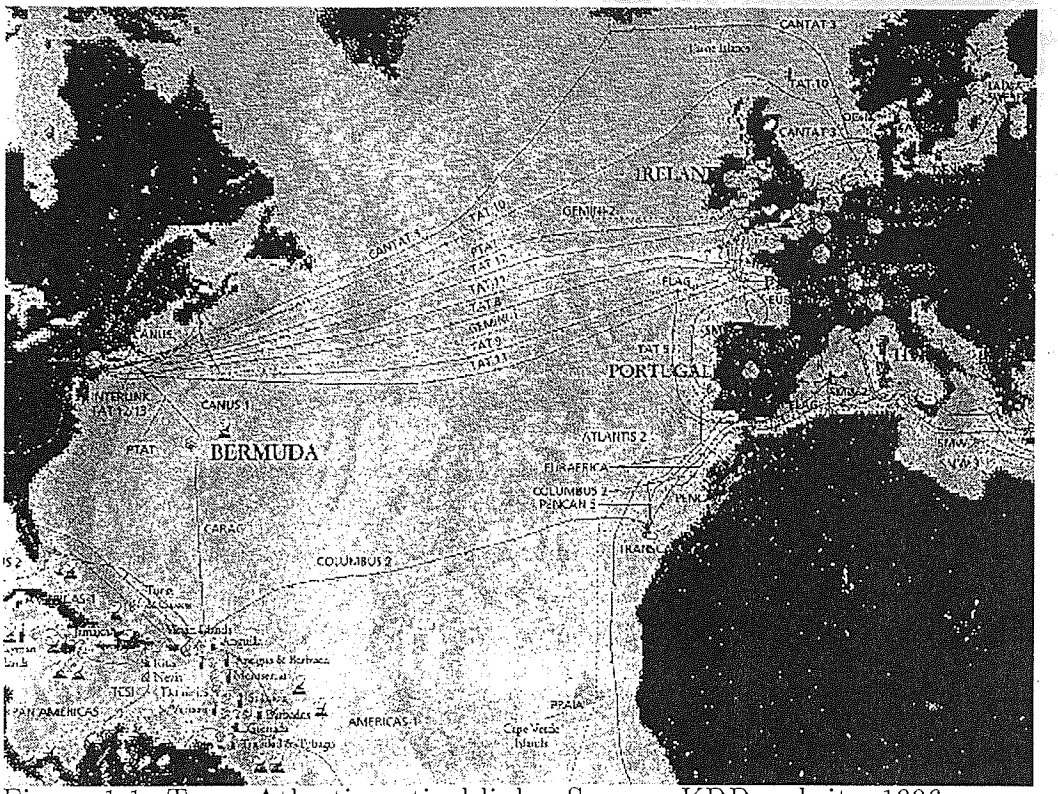

Figure 1.1: Trans-Atlantic optical links. Source: KDD website, 1996.

of the high-speed electronics required increases rapidly. It is also very difficult to make these regenerators flexible in their data-rate and wavelength handling capabilities. Many of these bulky electronics packages are also buried under the ocean floor; difficult to access if there is a fault and subject to high pressures, low temperatures, the possibility of attack from sea-life and damage from ocean-bed fishing trawlers. As a result, a high level of robustness and reliability is specified for these systems - usually the guaranteed lifetime is 25 years. Land-based networks also require expensive regenerating equipment, although this is usually easier to access and (in Europe at least) not subject to such environmental extremes.

Solitons offer the advantage of long-distance stability by balancing dispersion with non-linearity whilst EDFAs allow them to be re-amplified at regular intervals, rather than completely re-generated. If a non-return to zero (NRZ) system is to be made non-regenerative then non-linearities have to be minimised by keeping the average power

low (without the signal-noise ratio becoming too large) and the net dispersion zero.

1.1.2 Solitons

Put simply, the term 'soliton' covers wave phenomena where dispersion is balanced by non-linearity in the propagation material. The first observation of a 'soliton wave' was made by John Scott Russell on the Edinburgh-Glasgow canal in 1834 [2]. What Russell saw was a travelling water wave, formed by the motion of a canal barge, which then propagated along the canal 'without change of form or diminution of speed' for a couple of miles. Although Scott Russell made a good attempt at modelling this phenomenon, it was not until after his death that Korteweg and de Vries [3] derived the equation for the propagation of a wave on the surface of a shallow canal (hence the abbreviation KdV). In such circumstances, a wave can exist which balances the dispersion caused by gravity and the non-linear potential of the water raised above its normal level. Subsequently, similar phenomena have been predicted and observed in 'bores' on rivers (such as the Severn Bore), large ocean waves and optical behaviour in semi-conductors. The name 'soliton' was given to such pulses which pass through each other almost unperturbed by Zabusky and Kruskal in 1965 [4] because of their particle-like behaviour.

The solitons which are the subject of this thesis, however, are those which can exist in single-mode optical fibre with anomalous dispersion. These were predicted by Hasegawa and Tappert in 1973 [5] as a solution of the equation governing the propagation of light in such fibres which has the form of the Non-Linear Schrödinger Equation (NLSE). Here, solitons exist as a balance between the anomalous chromatic dispersion which causes the loss of data in Non-Return to Zero (NRZ) format and Self-Phase Modulation (SPM) which is the non-linear interaction of the pulse with

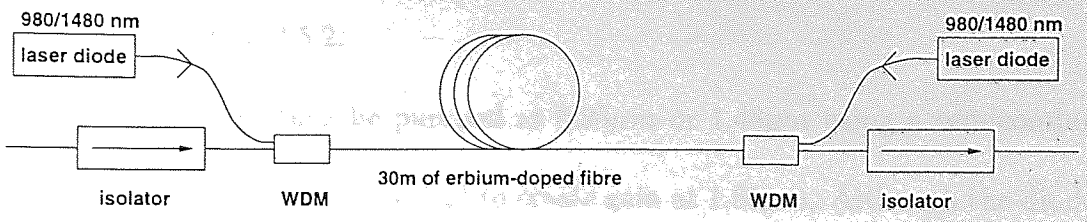

Figure 1.2: Schematic of a double-pumped erbium-doped fibre amplifier.

itself.

Soliton behaviour in fibre was demonstrated experimentally in 1980 by Mollenauer et al [6]. Since the invention of the erbium-doped fibre amplifier (EDFA) [7, 8] progress has been extremely rapid in making high data-rate, long-distance optical communications possible using solitons. The EDFA non-regeneratively boosts a signal's energy. The 'average soliton model' [9, 10], which proves that it is possible to have soliton behaviour in fibres which are not lossless, and the suppression of noise-induced timing jitter [11] have continued to push back the limits of soliton communications.

1.1.3 Erbium-Doped Fibre Amplifiers

The principle behind an optical amplifier (Fig. 1.2) is that light within the spontaneous emission bandwidth of a gain medium will coherently increase in power as it is transmitted through the inverted medium. In other words, it is a laser without the feedback.

Handily for optical communications, Er^{3+} ions can be added to optical fibre during manufacture. This fibre can then be used as the gain medium in an amplifier and can also be spliced directly into a fibre-optic communication system. The main drawback when using EDFAs is spontaneous noise - an inevitable side-effect in an optical amplifier, due to the quantum mechanical probability of ions in the excited state relaxing to the ground state without the stimulation of signal photons. The level of this problem

is addressed in section 2.5.2.

The Er^{3+} ions can then be pumped at $0.98\mu m$ or $1.48\mu m$ using a semiconductor laser diode (or diodes, as in figure 1.2) to create gain at $1.55\mu m$. Although the diode(s) requires electrical current and temperature control (although no temperature control is required in sub-sea systems where the water acts as a coolant), the electronics does not handle the data and is much cheaper and more straightforward in comparison with data-regeneration at $> 1Gbit/s$. The pump light can either (or both) be fed into the Er^{3+}-doped fibre in the same direction as the signal being amplified (co-pumping) or in the opposite direction (reverse or counter-pumping) [12].

The other optical components required are a wavelength multiplexer(s) for mixing the pump and signal, an isolator(s) to reduce feedback into the amplifier (which can lead to lasing) and/or to remove residual pump light from reverse pumping, and usually, an optical filter to remove residual pump light from co-pumping and generally improve the output signal.

1.1.4 Wavelength Division Multiplexing

A simple way of increasing the total data rate in an optical link is by transmitting more than one wavelength down the same fibre. Without modification (by, for example, adding different dopants to extend and flatten it) the 3dB bandwidth of an EDFA is about $20nm$ (see figure 1.3). It must be noted that it is the concatenated bandwidth which is more significant however. Unless the gain characteristic is *very* flat, the total gain characteristic becomes very narrow, very fast. This is not a problem in single-channel operation, but will lead to a large differential gain between WDM channels. Gain flattening has allowed the transmission of as many as $50 \times 10Gbit/s$ channels over single-mode fibre up to $1600km$ [13]. Closer channel spacing and extended bandwidth

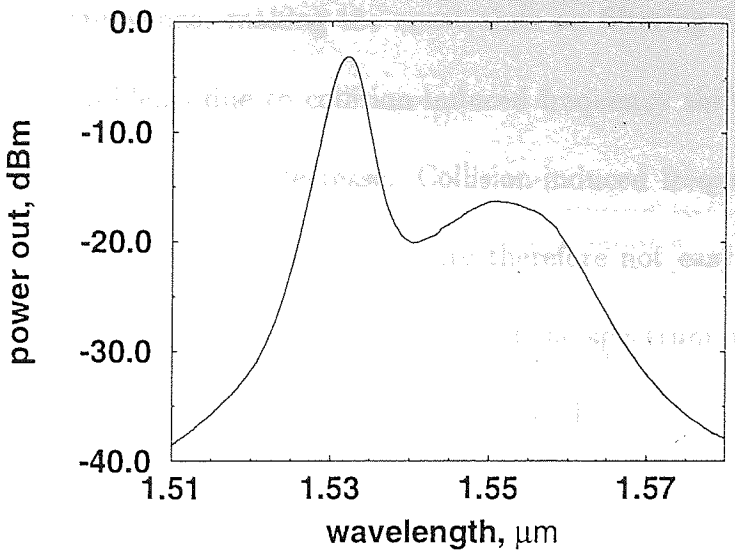

Figure 1.3: Typical emission spectrum of an erbium-doped fibre amplifier.

EDFAs could extend the total capacity well beyond $1Tbit/s$.

The currently agreed channel spacing for WDM in international telecoms is $100GHz$ or multiples thereof [14]. Closer channel spacings are certain to be agreed as the demand for total usable bandwidth increases. This is termed dense WDM (DWDM) to distinguish it from multiplexing signals from the two fibre 'windows' of $1.3\mu m$ and $1.5\mu m$. There is a limit to how closely channels can be spaced, however. If channels are very close together and the average dispersion is low, pulses in different channels will have a small difference in their group velocities.Then it will take a long time for pulses in the faster channel to overtake slower ones and if they overlap for too long, cross-phase modulation between the pulses can destroy them. Also, there is an absolute limit set by having to spectrally resolve the signals. For example, for $20ps$ FWHM pulses, the spectral width will be approximately $17.5GHz$ and this will be the limit of spectral resolution.

The channels simulated in this thesis are separated by $200GHz$ in order to resolve their spectra in detail after filtering. This is twice the currently agreed standard mentioned above. Organisations using WDM are quite likely to use multiples of the

standard in early configurations, making the constraints on filtering and wavelength allocation less strict. Problems due to collision-induced frequency shifts are likely to increase rapidly as channel spacings decrease. Collision-induced frequency shifts are very small compared to channel separation and are therefore not easy to detect, requiring the accurate calculation of the centre of mass of the spectrum of a pulse. The centre of mass of the spectrum, or mean frequency is given by

$$\frac{\int_{-\infty}^{\infty} \omega |u(\omega)|^2 d\omega}{\int_{-\infty}^{\infty} |u(\omega)|^2 d\omega}. \tag{1.1}$$

Pulses need to be adequately separated to allow integration across less than half that value make a close enough approximation to the integral from $-\infty$ to ∞. This was not true when a spacing of $100GHz$ (the ITU standard) was used, so double this value was chosen.

The alternative method of combining data is by interleaving them temporally at the same wavelength (Optical Time Division Multiplexing - OTDM). In this scheme, incoming channels have to be synchronised and the total channel data-rate becomes a multiple of the incoming data-streams, squeezing the neighbouring pulses closer together and increasing the likelihood that they interact with each other.

WDM, however, allows a huge total data-rate by passively multiplexing several relatively low-data rate channels. Star couplers (similar in behaviour to a prism), stretched-pair couplers or fibre-grating filters can all be used to passively combine or separate different wavelengths. As this thesis will show, this is not without its problems but these can be overcome without costly electronic control, by careful choice of system parameters.

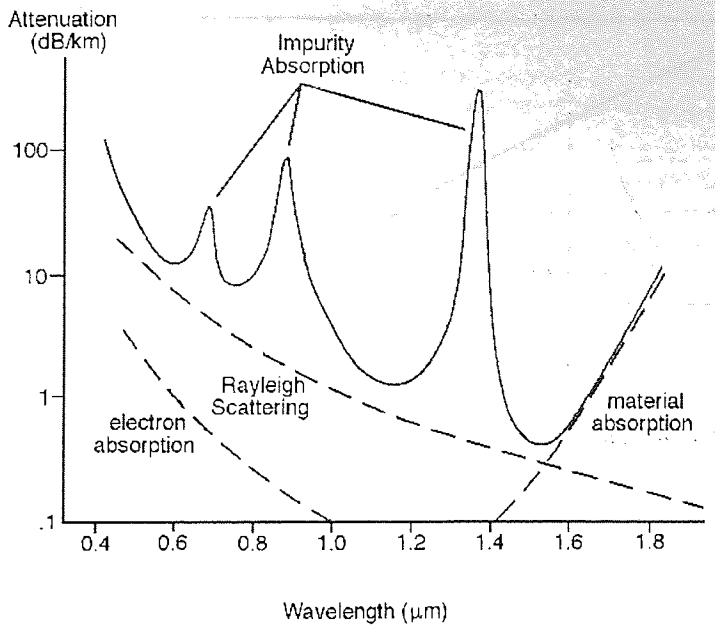

Figure 1.4: Loss characteristics of standard fibre.

1.1.5 Dispersion Management

The most common single-mode optical fibre is called 'standard fibre'. Its prevalence is partly because it is the simplest and cheapest to manufacture. It has two low-loss 'windows' at $\lambda = 1.3\mu m$ and $\lambda = 1.55\mu m$ (Fig. 1.4). The second of these has the lowest loss and coincides conveniently with the gain window of the EDFA. It is also possible to manufacture semi-conductor laser sources at this wavelength from aluminium gallium arsenide (InGaAsP) which operate at room temperature, are long lived and simple to stabilise.

Unfortunately, the dispersion at this wavelength is $\sim 17ps/(nm.km)$ (figure 1.5) which would require a $20ps$ pulse to have $1.07J$ of energy to fulfil the soliton criteria described in the next chapter. This is an almost impossible energy to obtain by use of an EDFA and certainly an impractical energy level for optical communications, not only because of the power requirements, but also because pulse behaviour would be highly non-linear and self-destructive. NRZ communications also degrade as dispersion increases. In this case, the bit pattern is 'smeared out' at a rate determined by the

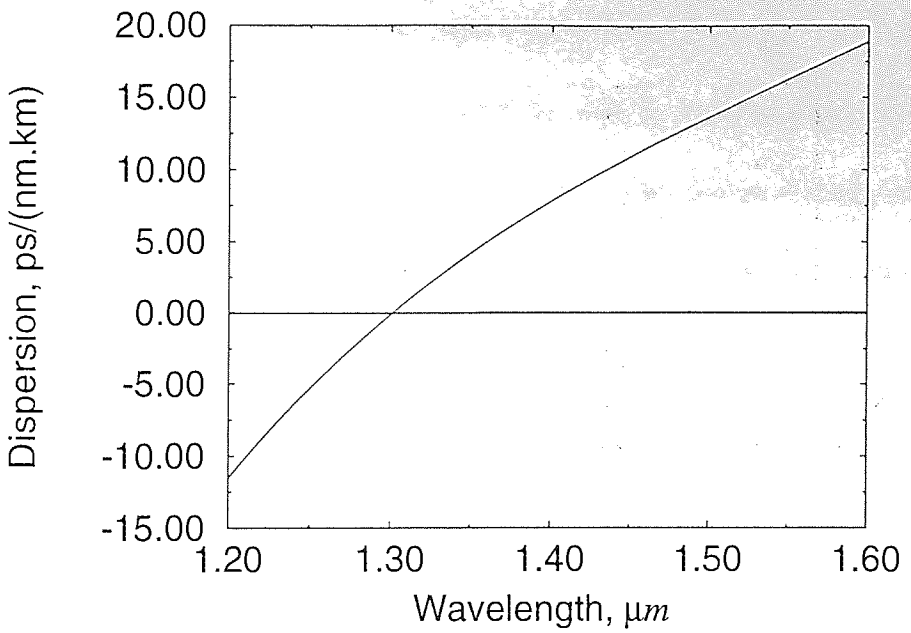

Figure 1.5: Dispersion characteristics of standard mono-mode fibre.

bandwidth of the signal (at least as great as the data rate) and the dispersion.

Alternatively, dispersion-shifted fibre can be employed. By manufacturing the fibre with different core dopants and modified refractive-index cross-section, the waveguide dispersion becomes important and the net dispersion is changed. This happens at the expense of a small increase in loss, i.e. loss is $0.2dB/km$ in dispersion shifted fibre and $0.17dB/km$ in standard fibre. Dispersion shifted fibre is manufactured for use in NRZ systems with a slightly negative dispersion and is periodically compensated using standard fibre. Pulses transmitted at the exact zero dispersion suffer more severely from higher-order dispersion effects.

A second solution is to use mostly standard fibre and periodically (approximately every $30 - 100km$) splice in a short section of highly normal (D negative) fibre, or a highly dispersive fibre grating, to bring the average down to an acceptable value for soliton transmission [15] (or similarly to extend the transmission distance of NRZ).

This is one form of dispersion management. Dispersion management is essentially where the values of dispersion are mixed to achieve the desired average value. Step-

wise dispersion maps, mimicking the exponential loss of energy between amplifiers [16, 17, 18, 19], have successfully been used in soliton transmission to increase the transmission distance. In uniform dispersion fibre, the soliton criteria are only met once between amplifiers. At all other points dispersive radiation is lost and/or the pulse changes shape towards one which does match the criteria. Approximating to the exponential profile reduces the level of these perturbations. Meanwhile, much attention has also been focussed on a wide variety of other dispersion configurations, e.g. [20, 21, 22, 23] and their various benefits and draw-backs, some of which are described more fully in the next chapter.

This thesis will look at a wide-range of dispersion profiles comprising of fibres with two values of dispersion and their effects on WDM soliton systems.

1.2 Aims and Overview of this Thesis

The aim of this thesis is to examine the effects which occur when the techniques of dispersion management and WDM are combined in soliton transmission. In particular, the very important phenomenon of collision-induced frequency shifts is examined. Regimes where these effects are critical in system design and where the use of dispersion management is beneficial are sought out.

First of all, the theory underpinning soliton dynamics is outlined. Chapter 2 then goes on to address the problems of using solitons for communications in the real world where there is loss of pulse energy with propagation. Various soliton control methods are described and their strengths and weaknesses analysed. Many are found to be incompatible with WDM or very difficult to implement. Dispersion management as a method of soliton control is compared to other methods and its adaptability to WDM

explained. It is shown that the limitations in soliton communication systems can be incorporated in a single diagram showing which designs are feasible. The increase in the range of feasible parameters due to dispersion management is then calculated.

In Chapter 3, an analytic expression for the frequency shift caused by the collision of two solitons of different wavelengths is explained. Previously deduced limitations to WDM soliton systems are then explained for uniform and stepped dispersions. The problem of Four-Wave Mixing (FWM) in soliton systems is highlighted. The conditions under which large amounts of FWM products will be generated are shown and shown to be relatively unimportant in the simulations within this thesis.

In Chapter 4, the theory of collision-induced frequency shift outlined in Chapter 3 is exploited outside the range of dispersion maps previously examined without loss. In doing so, the effects of dispersion are isolated. The results are examined to find a physical explanation for the phenomena observed. Numerical simulations are performed in order to ascertain the limits of accuracy of the theory used and those limitations are explained in terms of the soliton dynamics.

The addition of loss is considered in Chapter 5, bringing the theory and simulations closer to reality. Potentially optimal design criteria are then identified. Further numerical simulations, solving the Non-Linear Schrödinger Equation (NLSE), are performed of pseudo-random data-streams with a variety of channel configurations, dispersion map depths, pulse parameters and fibre characteristics in order to find system design restrictions and recommendations. The problem of Gordon-Haus timing jitter is investigated in order to confirm that it does not exacerbate the problems due to collision-induced jitter.

The added complication of third-order dispersion is considered in Chapter 6. Three approaches to WDM propagation in the presence of third-order dispersion are evaluated

by simulation. The practicality and relative merits of each are outlined.

Finally, some overall conclusions are drawn as to the physics of the phenomena observed and the practical lessons which can be learnt. Some suggestions for further work are also outlined.

Chapter 2

Theory of Soliton Dynamics

2.1 Outline

In this chapter, the basis of soliton theory is presented along with some of the problems encountered in trying to use them in an optical communications system. A comparison is then made between proposed solutions to these problems, one of which is dispersion-management.

This chapter is structured as follows. Firstly, some fundamental properties of light in optical fibre are outlined and their effects when dominant are described. Secondly, the equation governing the propagation of light in an optical fibre is described and one stable solution, the temporal (first-order, bright) soliton, is presented. The theory is then extended to cover propagation in a fibre with loss and it is shown that there is still a periodically stable solution, called the 'average soliton'.

The limitations of single-channel data transmission are identified then displayed in a single design diagram. The merits of most of the soliton control methods suggested, so far, are compared and their effect on the design diagram are shown.

2.2 Properties of Optical Fibre

Put simply, optical fibres are 'light tubes' - glass drawn out into thin strands, with a refractive index profile which traps light by total internal reflection. The fibre referred to in this thesis is single-mode at $1550nm$; the second optical window in glass. Strictly speaking, single mode fibre carries two differently polarised modes, the problems arising from which will be discussed later. Other properties to be outlined are loss, chromatic dispersion and non-linear effects.

2.2.1 Loss

Loss is an unavoidable problem in fibre-optic communications, although modern fibre can have losses lower than $0.2dB/km$. dB/km are the preferred units in communication system design and are defined by,

$$\alpha_{dB} = -\frac{10}{L}\log\left(\frac{P_T}{P_0}\right) \tag{2.1}$$

where L is the distance a signal, initially of power P_0 which has been reduced to P_T. Loss can be compensated for by the EDFA, described in the last chapter. Figure 2.1 shows how a sech-shaped pulse (the shape of the ideal soliton) propagates in a fibre with no characteristics other than loss. It can be seen that there is no distortion of the pulse shape but the amplitude decreases exponentially.

One of the first assumptions made in deriving the Non-Linear Schrödinger equation (NLSE) in the next section is the assumption that propagation can be assumed to be described by the evolution of a slowly varying envelope. Loss, in particular is found to be a function of the imaginary part of $\tilde{\chi}^{(1)}(\omega)$, itself part of the frequency-dependent

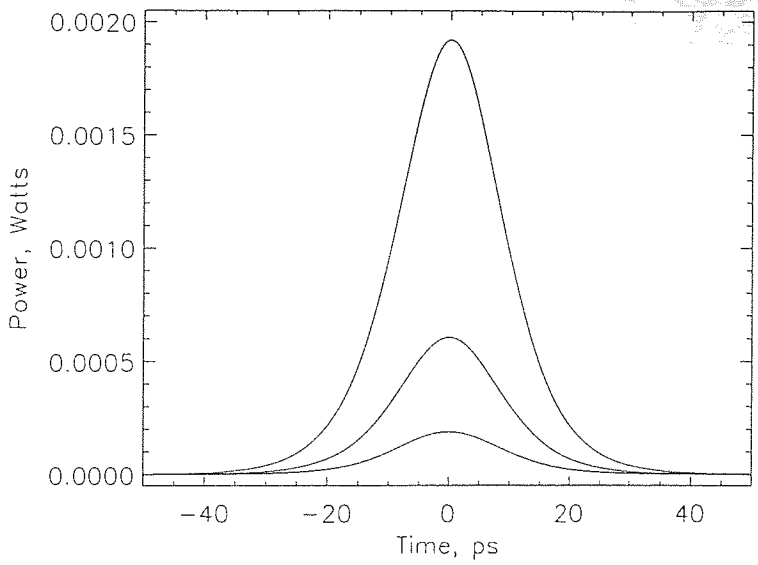

Figure 2.1: The effect of loss on a sech-shaped pulse in otherwise ideal fibre. Pulses shown after $0km$, $25km$ and $50km$ in $\alpha = 0.2dB/km$.

dielectric constant, by

$$\alpha(\omega) = \frac{\omega}{nc}\mathrm{Im}[\tilde{\chi}^{(1)}(\omega)] \tag{2.2}$$

where ω is the frequency, n is the refractive index and c is the speed of light in vacuum. In this equation, α is also the attenuation constant preferred by theoreticians, defined by

$$P_T = P_0 \exp(-\alpha L), \tag{2.3}$$

using the same notation as above.

2.2.2 Chromatic Dispersion

Another effect to have an important role in the NLSE is dispersion. Dispersion is an effect of the wavelength dependence of the propagation constant or wavenumber, β, which in turn is derived from the propagation equation of light.

Starting from Maxwell's equations, assuming the separability of linear and, the much smaller, non-linear polarisation, and also low loss, we can obtain a general equa-

tion for the electric field of light propagating in a material such as glass,

$$\nabla^2\tilde{\mathbf{E}} + n^2(\omega)\frac{\omega^2}{c^2}\tilde{\mathbf{E}} = 0, \tag{2.4}$$

which, given conditions of cylindrical symmetry and reduction to independent variables, solves for $\tilde{E}_z$ to give,

$$\tilde{E}_z(r,\omega) = \tilde{A}(\omega)F(\rho)\exp(im\phi)\exp(i\beta z), \tag{2.5}$$

where A is the normalisation constant, and $F(\rho)\exp(im\phi)$ is the field profile (which can then be re-expressed as $F(x,y)$).

The wavenumber can be shown to be linked to the field profile by

$$\frac{\partial^2 F}{\partial x^2} + \frac{\partial^2 F}{\partial y^2} + [\varepsilon(\omega)k_0^2 - \tilde{\beta}^2]F = 0, \tag{2.6}$$

and correspondingly to the normalisation constant by

$$\begin{aligned} 2i\beta_0\frac{\partial \tilde{A}}{\partial z} + (\tilde{\beta}^2 - \beta_0^2)\tilde{A} &= 0 \\ i[\beta(\omega) + \Delta\beta - \beta_0]\tilde{A} &= 0, \end{aligned} \tag{2.7}$$

where $\tilde{\beta}(\omega) = \beta(\omega) + \Delta\beta$. $\Delta\beta$ is related to the modal distribution, F, and a small perturbation to the refractive index, Δn, given by

$$\Delta n = n_2|E|^2 + \frac{i\alpha}{2k_0}, \tag{2.8}$$

($k_0 = \omega/c$), which is where non-linearity and loss will be brought into the NLSE later.

Dispersion terms are then derived from the wavenumber, $\beta(\omega)$ and its dependence on frequency by Taylor expansion,

$$\beta(\omega) = \beta_0 + (\omega - \omega_0)\beta_1 + \frac{1}{2}(\omega - \omega_0)^2\beta_2 + ... \tag{2.9}$$

where

$$\beta_n = \left(\frac{d^n\beta}{d\omega^n}\right)_{\omega=\omega_0}. \tag{2.10}$$

Substituting equation 2.9 into equation 2.7 we can solve after taking the inverse Fourier transform, to get

$$\frac{\partial A}{\partial z} = -\beta_1\frac{\partial A}{\partial t} - \frac{i}{2}\beta_2\frac{\partial^2 A}{\partial t^2} + i\Delta\beta A. \tag{2.11}$$

The similarity between this and the NLSE is quite obvious - looking ahead to equation 2.22.

Many disperion terms terms can be included in the further derivation but unless the pulses transmitted are shorter than $1ps$ long or the value of β_2 is negligible, it is possible to ignore any terms after it. In physical terms, dispersion is responsible for pulse broadening with propagation, as different wavelengths, with different group velocities walk away from each other.

Removing β_1 (group velocity dispersion) and $\Delta\beta$ (non-linearity and loss) from equation 2.11 we get

$$i\frac{\partial A}{\partial z} = \frac{1}{2}\beta_2\frac{\partial^2 A}{\partial t^2}, \tag{2.12}$$

which is easily solvable in frequency space to give,

$$\tilde{U}(z,\omega) = \tilde{U}(0,\omega)\exp\left(\frac{i}{2}\beta_2\omega^2 z\right)d\omega, \tag{2.13}$$

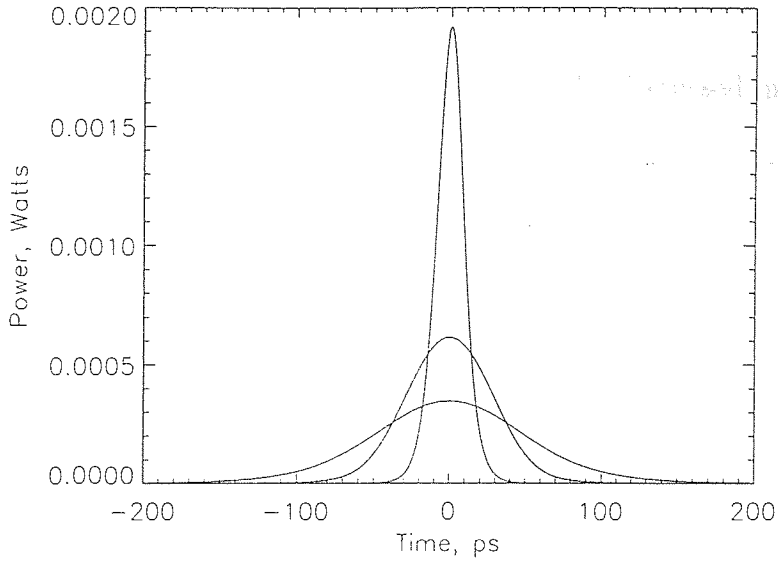

Figure 2.2: The effect of dispersion on a sech-shaped pulse in otherwise ideal fibre. Pulses shown after $0km$, $25km$ and $50km$ in $D = 17.0ps/(nm.km)$.

$\tilde{U}(0,\omega)$ being the Fourier transform at $z = 0$.

A simple picture of the effect of dispersion is shown in figure 2.2. In this simulation, the fibre is ideal except for a value of dispersion of $D = 17.0ps/(nm.km)$, such as is found in standard fibre. As in the loss-only case, the amplitude decreases with distance but this time it is because different wavelengths are travelling at different group velocities, hence the term group velocity dispersion. The spectrum and total energy of the pulse is un-changed.

The pulse width, as can be predicted from applying equation 2.13, increases following,

$$t_1 = t_0 \left[1 + \left(\frac{z_i \beta_2}{t_0^2} \right)^2 \right]^{1/2} . \tag{2.14}$$

Short pulses therefore broaden more quickly than long ones in the same dispersion.

2.2.3 Non-Linearities

The problems which arise due to non-linear effects will be discussed in a later section. This section will attempt to outline their existence and show how they too can be included in the NLSE.

The refractive index of glass is intensity dependent and can be expressed as

$$n = n_1 + n_2 I, \tag{2.15}$$

where,

$$n_2 = \frac{3}{8n}\chi^{(3)} \tag{2.16}$$

A non-linearity constant can be defined as

$$\gamma = \frac{n_2 \omega_0}{c A_{eff}} \tag{2.17}$$

where A_{eff} is the effective area - a measure of the cross-sectional field distribution, given by,

$$A_{eff} = \frac{\left(\int_{-\infty}^{\infty}\int_{-\infty}^{\infty}|F(x,y)|^2 dxdy\right)^2}{\int_{-\infty}^{\infty}\int_{-\infty}^{\infty}|F(x,y)|^4 dxdy}, \tag{2.18}$$

which simplifies to $A_{eff} = \pi w^2$ for a gaussian beam profile, where w is approximately the core radius of the fibre.

Typically, n_2 in silica fibre is approximately $2.6 \times 10^{-16} cm^2/W$, ω_0 is $10^{15} s^{-1}$, and A_{eff} is approximately $50\mu m^2$ for a wavelength of $1.5\mu m$ in dispersion-shifted, single-mode fibre.

This can be substituted into the expression for $\Delta\beta$ in equation 2.11 along with

equation 2.8 to give,

$$\frac{\partial A}{\partial z} + \beta_1 \frac{\partial A}{\partial t} + \frac{i}{2}\beta_2 \frac{\partial^2 A}{\partial t^2} + \frac{\alpha}{2}A = i\gamma|A|^2 A. \tag{2.19}$$

Removing the GVD, β_2 and loss terms from equation 2.11, gives us

$$\frac{\partial A}{\partial z} = i\gamma|A|^2 A, \tag{2.20}$$

which is readily solvable in the time domain to give

$$A(z,t) = A(0,t)\exp(i\gamma|A(0,t)|^2). \tag{2.21}$$

That is, there is a phase shift but no change in pulse shape.

This is self-phase modulation (SPM), which is an intensity-dependent phase-shift of the pulse's spectrum. The other main effect this term has is cross-phase modulation (XPM), where one pulse's intensity acts to distort that of another, depending on their local intensities.

Figures 2.3 and 2.4 show how SPM causes an evolution in a pulse's spectrum and chirp. The temporal pulse envelope is undistorted. With further propagation, more and more, smaller and smaller peaks in the spectrum will appear, in extreme cases leading to supercontinuum generation.

Other non-linear effects, not covered by the effects of γ, include polarisation mode-dispersion, Raman and Brilliuon scattering, which are discussed in more depth later. Polarisation mode dispersion, along with other effects due to birefringence, can be modelled by expressing the situation as two coupled NLS equations. The others have to be added in any simulation as a perturbation and cannot be included as other terms

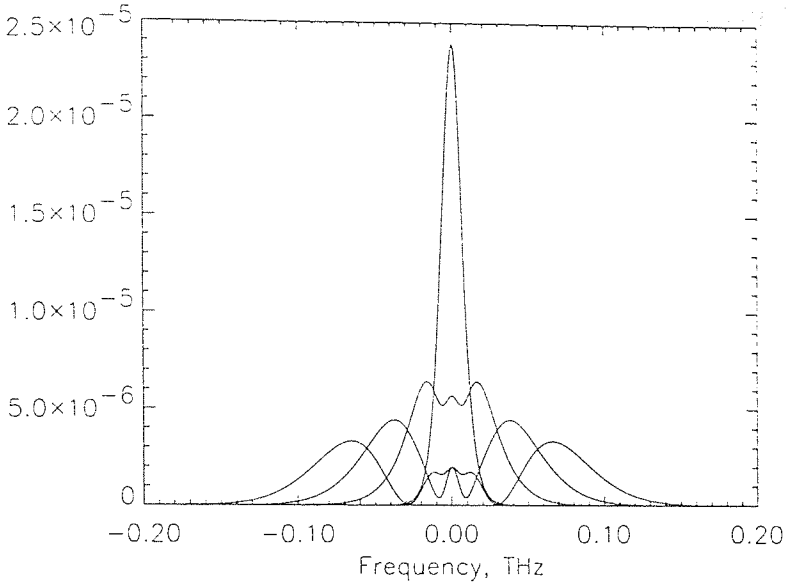

Figure 2.3: The effect of SPM on the spectrum of a sech-shaped pulse in otherwise ideal fibre. Pulses shown after $0km$, $25km$, $50km$ and $75km$ with a peak power of $0.05W$.

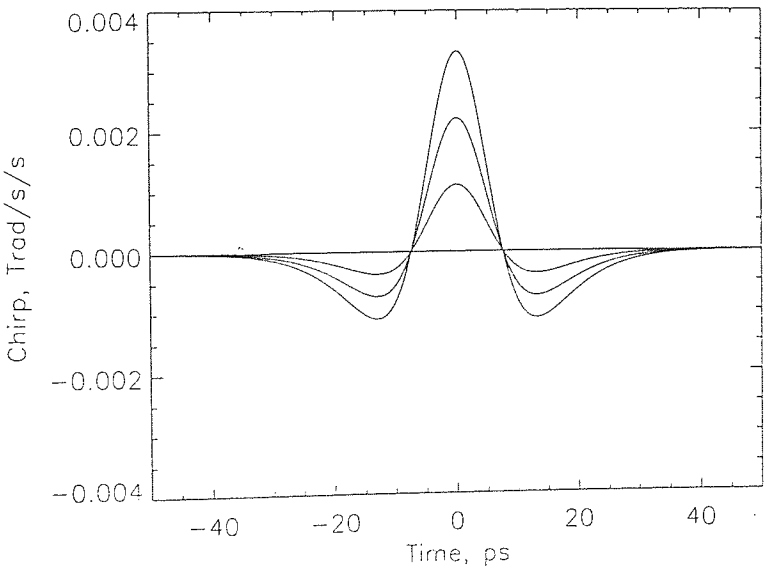

Figure 2.4: The effect of SPM on the chirp of the same sech-shaped pulse as above in otherwise ideal fibre. Pulses shown after $0km$, $25km$, $50km$ and $75km$ with a peak power of $0.05W$.

are. There are two other terms which can be added to the list of those which can be included in the NLSE and they are for self-steepening effects and self-frequency shift.

2.3 The Non-Linear Schrödinger Equation

While working at Bell Labs in New Jersey, USA, in 1973, Akira Hasegawa and Frederick Tappert derived the equation for the evolution of an optical pulse envelope in an optical fibre with anomalous dispersion [5]. The equation is of the form of a non-linear Schrödinger equation,

$$i\frac{\partial A}{\partial z} - \frac{1}{2}\beta_2\frac{\partial^2 A}{\partial T^2} - \frac{i}{6}\beta_3\frac{\partial^3 A}{\partial T^3} + \frac{\alpha}{2}A + \gamma|A|^2 A = 0 \tag{2.22}$$

where $A(z,T)$ is a complex amplitude function describing the E-field envelope of a pulse. The equation can be obtained from 2.19 by including β_3, the third order dispersion in ps^3/km, and changing to time coordinates T, relative to the pulse and normalised to the pulse width ($T = (t - cz/n)/\tau$). α is the loss of the fibre in km^{-1} and γ, the nonlinearity coefficient, given in equation 2.17.

Hasegawa and Tappert also gave one solution to this equation in the same paper (assuming that loss and third-order dispersion are negligible), the ' "bright" pulse, or envelope soliton'. This can be derived by first normalising equation 2.22 so it becomes,

$$i\frac{\partial u}{\partial z'} + \frac{1}{2}\frac{\partial^2 u}{\partial t^2} + |u|^2 u = 0 \tag{2.23}$$

where

$$u = \left(\frac{\gamma T_0^2}{|\beta_2|}\right)^{\frac{1}{2}} A, \tag{2.24}$$

$$z' = \frac{z}{L_D} \qquad \text{and} \qquad t = \frac{T}{T_0}, \tag{2.25}$$

where $L_D = T_0^2/|\beta_2|$ is the dispersion length and T_0 is the initial pulse width.

The simplest solution to this equation is,

$$u(z', t) = \text{sech}(t)e^{iz'/2} \tag{2.26}$$

and is known as the first-order soliton. The pulse phase increases linearly with z and pulse properties are obviously periodic with z'. The soliton period is defined as the normalised distance, $\pi/2$. That is,

$$z_0 = \frac{\pi}{2}\frac{T_0^2}{|\beta_2|} = 0.322\frac{\pi}{2}\frac{\tau^2}{|\beta_2|}, \tag{2.27}$$

where τ is the pulse width (FWHM) in real units. The soliton period is $1/8th$ of a complete phase rotation in eq'n 2.26.

At this point, it is useful to introduce the dispersion term, D, given by,

$$D = -\frac{2\pi c}{\lambda^2}\beta_2, \tag{2.28}$$

and measured in $ps/(nm.km)$ which is used most frequently in designing optical systems because it is easy to calculate accumulated dispersion with propagation.

Figure 2.5 shows the temporal shape of a first-order soliton with $20ps$ FWHM in fibre with dispersion $D = 0.5ps/(nm.km)$.

The most important relationship between these parameters is,

$$E_s = \frac{2|\beta_2|cA_{eff}}{n_2\omega_0}\frac{1.76}{\tau}, \tag{2.29}$$

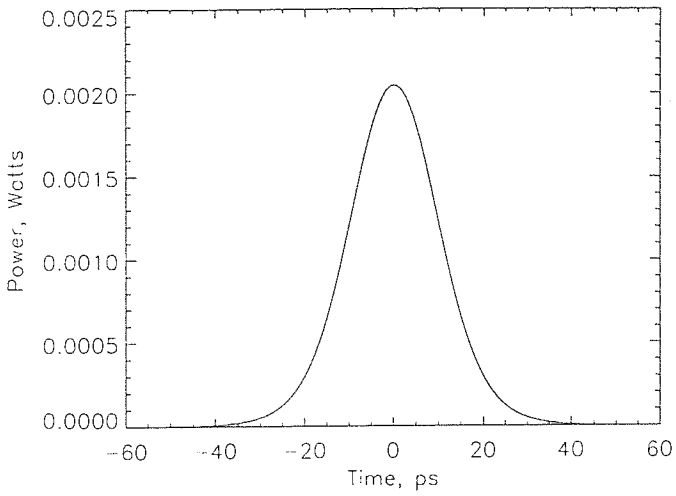

Figure 2.5: Temporal envelope of a first-order soliton in fibre with dispersion $D = 0.5ps/(nm.km)$ and FWHM $\tau = 20ps$.

the energy relationship for a first-order soliton with half-width τ, the energy contained in the soliton E_s and the fibre characteristics given. This simplifies to [24]

$$E_s = 1.53\frac{D}{\tau} \tag{2.30}$$

for typical optical communications fibre, single-mode at $\lambda = 1.5\mu m$. That is, the effective area, $A_{eff} = 50\mu m^2$. D is the dispersion in ps/(nm.km), τ is the pulse width (FWHM) in ps, and E_s is the pulse energy in pJ.

The limitations to the accuracy of this equation are set by the thresholds above which other effects become significant. Realistic levels of loss cannot be ignored for propagation over more than a few tens of metres. This is discussed in the following section.

2.4 Soliton Dynamics with Loss

The non-linear Schrödinger equation above assumes that loss (attenuation) in the fibre is negligible compared to the other effects. It has proved impossible to manufacture optical fibre with loss much less than $0.2dB/km$. The advent of the erbium-doped fibre amplifier [7, 8] (EDFA) made it possible to periodically compensate for this loss in the $\lambda = 1.5\mu m$ window. Several studies showed that a soliton's properties would survive periodic amplification and loss, both in theory and practice, as follows.

In 1980, Mollenauer et al, at Bell Labs, obtained experimental verification [6] of the soliton phenomenon, followed by transmission of solitons, first over $10km$ [25] and later $4000km$ [26] using Raman gain to compensate for loss.

Hasegawa and Kodama [27, 28] further developed the soliton theory, showing that, in principle, it was both possible for solitons to survive periodic amplification and loss, although the initial proof used the addition of a CW wave of the same phase and wavelength as the soliton rather than an amplifier model. From this, they claimed that data transmission was possible with soliton data-streams.

As experimental achievements, in terms of distance and data rate, progressed, so did the theoretical understanding of soliton dynamics. Notably, soliton theory has been expanded to include investigations of the interactions between neighbouring solitons in a pulse train [29, 30, 31, 32] and collision dynamics between solitons of different wavelengths [33]. The latter of these would later be expanded to give the analytic theory used in much of this thesis.

Although soliton transmission with periodic amplification and loss had been proven to be possible in principle (also examined in [33]), it was not until 1990/91 that an exact solution was derived by Mollenauer et al [34], and independently by Hasegawa

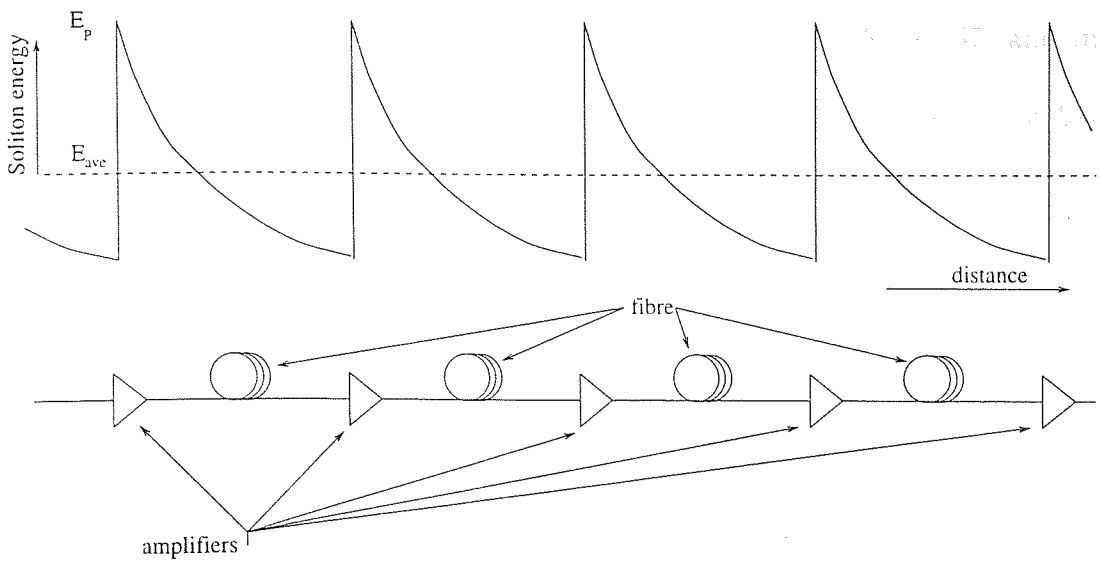

Figure 2.6: Average soliton evolution over periodic amplification system.

and Kodama [9] (the 'guiding-center' soliton) and Blow and Doran [10] (the 'average' soliton) which could be used to predict the necessary input power and pulse width for stable soliton transmission in a periodically amplified system.

In the average soliton model, the average pulse energy in any fibre link between amplifiers is equal to the soliton energy given by equation 2.30. This holds as long as the amplifier spacing is significantly less than the soliton period, and the dispersion in the link is uniform. Figure 2.6 shows how pulse energy evolves in a chain of lumped amplifiers. The pulse only fulfils the soliton condition at one point between each amplifier, being boosted in power at each amplifier and then decaying exponentially as it travels down the fibre.

In parallel with this, experimental advances were bringing the possibility of long-distance communication at high data rates without optical regenerators closer and closer. The combination of sources at $\lambda = 1.5\mu m$ and the highly efficient erbium doped fibre amplifier [7, 8], however, finally allowed transmission results from soliton experiments to rival those achieved using NRZ pulses (non-return to zero, where the optical pulses are not discrete). Both systems have achieved trans-oceanic transmission

distances for single-channels of up to and over $10Gb/s$, e.g. [35, 36, 37] and more recently the total data rate has been pushed to over $100Gb/s$ by the use of WDM [38, 39].

2.5 Soliton Transmission Limitations

In the following sections, the limits to soliton transmission in terms of data-rate, amplifier spacing and total distance are highlighted. Where possible, expressions are given for the maximum distance over which data can be transmitted due to each limitation.

2.5.1 Amplifier Spacing

Having replaced regenerators with amplifiers, these amplifiers become a significant source of cost in installing a point-point link. As the amplifier spacing is increased, the number of amplifiers required for a point-point link is reduced. Therefore, the greater the spacing between amplifiers, the lower the cost. The fundamental limitation on amplifier spacing is the variation of phase, i.e. the soliton period. This is referred to as the average soliton limit. Effects due to phase variation of the soliton become evident if the amplifier spacing is not less than 10 times smaller than the soliton period [40], although the effects are not large enough to degrade data transmitted over transoceanic distances. As the phase of the amplifier-spacing approaches that of the soliton frequency side-bands are formed [41], draining energy from the signal wavelength. An example of this is given in figure 2.7 where the amplifier spacing is exactly equal to the soliton period.

A guide to use in avoiding problems arising from these effects is that the soliton

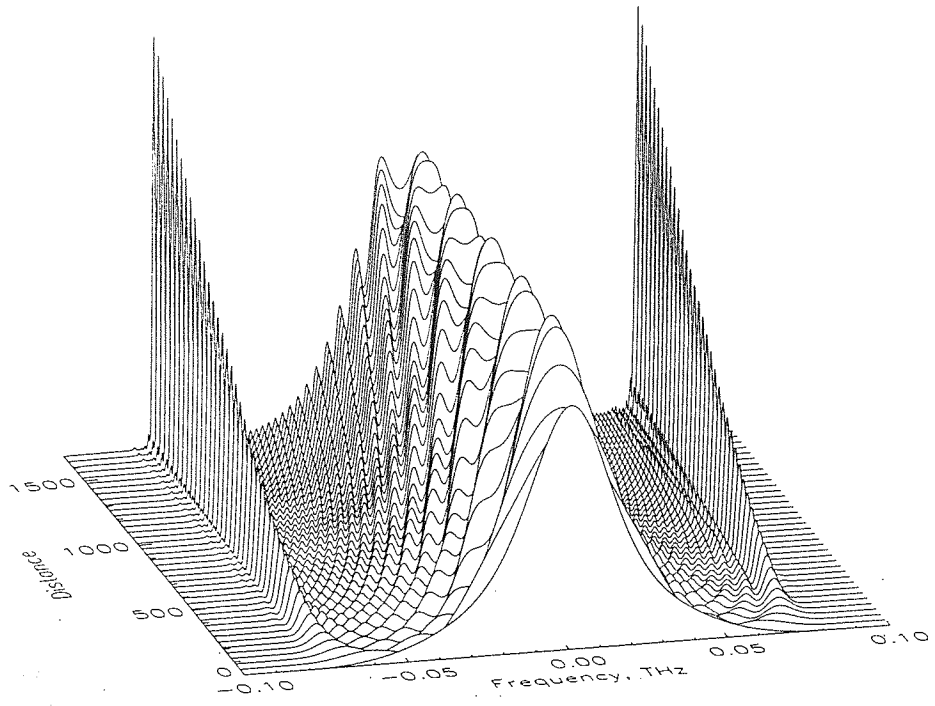

Figure 2.7: Evolution of the spectrum of a $10ps$ soliton transmitted in fibre of dispersion $0.938ps/(nm.km)$ with amplifiers every $42.3km$ which is also the soliton period.

period must be at least 5 times the amplifier spacing. That is,

$$z_a < \frac{0.322}{5}\left(\frac{\pi\tau^2}{2|\beta_2|}\right) \tag{2.31}$$

Where τ is the pulse width (FWHM) in ps and β_2 is the dispersion in ps^2/km. Hence, for example, for a $20ps$ soliton in an average dispersion of $0.5ps/(nm.km)$ at $\lambda = 1.55\mu m$, the maximum amplifier spacing would be $63.5km$. From this example, it can be seen that soliton-amplifier phase interaction is not a problem with these parameters. However, as the single-channel data-rate goes up, the pulse width will necessarily have to reduce.

Figure 2.8 shows the limits on amplifier spacing and pulse width due to sideband formation over a range of dispersions for a $10Gbit/s$ single-channel transmission over

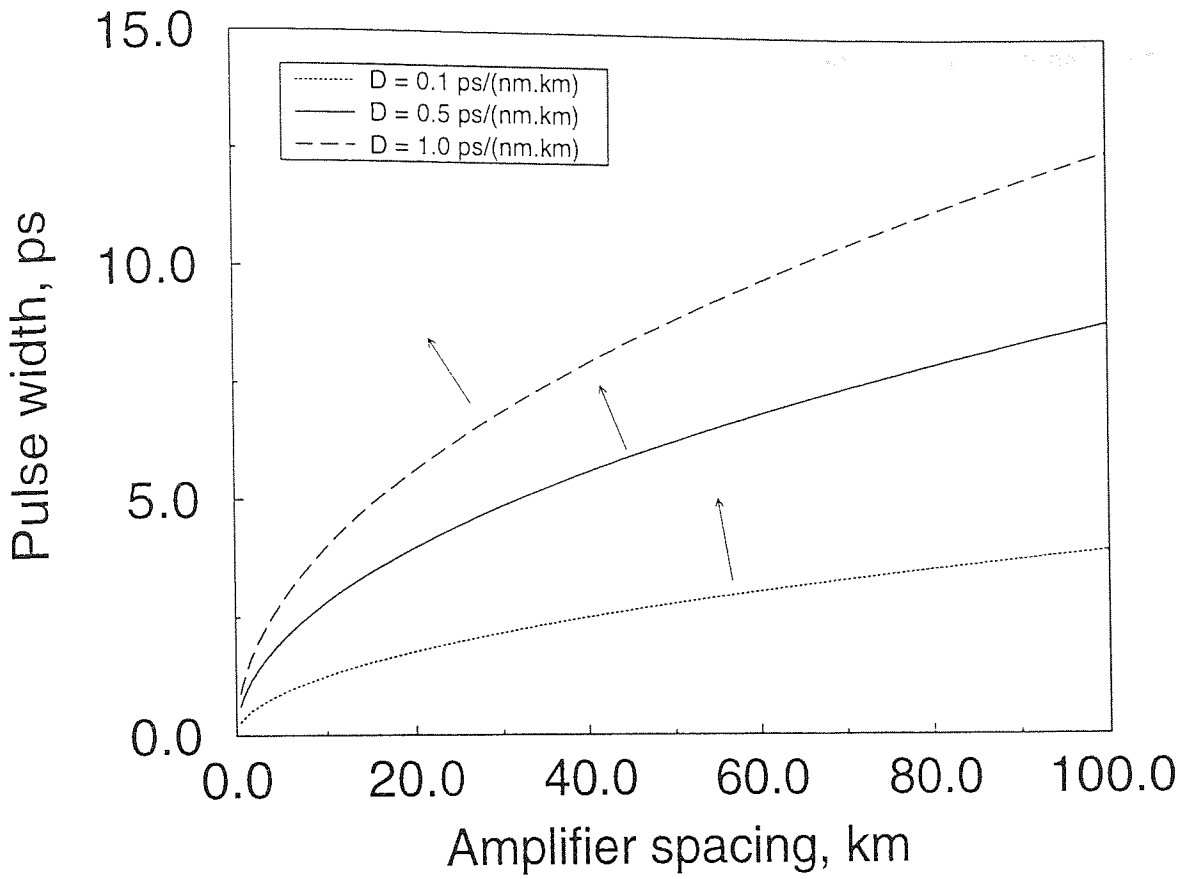

Figure 2.8: Limitations on amplifier spacing and pulse width due to the average soliton limit. Data rate is $10Gbit/s$ and total propagation distance, $L = 6000km$. The arrows show which side of each line operation is permissible.

$6000km$.

2.5.2 Signal-Noise Ratio

In common with NRZ systems, soliton communication systems which use EDFAs suffer from spontaneously emitted noise. This builds up (if not removed by filtering, or similar) until there is enough of it to swamp the data - or at least to cause unacceptable errors.

From the amplifier equations in [12] the noise per unit bandwidth at each amplifier is $n_{sp}(G-1)h\nu$, where G is the power gain and η_{sp} is the spontaneous emission factor ($n_{sp} = 1$ for an ideal amplifier). The total noise, P_{noise}, after N amplifiers, at a receiver with bandwidth B, is $NBh\nu n_{sp}(G-1)$.

If the number of 'ones' and 'zeros' in the bit-stream are approximately equal then the average power is $RE_{sol}/2$, where R is the bit-rate and,

$$E_{sol} = \frac{1.17D}{\tau}\left(\frac{GlnG}{G-1}\right) \tag{2.32}$$

is the soliton energy just after every amplifier (when $\lambda = 1.55\mu m$, combining equation 2.29 with the average soliton factor). Hence the SNR is given by

$$SNR = \frac{E_{sol}}{P_{noise}} = \frac{1.17D}{\tau}\left(\frac{GlnG}{G-1}\right)\frac{1}{NBH\nu n_{sp}(G-1)}, \tag{2.33}$$

or, in other words, the maximum pulse width for transmission over distance L, with amplifier spacing L_a, is given by

$$\tau_{SNR} = 1.17D\left(\frac{GlnG}{(G-1)^2}\right)\frac{L_a}{LBH\nu n_{sp}SNR_{max}}. \tag{2.34}$$

2.5.3 Gordon-Haus Jitter

Amplifiers also bring the main system limitation, first identified by Gordon and Haus in 1986 [11]. Stochastic noise from each amplifier adds a random change to each soliton's average frequency. Each soliton then has a slightly different group velocity and may walk out of its allocated time window and subsequently lead to errors at the receiving end.

For idealised amplifiers and 'average soliton' conditions, Marcuse [42] derives the distance limit set by Gordon-Haus jitter alone to be,

$$L^3_{max} \leq 0.1372\frac{\tau t_w^2 A_{eff} L_a Q}{n_{sp} n_2 D h(G-1)} \tag{2.35}$$

where, τ is the pulse width (FWHM), $2t_w$ is the expected arrival time window of the soliton (i.e. the bit period), A_{eff} is the effective area of the fibre, L_a is the amplifier spacing, n_2 is the non-linear coefficient of the fibre (in units of cm^2/W) [43], h is Planck's constant, G is the gain and n_{sp} is the spontaneous emission factor of the amplifiers. Q is the 'average soliton factor', given by,

$$Q = \frac{\alpha L_a}{1 - \exp(-\alpha L_a)}, \tag{2.36}$$

which takes account of the variation in amplitude between amplifiers.

Note that the L_{max} increases as the cube root of pulse width ($\tau^{1/3}$), $t_w^{2/3}$ and $D^{-1/3}$. Hence, to optimise this parameter, we would like as wide a pulse, as low a data rate *per channel* and as small a dispersion as possible.

Figure 2.9 illustrates the practical limits set by Gordon-Haus jitter on $10Gbit/s$ single-channel data transmission over $6000km$ for a range of dispersions. The sharp up-turn for very small amplifier spacings is due to the excess gain required of each amplifier to overcome losses due to splices and isolators, etc.. In this case, the excess gain has been estimated to be $0.1dB$.

Several factors can be used to decrease the Gordon-Haus effect such as filtering (of fixed or sliding central frequency), phase and amplitude modulation, partial re-generation, alternating amplitude modulation and dispersion management. These are discussed in section 2.6.

2.5.4 Soliton-Soliton Interaction

The high pulse width/low data rate relationship is also limited by the requirement that we avoid neighbouring soliton-soliton interaction [29, 30]. An attractive force between

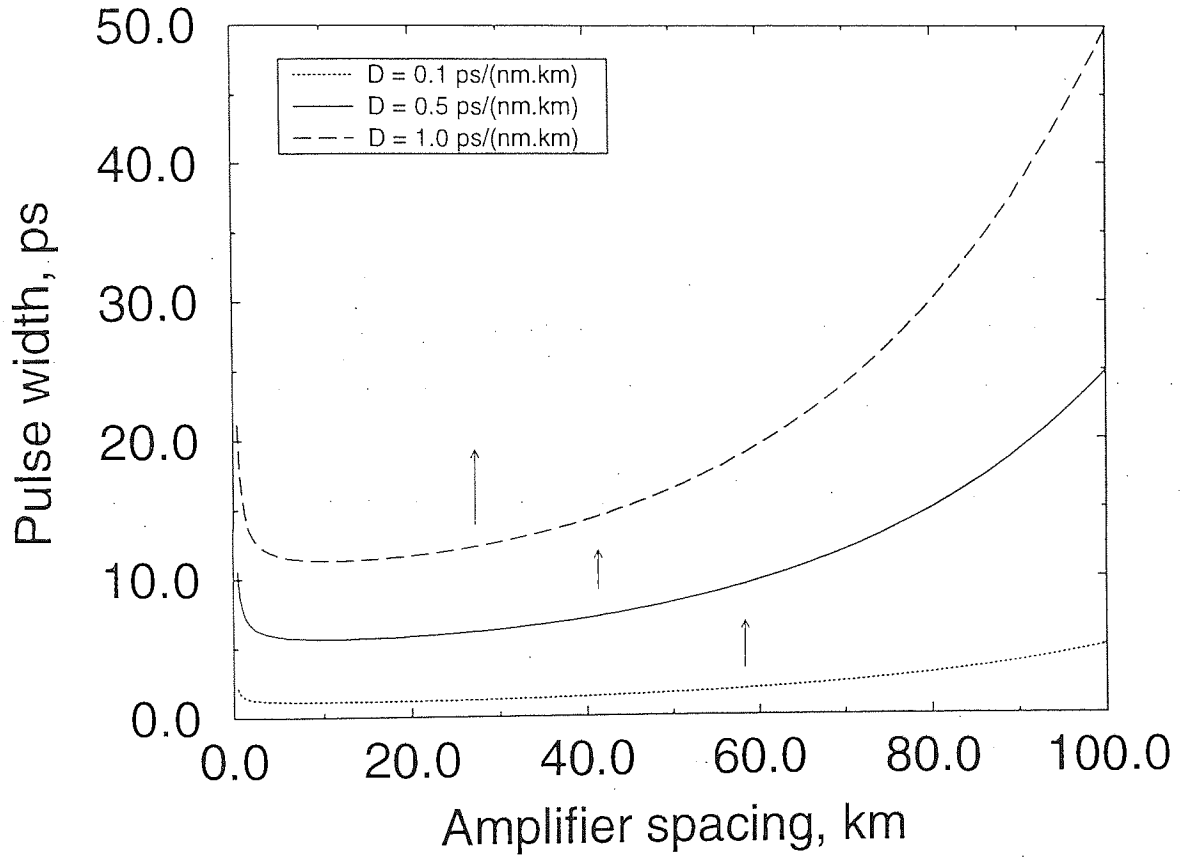

Figure 2.9: Limitations to amplifier spacing and pulse width due to Gordon-Haus jitter after $6000km$ at $10Gbit/s$ per channel. Other parameters are, $\lambda = 1.55\mu m$, $A_{eff} = 50\mu m$, $\alpha = 0.2dB/km$ and $n_2 = 2.6 \times 10^{-20} m^2/W$. The arrows show which side of each line operation is permissible.

neighbouring solitons of the same phase in a pulse train can be deduced by regarding them, more correctly, as two parts of a second-order soliton, half-way through its phase evolution. Solitons in anti-phase repel one another and solitons in quadrature neither attract nor repel. An approximate rule is that $\tau \leq 2/5t_w$ (t_w is half the bit-period, as defined in [42]). A more accurate design rule is to make the total system length less than half the collision distance due to soliton attraction. Hence,

$$L_{max} \leq \frac{1}{2}\left(\left(\frac{\tau}{1.76}\right)^2 \frac{\pi}{2\beta_2}\right) \exp\left(\frac{1.76}{2R\tau}\right) \tag{2.37}$$

where R is the data-rate (from [44]).

This attractive force only exists for solitons of the same amplitude and phase [30, 32, 31] because it is only the identical portions of the two solitons which are in a bound state. Hence, by varying either of these factors between neighbouring solitons, it is possible to increase the maximum transmission distance [45]. Slow amplitude (half-data rate) modulation schemes reduce the amount of interaction and have been shown to be effective experimentally [46, 47] but this may be impractical in terms of system design as the initial modulation may be lost after repeated re-amplification. In all the simulations in this thesis, pulses in the same channel are assumed to be at the same phase and initial amplitude.

2.5.5 Non-Linear Effects

Optical Kerr Effect

Self-phase modulation (SPM), is only one of the possible non-linear effects which can be experienced by optical pulses. It is a manifestation of the optical Kerr effect, due to the interaction between the light and electrons in bound states of the silicate lattice.

Generally speaking, the interaction leads to a change in the refractive index, n, given by equation 2.15, and hence dependent on $\chi^{(3)}$, the third order susceptibility of the material [48]. Other, and usually detrimental, effects due to the optical Kerr effect include cross-phase modulation (XPM) and four-wave mixing (FWM).

Brillouin Scattering

Two other $\chi^{(3)}$ effects are; Raman scattering (see below) and Brillouin scattering, which is an acoustic interaction with the lattice. Brillouin scattering effects signals with very narrow spectra (e.g. a few tens of MHz) and is therefore not a serious problem in soliton transmission. Also, the scattered light propagates in the opposite direction to the data signal, so uni-directional data propagation is not effected and the noise can be removed by the use of isolators, which are usually included in the design of EDFAs anyway.

Raman scattering and Self-Frequency Shift

Raman scattering is due to photons interacting with the infrared optical vibrations of the lattice. The photons are absorbed, a quantised lattice vibration (phonon) at an infrared frequency and a photon of frequency given by the difference between the original photon and phonon is emitted. It is also possible, but much less likely that a photon and phonon combine to make an up-shifted phonon. Hence, when scattering occurs, side-bands grow - one at lower frequency, much more intense than the one at higher frequency.

The scattering process can also be stimulated by a pump signal at the side-band frequency so that the interaction occurs more quickly. Because of this, Raman scattering is also strongly cumulative and can lead to a sequence of scattered sub-sidebands.

The peak resonance in glass is about $90nm$ at $1.55\mu m$, putting it outside the total bandwidth being exploited in this thesis, across the EDFA window. However, Raman scattering can occur between channels of any wavelength separation, so WDM systems can incur penalties due to cross-talk between channels. The numerical results in this thesis do not consider Raman effects, however, as it was intended to isolate the effect of collision-induced frequency shift.

If Raman scattering was to be included then the time delayed nonlinear response of the material has to be taken into consideration in deriving the NLSE. The response has a component due to the Raman gain coefficient which in turn depends on the vibrational frequencies of the glass. Being a property of the material, made up of overlapping bands, these frequencies have to be obtained by experiment.

When solitons are shorter than a picosecond FWHM, their spectrum becomes wide enough for pumping of the wavelengths in the wings of the spectrum. When this occurs, there is a continuous downshift of the average frequency called the soliton self-frequency shift (SSFS). The rate of SSFS is given by,

$$\frac{d\omega_0}{dz} = \frac{-4\tau_R\beta_2}{15\tau^4}, \tag{2.38}$$

where τ_R is the Raman pulse-width, below which self-frequency shift becomes significant and ω_0 is the central frequency of the soliton. From experimental results, $\tau_R \approx 1ps$, hence SSFS is not significant for any of the pulses studied in this thesis.

Non-Linear Polarisation Dispersion

An assumption made in deriving the NLSE used in this thesis is that the optical field is scalar. There are, in fact, two orthogonal polarisation axes and energy in each axis

interacts with the other by XPM. In a perfect (circular, untwisted) fibre, this leads to a rotation of the polarisation with propagation and no detrimental effects. Real telecoms fibre is randomly birefringent, however, and the two polarisations therefore have different group velocities and randomly varying polarisation rotation rates. The different group velocities lead to polarisation mode dispersion, which, like chromatic dispersion, smears the pulses out with propagation distance. For linear (NRZ) pulses, this effect can be of the order of picoseconds per km.

As early as 1982 it was shown that polarisation rotation's intensity dependence could be used to discriminate between optical pulses and noise [49]. In 1987, Menyuk [50] showed that because solitons in both polarisation modes of fibre with constant birefringence could be expressed by coupled versions of the NLS, PMD is suppressed if the predicted walk-off over a soliton period is less than the input pulse width. This effect is called soliton trapping and, analogous to the balance of chromatic dispersion and SPM which maintains the soliton's shape over large distances, the PMD is balanced by XPM between the polarisations.

Numerical simulations have subsequently shown that solitons are resistant to PMD in randomly birefringent fibre [51] when the fibre polarisation parameter $\Delta\beta/h^{\frac{1}{2}}$ (where $\Delta\beta$ is the birefringence and h is the rate at which light is coupled between the fast and slow axes), obeys

$$\frac{\Delta\beta}{h^{\frac{1}{2}}} < 0.3D^{\frac{1}{2}} \tag{2.39}$$

where D is the chromatic dispersion. Recently, it has also been shown that dispersion management and power-enhancement do not significantly change soliton's resistance to PMD [52].

2.6 Soliton Control

Several methods have been employed to combat the effects listed above, extending the transmission distance and increasing the single-channel data rate. These include filtering (static and sliding frequency), phase modulation, amplitude modulation, non-linear gain, phase conjugation, pulse shepherding and dispersion management [53, 54, 55, 56, 57, 40, 58, 59, 60, 61]. Some of these are more difficult to implement in a WDM system than others.

2.6.1 Filtering

Filtering is beneficial to soliton transmission for two reasons. Firstly, background noise, including amplified spontaneous emission (ASE) from the amplifiers required to compensate for fibre loss, is reduced, improving the signal-noise ratio. Secondly, Gordon-Haus jitter is suppressed.

Soliton self-shaping re-centres the soliton spectrum around the centre frequency of the filter used. The walk-off from the soliton's timing window is therefore reduced [53, 54, 55, 56]. The reduction in walk-off is at the cost of increased amplifier gain and hence amplifier noise. Hence, the filter cannot be narrow enough to eliminate timing jitter completely. However, the build-up of rms timing jitter is now proportional to $z^{1/2}$ rather than $z^{3/2}$ as it was in the unfiltered case.

The system can be improved further by using filters with a centre frequency which slides in value along a chain of amplifiers [57, 37]. ASE, behaving linearly, is completely filtered out after ≈ 5 amplifier spans whereas solitons, behaving non-linearly, follow the centre frequencies of the filters and timing jitter is further eliminated. Again some excess gain is required to compensated for signal power lost in filtering, but now more

gain and narrower filters can be used without penalty and timing jitter is suppressed completely. Sequences of filters, down-sliding in frequency act more efficiently than up-sliding sequences because of higher-order effects of the narrow filters used [57].

It has also been shown that both static and sliding-frequency filters suppress interaction between neighbouring solitons in a pulse train (see [62] for a summary of the effects).

The use of filters fixes the signal wavelength used. Comb-type filters are easy to manufacture and can be used to extend the technique to WDM systems. In single or multiple-wavelength systems, sliding-frequency sequences of filters can be used in lumped amplification links.

2.6.2 Phase and Amplitude Modulation

It has also been shown that the phase-modulation of a soliton data-stream, with the maximum positive chirp coinciding with each soliton can reduce both soliton-soliton interaction and Gordon-Haus jitter [40] and that even just one phase modulator at the half-way point of an optical link can reduce timing variance due to Gordon-Haus jitter by a factor of five [63]. Some dispersive radiation is also produced which can be filtered out with quite broad-band filters.

Phase modulation needs to be applied to each channel of a WDM system separately, requiring de-multiplexing and re-multiplexing of the data. Also, the data-rate and timing have to be extracted in order to synchronise the modulation with the data in each channel. That is, phase-modulated jitter reduction would require clock recovery and phase modulators and for each channel. Compared to filtering, such equipment would be expensive, cumbersome and difficult to maintain. An alternative has been suggested, that the transmission length be designed such that all channels are synchro-

nised at the phase modulator [64], but this design limitation, which would also fluctuate with temperature, is not attractive in designing a robust, 'plug-together' network.

Another system for improving soliton timing is amplitude modulation synchronised so that the minima in loss due to the modulator coincide with the expected arrival times of the solitons [58]. As with static-frequency filtering, the rate of growth of timing jitter becomes proportional to $z^{1/2}$ but with the addition of filtering, the jitter cannot grow beyond a fixed value [55].

Again, a WDM system would require de-multiplexing and re-multiplexing every time the signal was to be modulated; this time, at regular intervals during transmission, making it even less practical than phase modulation.

2.6.3 Nonlinear Effects

It is possible to directly exploit the non-linear properties of solitons by either using an amplifier along with a non-linear absorber such as a non-linear optical loop-mirror (NOLM) [65, 66] or saturable absorber [59, 67, 68], or polarisation rotation along with polarisation dependent loss [69].

A non-linear absorber acts as a filter to back-ground noise but allows large-energy pulses to propagate. As such, a switching power has to be decided on, above which loss is low. NOLMs [66], for example, have a power dependent switching characteristic such as in figure 2.10 with an optimum input power. Hence, this method of pulse stabilisation is only effective in single-channel systems as co-incident pulses will suffer a lower transmission ratio than a single pulse. Single channel bifurcation of central frequencies has also been observed in some simulations of soliton transmission with NOLMs used as saturable absorbers [66] which would lead to large timing errors at the receiver.

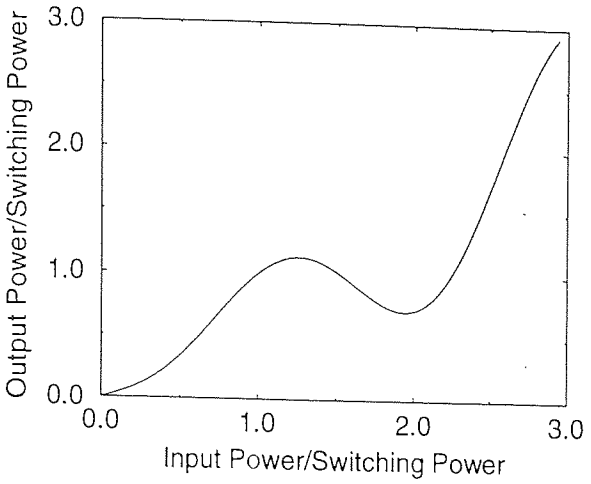

Figure 2.10: Transmission characteristic of a NOLM with coupling ratio 0.2. Switching power would be tailored to that the peak power of a first-order soliton.

Saturable absorbers such as multiple-quantum-well (MQW) devices can also be used as low-level noise filters [67]. Amplifier spacing can then be increased whilst soliton-soliton interaction and Gordon-Haus jitter are reduced because intensity fluctuations due to ASE are smoothed out. MQW saturable absorbers have a strong wavelength dependence however, excluding them from use in WDM systems.

Between any two amplifiers in a concatenated chain, solitons will undergo a certain amount of non-linear polarisation-rotation whilst the ASE from the previous amplifiers will not (behaving linearly) [69]. Polarisation-dependent filters at the end of each segment, aligned to match the solitons will then filter out any ASE. This requires polarisation control at each amplifier to ensure that all data survives. Different WDM channels, however, would undergo different amounts of polarisation rotation and only one channel would survive the polarisation-dependent absorber.

2.6.4 Phase Conjugation

It is possible to use the same fibre to perform dispersion compensation 'on itself' by optical phase conjugation of the signal at the half-way point in any optical link [60]. This can be achieved by the stimulation of four-wave-mixing (FWM) using a pump

signal to produce a copy of the signal with shifted wavelength and opposite sign of chirp. This has been achieved for NRZ signals by using FWM in dispersion shifted fibre [70, 71] and in a semiconductor laser amplifier [72].

The technique has been shown to be applicable to single-channel soliton systems [60]. It has the benefit of being passive and not requiring clock-recovery circuitry. The method used is stimulation of four-wave mixing (FWM) by injection of a pump signal. Such a method would be directly applicable to WDM, with one pump signal creating a phase conjugate of each wavelength channel.

Phase-conjugation by the use of parametric amplification has also been shown to be a possible method of pushing single-channel soliton propagation to data rates greater than $100Gb/s$ as it compensates for Raman scattering [73, 74]. The scheme proposed also required dispersion tailored fibre.

2.6.5 Soliton Shepherding: Use of XPM

Some schemes have been proposed which exploit the action of cross-phase modulation (XPM) to re-time or 'shepherd' data-carrying solitons. This, in turn, reduces the build-up of Gordon-Haus jitter. A clock-stream of pulses can be co-propagated with the data but at an orthogonal polarisation [75] which modulates the phase of the signal pulses in much the same way that soliton self-trapping reduces polarisation mode dispersion (PMD). This shifts the signal pulses' central frequency, pushing them back to their original time-slot. In practical terms, the output of the laser being used as a pulse source could be split in two. One pulse stream could be modulated with data then multi-plexed with the un-modulated clock stream at 90° to the data. At the receiver, the clock stream could be removed with a polarising filter. The authors who proposed this method did not mention the problem of polarisation mode dispersion. In randomly

birefringent fibres, conventional solitons need to have roughly half their energy in each polarisation state for soliton trapping. Random birefringence may actually destroy the soliton-soliton interaction which keeps the clock pulses in place and data may be lost.

Alternately, the clock-stream pulses can be at a slightly different wavelength from the signal and co-propagated over short lengths of fibre at intervals along the transmission fibre [61], with the same effect. This has been achieved experimentally by modulating a dfb laser at the rate of data circulating in a loop. The data rate was recovered electronically. The clock stream was multiplexed into a short segment of the loop, over which there was no significant walk-off between the data and the shepherding pulses.

A more complex method of improving the signal is all-optical signal regeneration [76, 77]. The data is used to mode-lock a fibre ring-laser whose output pulses are then at the data rate but with minimal timing jitter. This recovered clock pulse stream is then modulated with the data stream using a NOLM. The output pulses are then at the wavelength of the fibre ring-laser.

Soliton shepherding and all-optical signal regeneration can only be implemented in WDM if the channels are separated in order to perform the correcting process. A co-propagating clock-stream system should be compatible with WDM but may be difficult to implement (each channel requiring its own, synchronised support channel).

2.6.6 Dispersion Management

Dispersion management is defined as tailoring the average dispersion to that required by using a combination of local dispersions. For example, standard fibre, as is installed in most of the world's optical networks, can be compensated with a short portion of highly normal dispersion fibre [15] giving a net dispersion small enough to make

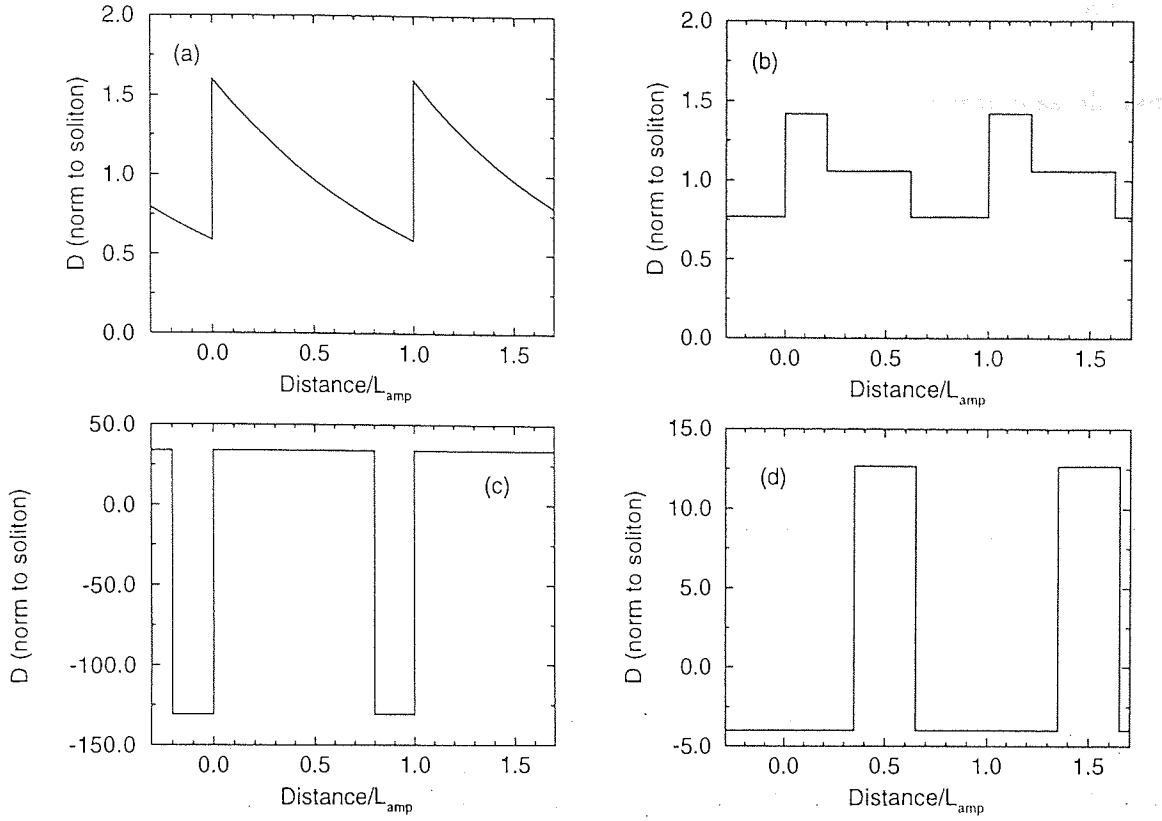

Figure 2.11: Four possible dispersion maps. Dispersions have been normalised to the average value and distances are given in amplifier spacings. (a) matches the dispersion to the exponential decrease in soliton energy between amplifiers, (b) approximates to the exponential decrease in energy in a 3-step profile, (c) shows, in the same units, how large local dispersions can be used to form a low average dispersion and. (d) shows an arbitrary dispersion map where the amplifiers are not located at points where there is also a change in local dispersion.

soliton propagation viable. In WDM it is also desirable to compensate for third-order dispersion, flattening the second-order.

Four possible dispersion management schemes for a link comprising of fibre and concatenated amplifiers are illustrated in figure 2.11. As will be seen in later chapters, there are benefits to these, and other, dispersion management schemes when used in WDM systems.

NRZ systems have used dispersion compensation for some time in an attempt to have zero net dispersion and to reduce four-wave mixing. Any finite dispersion degrades NRZ pulses with propagation. The bit-pattern is smeared out by a factor determined by the dispersion, the bandwidth (which has a minimum value of the single-channel

data-rate) and the distance propagated.

Dispersion management in single channel soliton systems have several possible benefits. It may be difficult and/or expensive to accurately manufacture fibre with dispersion low enough for soliton conditions to be met with reasonable power levels (i.e. achievable with diode-pumped EDFAs and not high enough to cause Raman scattering).

Average soliton dynamics are limited by the amount they deviate from the soliton condition, i.e. the energy equation 2.29. The main problem observed is dispersive radiation which can lead to the destruction of the soliton [40]. If the fibre is manufactured with an exponentially tapered dispersion profile, such that the energy equation is satisfied at all times, then there is no dispersive radiation [78, 10]. However, such fibre is very difficult to manufacture, has to be tailored to each amplifier-span in an optical link, is uni-directional and all samples manufactured so far have been highly wavelength sensitive.

A step-profile approximation of the exponential profile has also been found to increase the feasible amplifier spacing in a single-channel soliton system [17].

Exponentially tapered fibre, step approximations to it and the range of dispersion maps considered in this thesis may be considered 'weak' or 'moderate' dispersion management. Deep dispersion profiles may be defined as ones which are associated with significant energy enhancement factors, as described in the next section. Deep dispersion profiles, such as dispersion-compensated standard fibre, also reduce Gordon-Haus jitter [79].

2.6.7 Energy Enhancement

Perhaps the main advantage of dispersion management is the power-enhancement factor identified by Smith et al [80]. In the idealised, lossless case, Smith showed that the stable soliton energy, E_{sol} grows with the depth of the dispersion map used and inversely with the square of the pulse width. A non-analytic explanation for this is that more energy is required to fulfil the soliton criteria as the pulses evolve with propagation. That is, in strong local dispersion, the pulses become chirped very rapidly and appear to 'breathe'. Hence, the self-phase modulation which balances the effects of dispersion is weaker over a significant part of the cycle.

If the map uses alternate segments of fibre of lengths l_1 and l_2 and dispersions $\ddot{\beta}_1$ and $\ddot{\beta}_2$ with average value $\ddot{\beta}_{av}$, then,

$$E_{sol} = E_0 \left[1 + 0.7 \left(\frac{(\ddot{\beta}_1 - \ddot{\beta}_{av})l_1 - (\ddot{\beta}_2 - \ddot{\beta}_{av})l_2}{\tau^2} \right)^2 \right]. \tag{2.40}$$

where τ is the FWHM pulse width. The strong relationship with τ sets a realistic limit to the use of the equation even in the lossless case. Where the amount of breathing and/or energy enhancement becomes large, the equation no longer holds. That is, when the predicted enhanced energy is about ten times that of the unenhanced energy, a deviation from the prediction would be expected.

In fact, as dispersion depth increases, the periodically stable pulse shape also changes from sech, through gaussian to more complex pulse-shapes [21]. In the presence of loss, it has also been observed that there can be a modification of the enhancement factor [81]. A reduction in enhancement factor is most noticeable when the periodicity of the dispersion and the periodicity of amplification are the same and when the amplifiers are sited at points where there is a change in the dispersion - a situation

which is easily avoidable in designing a real transmission system. The reduction of enhancement factor is taken into consideration in later chapters.

The main benefits of the enhancement factor are due to the possibility of using very low average dispersions without incurring an unacceptable signal-to-noise (SNR) penalty and reducing Gordon-Haus jitter as discussed in the next section.

2.7 Design Diagrams

It is possible to combine the design limitations listed above in a single diagram which displays the usable range of parameters. This concept was first proposed by Doran [82] and expanded on by Wright et al [44, 83].

Figure 2.12 shows the window (eye) in which it would be feasible to construct a $6000km$, $10Gbit/s$ transmission system with lumped amplification. In this example, it can be seen that the main limits to increased amplifier spacing are the acceptable signal-to-noise ratio (SNR) limit and the Gordon-Haus jitter limit.

One benefit of dispersion management is the power-enhancement factor identified by Smith [80] which opens out the eye formed by the SNR and Gordon-Haus jitter lines. Figure 2.13 shows how the usable range of parameters varies with depth of dispersion map. Parameters which would correspond to an enhancement factor of greater than 11 have been dis-allowed, which causes the discontinuity in the Gordon-Haus lines. The limitation was imposed to avoid unrealistic peak powers and pulse widths (as explained in the last section). That is, the enhancement factor proposed by Smith at al becomes less relevant as profiles get beyond this order of magnitude. The combination of the equations for Gordon-Haus jitter and enhancement factor, if unchecked, give solutions for pulses of zero width due to the τ^4 term in equation 2.40.It can be seen that a set

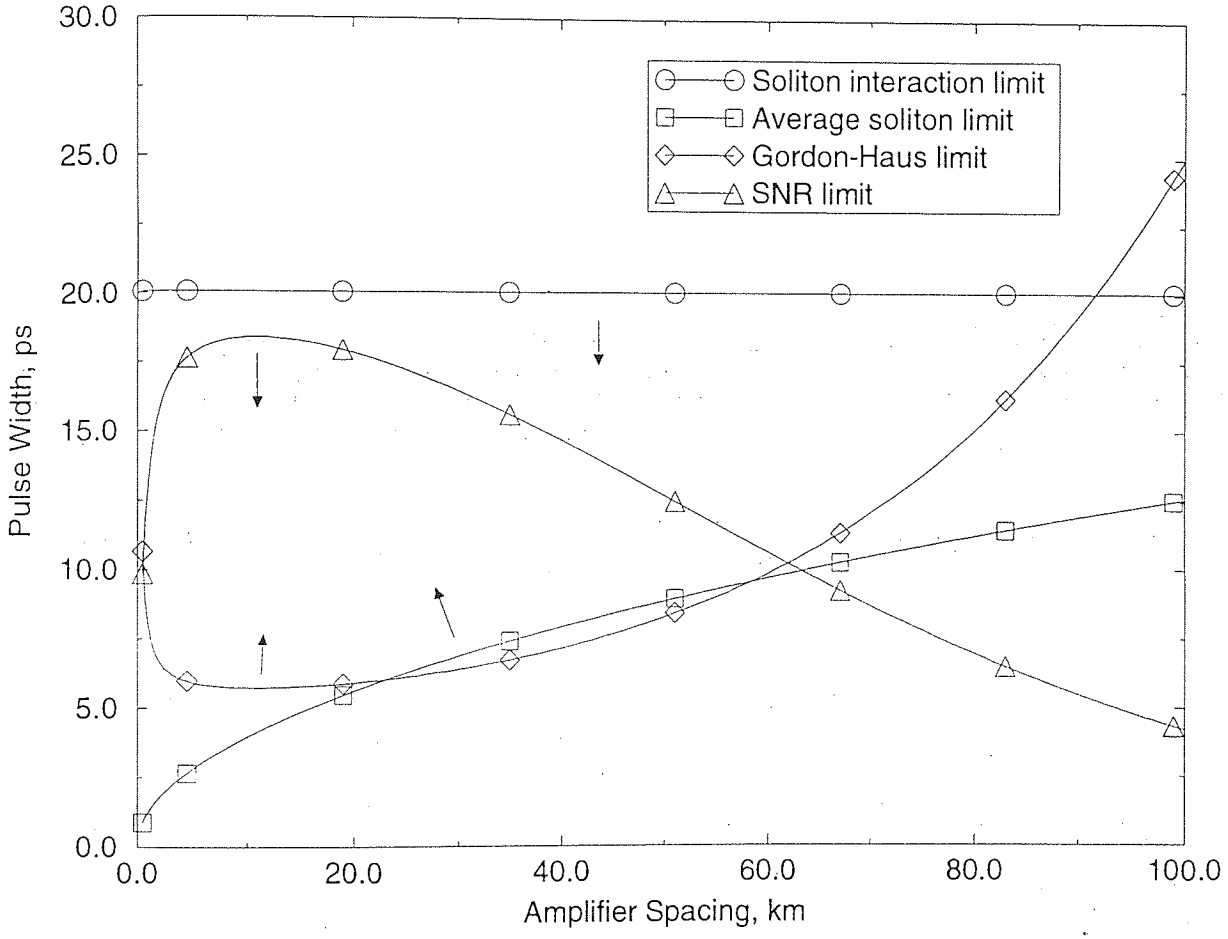

Figure 2.12: Design diagram for 6000km transmission of a single $10Gbit/s$ channel of solitons. Other parameters are, $\lambda = 1.55\mu m$, $D = 0.5ps/(nm.km)$, $\alpha = 0.2dB/km$, $A_{eff} = 50\mu m$, and excess gain due to amplifier components and splices $= 0.1dB$. The arrows show which side of each line operation is permissible.

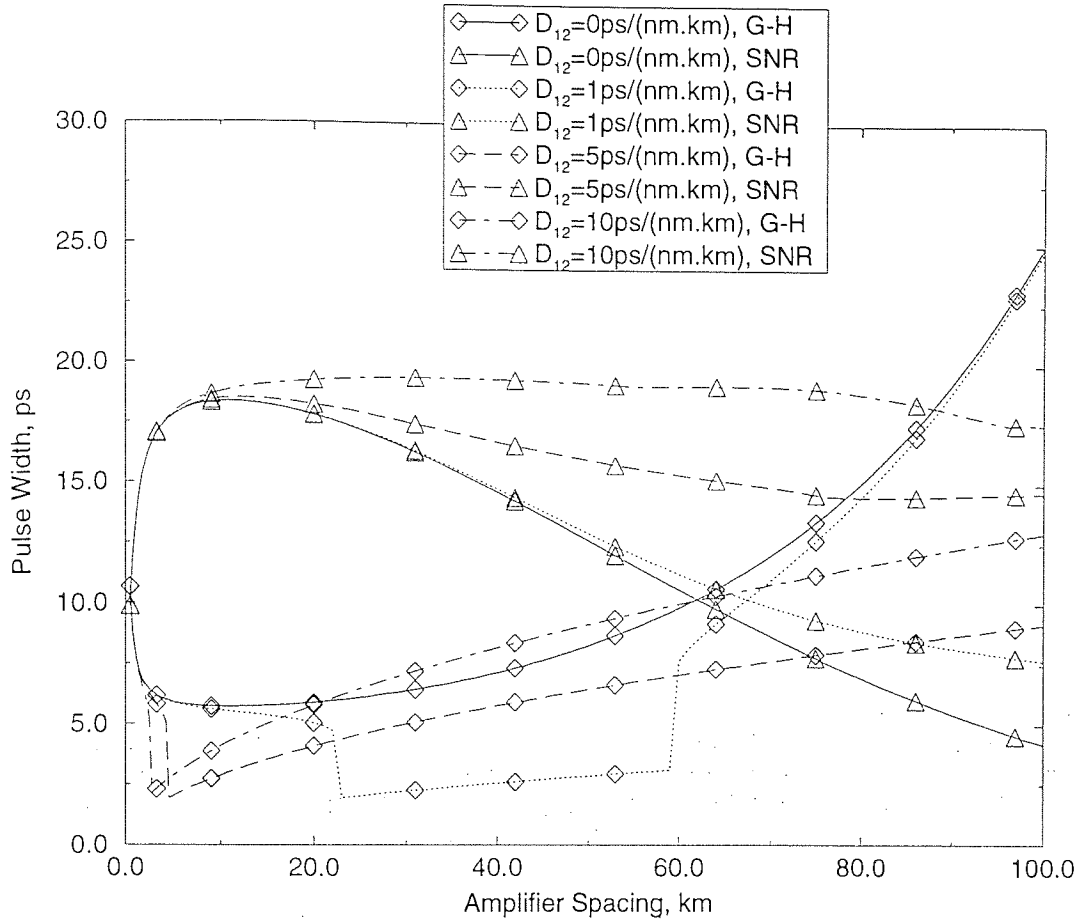

Figure 2.13: Design diagram for 6000km transmission of a single $10Gbit/s$ channel of solitons. A range of two-step dispersion maps have been included to show their effect by the predicted enhancement factor. Dispersion depth is given by $D_{12} = D_1 - D_2$, where $D_{1,2}$ are the component dispersions of the map. Other parameters are, $\lambda = 1.55\mu m$, $D_{ave} = 0.5ps/(nm.km)$, $\alpha = 0.2dB/km$, $A_{eff} = 50\mu m$, and excess gain due to amplifier components and splices $= 0.1dB$. G-H = Gordon-Haus limit, SNR = signal-to-noise ratio.

of parameters have been opened up for much larger amplifier spacings and the average soliton limit has become the main limiting factor across much of the range of amplifier spacings.

The window of usable design parameters has opened out significantly, however, particularly making it possible to use larger amplifier spacings and subsequently saving on component costs. The rest of this thesis is concerned with detrimental effects caused by wavelength multiplexing. It will be shown that dispersion management can also be beneficial in reducing these effects.

Chapter 3

Analytic Theory of Solitons in WDM Collisions

3.1 Introduction

Various developments of the analytic theory have advanced knowledge of the behaviour of optical soliton transmission systems since the discovery of optical solitons in 1973. The need to utilise WDM to increase the total data capacity of such systems has also increased as it has become apparent that data rates approaching the limits of single-channel soliton transmission will soon be required in telecommunications.

Several effects, not observed in single-channel systems, all due to the non-linearity of soliton propagation, have to be taken into consideration. Included in these are pseudo-phase-matched four-wave-mixing, collision-induced residual frequency shift and collision-induced frequency shifts at the detector.

In a collision between solitons of different wavelength, the solitons are perturbed by each other, shifting in central frequency, accelerating towards each other in the first half of the collision and away from each other in the second half. In the lossless

case, these perturbations are symmetric over a complete collision and there is no net frequency shift (an elastic collision). However, with loss and re-amplification, collisions are asymmetric, the solitons receive a change in their average frequency [84] and four-wave mixing products are produced [85]. The group velocities of solitons in a data stream are randomised by their frequency shifts with respect to each other and pulses walk away from their expected temporal positions.

The core of this thesis is concerned with minimising these frequency shifts by using dispersion management.

3.2 Non-Collision-Induced Effects of the WDM of Solitons

3.2.1 Initial Conditions

The initial pulse positions in the WDM channels make a very large difference to the maximum transmission distance [84, 44]. If two channels have their pulses superimposed when launched, all coincident pulses will receive a strong frequency shift due to the partial collision that they undergo initially. For this reason, all simulations used in this thesis have the initial pulses as well separated as possible depending on the data rate.

Another initial condition which has been shown to be very important in stabilising the transmission of solitons in dispersion management is the chirp of the soliton [80, 81, 86]. Before transmission through the periodic dispersion, the pulses have to be 'matched' to the stable cycle of pulse fluctuations. That is, as well as injecting a pulse of the correct (*sech*) shape and energy (set by the enhancement factor and exponential

loss cycle), they must also be of the correct chirp and phase. At one point in the cycle, the pulse is transform limited. In the lossless case, matching can be achieved by passing the pulses through a half-segment of the second fibre in the sequence, i.e. at this point in the cycle, the pulses are transform limited. With the introduction of loss, particularly when the periodicity of the dispersion map is the same as the amplifier spacing, the amount of fibre needed to achieve this gets smaller. That is, the point in the dispersion map where the pulses are transform limited shifts to later in the cycle. The amount of shift has not been quantified and is found by iteration.

3.2.2 Third-Order Dispersion

The effect of third order dispersion (the variation in dispersion with wavelength) is much more significant in WDM soliton systems than in single channel systems. In particular, it is preferable to have a small value of average dispersion in order to minimise Gordon-Haus and collision-induced timing jitter. It is possible to tailor a system with a very small dispersion (say $0.1ps/(nm.km)$) at one wavelength by combining standard and dispersion-shifted fibre. With a typical value for third-order dispersion ($0.07ps/nm/(nm.km)$) a second WDM channel, with wavelength $1nm$ longer than the first will see dispersion of $0.17ps/(nm.km)$. This problem is addressed in Chapter 6, where data propagation is simulated.

3.2.3 Four-Wave Mixing

Non-linear effects due to the third-order susceptibility ($\chi^{(3)}$) can cause energy to be lost from the data, either to back-ground noise or cross-talk. Third-order harmonic generation is not detrimental to data propagation at the pulse powers studied in this thesis. Four-wave mixing, however, is predicted to be significant in some systems with

pulse powers of the order of those used here. FWM can be either transient or residual. That is, side-bands can be produced during a collision between solitons or can build up during a collision and energy can be permanently lost to the new frequencies produced.

Four-wave mixing (FWM) is a parametric process through which co-propagating electromagnetic waves of two different frequencies ω_1 and ω_2 interact to produce waves at ω_3 and ω_4, where the frequencies involved must obey [48],

$$\omega_3 + \omega_4 = \omega_1 + \omega_2. \tag{3.1}$$

The phase-matching condition,

$$\Delta k = k_3 + k_4 - k_1 - k_2 \tag{3.2}$$

$$= (n_3\omega_3 + n_4\omega_4 - n_1\omega_1 - n_2\omega_2)/c = 0, \tag{3.3}$$

where k_j is the phase per unit length and n_j is the refractive index at frequency ω_j, and c is the speed of light, also has to be satisfied for efficient frequency conversion. Figure 3.1 shows the build-up of permanent FWM products after a single two-soliton collision. This diagram shows the evolution of the pulses spectra with distance travelled along the y-axis. The collision occurs after $400km$. In this instance, the FWM products have $\sim 50dB$ less peak power than the signal solitons.

When four-wave mixing (FWM) occurs, side-bands are produced during collisions between solitons of different wavelengths. After experimental evidence [57] was found of four wave mixing products possibly being a significant problem in soliton transmission, Mamyshev and Mollenauer [87] highlighted the pseudo-phase-matching between soliton period and amplifier spacing as being responsible for the worst possible FWM product

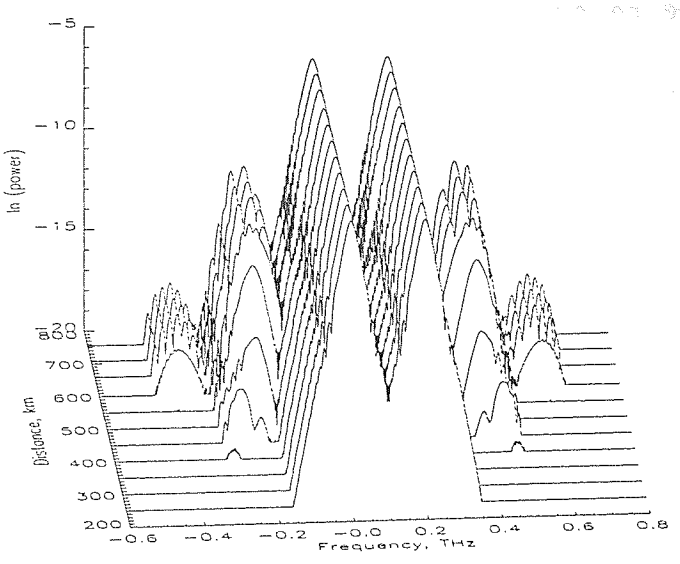

Figure 3.1: Four-wave mixing during the collision of two solitons, $1.6nm$ apart in fibre with loss, $\alpha = 0.2dB/km$ and dispersion, $D_{ave} = 0.5ps/(nm.km)$, pulse width $\tau = 20ps$, amplifier spacing, $L_{amp} = 50km$. Log of power is plotted against optical frequency as the two pulses propagate. They begin to collide after $400km$ and have fully separated by $700km$. In these conditions it can be seen that FWM products are $\sim 50dB$ below signal level.

growth, i.e.,

$$L_{amp} = \frac{2\pi n}{\Delta k}, \tag{3.4}$$

where n is an integer, and Δk is the phase mis-match between FWM products, defined in equation 3.2. In this instance, the phase-matching condition is met whenever solitons in different channels collide and FWM products accumulate. Ablowitz et al [85] also provided an analytic model which agrees with the occurance and magnitude of growth of FWM products seen in numerical simulations and predicts the undesirable resonances observed in [87].

As with collision-induced frequency shifts, FWM products can also be minimised by using or approximating to an exponential taper of dispersion between amplifiers [87] which reduces the perturbative effects due to loss, making collisions physically equivalent to the lossless case. FWM products are always produced during collisions, however these are transient in the lossless case or when the fibre dispersion tapers with

loss. Levels of FWM were periodically inspected in the simulations used in this thesis. In all the cases where dispersion management is successful in reducing collision-induced frequency shifts, no significant amounts of FWM products were observed.

In [84], where the adiabatic theory of collision-induced frequency shift was first derived, four-wave-mixing products were identified but ignored as negligible. The results of this thesis would indicate that this was a valid assumption over the range of parameters studied.

3.3 Collision-Induced Frequency Shift

In 1986, Mollenauer, Gordon and Islam produced a comprehensive investigation of soliton propagation in systems with periodically compensated loss, including an investigation of the limits of WDM [33]. Their analytic work was also extensively backed up by numerical simulations and drew some general conclusions about usable WDM channel separations.

Mollenauer et al extended their analysis in 1991 [84] to give an expression for the residual frequency shift after the collision of two solitons of different wavelengths.

They returned to the non-linear Schrödinger equation in the form,

$$-i\left(\frac{\partial u}{\partial z}-\frac{\gamma(z)}{2}u\right)=\frac{\Delta(z)}{2}\frac{\partial^2 u}{\partial t^2}+|u|^2u \tag{3.5}$$

where the loss coefficient, γ averages to zero and the dispersion parameter, $\Delta = D/\bar{D}$ averages to one over a distance much less than the soliton period.

This can be transformed into

$$-i\frac{\partial u'}{\partial z'} = \frac{1}{2}\frac{\partial^2 u'}{\partial t^2} + g|u'|^2 u', \tag{3.6}$$

where $g(z') = G(z)/\Delta(z)$, $u' = u/\sqrt{G}$, $dz' = \Delta dz$ and $z' = 0$ when $z = 0$. $G(z)$ is the variation in gain (or loss) dependent on distance and is periodic.

Taking the solution to eq'n 3.6 to have soliton form,

$$u' = \mathrm{sech}(t + \Omega z')\exp(-i\Omega z' + i\phi), \tag{3.7}$$

where $d\phi/dz' = g - (1+\Omega^2)/2$. As Mollenauer et al pointed out, this is only an approximate solution which is accurate where the loss coefficient and dispersion parameter vary over a short scale compared to the soliton period.

Adding two such solutions for solitons whose frequencies do no not overlap (i.e. pulses from two different WDM channels), $u' + v'$ we can re-substitute into eq'n 3.6 (and ignore the cross-products associated with FWM) to get,

$$-i\frac{\partial u'}{\partial z'} = \frac{1}{2}\frac{\partial^2 u'}{\partial t^2} + g(|u'|^2 + 2|v'|^2)u', \tag{3.8}$$

and,

$$-i\frac{\partial v'}{\partial z'} = \frac{1}{2}\frac{\partial^2 v'}{\partial t^2} + g(2|u'|^2 + |v'|^2)v'. \tag{3.9}$$

We are interested on the effect on one soliton's mean frequency, $\langle\omega\rangle$, by interaction with the other soliton. The mean frequency of a pulse is defined as,

$$\langle\omega\rangle = W^{-1}\mathrm{Im}\int \frac{\partial u'^*}{\partial t}u' dt. \tag{3.10}$$

Also, the mean temporal position is defined as,

$$\langle t \rangle = W^{-1} \int t|u'|^2 dt, \tag{3.11}$$

where the pulse energy is,

$$W = \int |u'|^2 dt. \tag{3.12}$$

Differentiating with respect to z' gives,

$$\frac{dW}{dz'} = 0, \tag{3.13}$$

and

$$\frac{d\langle t \rangle}{dz'} = -\langle \omega \rangle. \tag{3.14}$$

Using eq'n 3.8 then gives,

$$\frac{d\langle \omega \rangle}{dz'} = \frac{2g}{W} \int \frac{\partial |u'|^2}{\partial t} |v'|^2 dt. \tag{3.15}$$

Substituting eq'n 3.7, and it's equivalent for v' with mean frequency $-\Omega$ into eq'n 3.15 to get,

$$\frac{d\Omega}{dz'} = g \int dt \left(\frac{\partial}{\partial t} \text{sech}^2(t + \Omega z') \right) \text{sech}^2(t - \Omega z') \tag{3.16}$$

which applies to both solitons. When the frequency shifts are much smaller than the frequency separation of the solitons, their effect on the integral can be taken as negligible, hence,

$$\frac{d\Omega}{dz'} = \frac{g}{2\Omega} \int dt \quad \text{sech}^2(t + \Omega z') \text{sech}^2(t - \Omega z'). \tag{3.17}$$

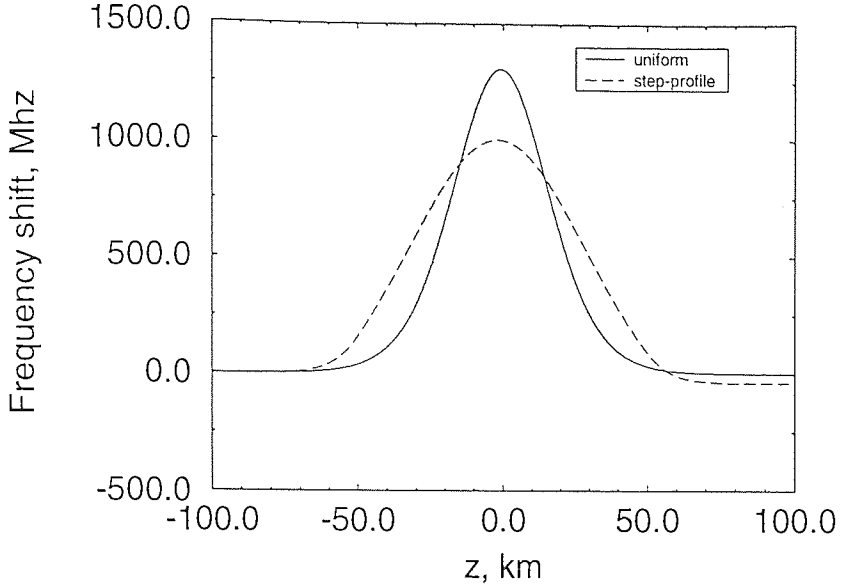

Figure 3.2: Frequency shift during the collision of two solitons, $1.6nm$ apart in fibre with $\alpha = 0$ and (a) - solid line - $D = 0.5ps/(nm.km)$ and (b) - dashed line - a stepped dispersion profile, equal step-lengths, $L_{1,2} = 100km$ and dispersions $D_1 = 0.75ps/(nm.km)$ and $D_2 = 0.25ps/(nm.km)$. In (b) $D = D_2$ across $-50km < z < 50km$. The distance, $z = 0$ at the collision centre in both cases.

At this point, we can get a simple picture of what this looks like in the lossless case with uniform dispersion. In this case, $g = 1$, $z' = z$ and eq'n 3.17 reduces to,

$$\delta\Omega = -\frac{1}{2\Omega}\int dt \quad \mathrm{sech}^2(t+\Omega z)\mathrm{sech}^2(t-\Omega z) \tag{3.18}$$

$$= -\frac{2}{\Omega}\frac{[2\Omega z\cosh(2\Omega z) - \sinh(2\Omega z)]}{(\sinh(2\Omega z))^3}. \tag{3.19}$$

This predicts the mean frequency of each soliton as they collide. Figure 3.2 plots the shift in the mean frequency of one soliton (the other undergoes the opposite sign of shift - hence the minus sign is dropped beyond this point) during the collision of two solitons, $1.6nm$ apart in lossless fibre with dispersion $D = 0.5ps/(nm.km)$ and in a stepped profile where the average dispersion $D_{ave} = 0.5ps/(nm.km)$.

The frequency shift does not necessarily return to zero after a collision in lossy and/or non-uniform dispersion fibre (e.g. in the second plot of central frequency in figure 3.2). To calculate the net frequency shift, we can integrate eq'n 3.17 over z' to

get

$$\delta\Omega = -\frac{1}{2\Omega}\int dz' \frac{dg}{dz'} \int dt \quad \mathrm{sech}^2(t+\Omega z')\mathrm{sech}^2(t-\Omega z'). \tag{3.20}$$

This can then be reduced by doing a spatial resolution of g because g is periodic in z. That is,

$$g(z') = \int dk \quad \bar{g}(k)\exp(ikz'). \tag{3.21}$$

After substitution into eq'n 3.20, we get,

$$\delta\Omega = \mathrm{Im}\frac{32}{\pi^2}\int_0^\infty dk \frac{\bar{g}(k)}{k}\frac{x^4}{\sinh^2 x}, \tag{3.22}$$

where,

$$x = \frac{\pi k}{4\Omega}. \tag{3.23}$$

In a periodic variation of dispersion and gain, $g(z')$ reduces to a sum over spatial harmonics of the fundamental period (i.e. $L_{amp} = L_{pert}$ in all the cases considered in this thesis, where L_{pert} is the periodicity of the dispersion map), with wave numbers

$$k = \frac{2\pi n}{L'_{pert}}, \tag{3.24}$$

and eq'n 3.22 becomes

$$\delta\Omega = \frac{16L'_{pert}}{\pi^3}\sum_{n=1}^{\infty}\mathrm{Im}(\bar{g}_n)\frac{n^3x^4}{\sinh^2(nx)}, \tag{3.25}$$

where

$$x = \frac{\pi^2}{2\Omega L'_{pert}} \tag{3.26}$$

and $\bar{g}_n$ is the average of $g(z')\exp(-i2\pi nz'/L'_{pert})$. That is,

$$\bar{g}_n = \frac{1}{L'_{pert}} \int_0^{L_{pert}} \frac{G}{\Delta} \exp\left(-\frac{i2\pi nz'}{L_{pert}}\right) dz' \tag{3.27}$$

If $\delta f = 0.5612(\Omega/\tau)$ is the channel spacing in real units then (using g_n for $\bar{g}_n$ from now on to reduce clutter) eq'n 3.25 can be expressed as,

$$\delta(\frac{\delta f}{2}) = 0.2274 \frac{L_{pert}}{z_0 \tau} \sum_{n=1}^{\infty} \mathrm{Im}(g_n) \frac{n^3 x^4}{\sinh^2(nx)}. \tag{3.28}$$

and

$$x = \frac{\pi^2}{2\Omega L'_{pert}} = 2.7995 \frac{L_c}{L_{pert}}. \tag{3.29}$$

The collision length, $L_c = 0.6298 z_0/(\tau \delta f)$, begins and ends where the solitons overlap at their half power points

In real units the periodic power variation,

$$G(z) = \frac{\alpha L_{pert}}{(1 - e^{-\alpha L_{pert}})} e^{-\alpha z} = \Lambda^2 e^{-\alpha z}, \tag{3.30}$$

and $\Delta(z)$ is the periodic dispersion variation, both normalised to unity. Λ^2 is the average soliton factor and as above, z' is the inhomogeneous distance along the fibre span,

$$z' = \int_0^z \Delta(z) dz. \tag{3.31}$$

These equations can be plotted in a variety of ways which illustrate the effect that they describe. Possibly the most revealing are those of frequency shift against collision centre and maximum residual frequency shift against collision distance.

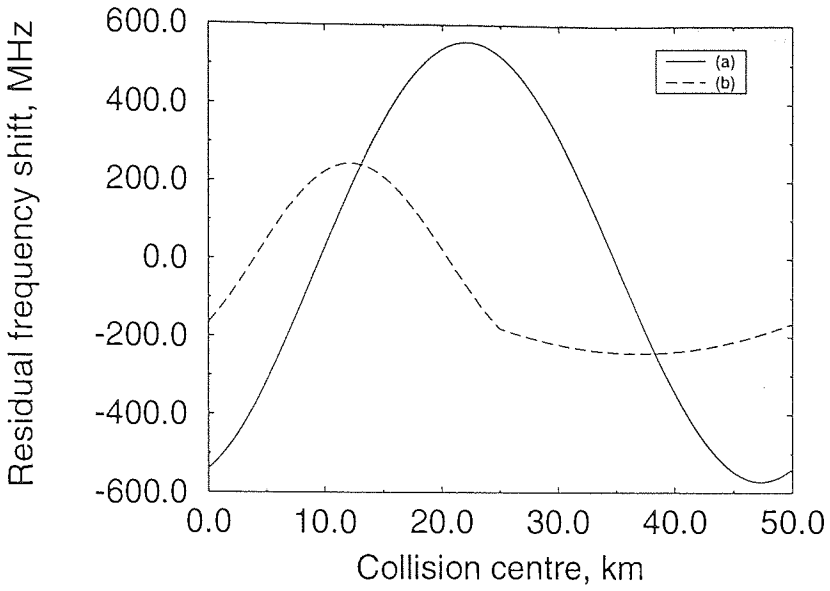

Figure 3.3: Frequency shift against collision centre for two solitons, $1.6nm$ apart in fibre with $\alpha = 0.2dB/km$ and $D_{av} = 0.5ps/(nm.km)$. (a) Uniform dispersion and (b) $D_1 - D_2 = 1.0ps/(nm.km)$.

3.4 Two-Step Profiles

As in figure 3.2, the collision centre is taken as the point where the two solitons are completely overlapping. In uniform dispersion, lossless fibre, the position of the collision centre is immaterial. However, as soon as any variation in pulse energy or dispersion is introduced, the collision becomes asymmetric and there is a net frequency shift. With loss present, the asymmetry becomes most noticeable when the collision occurs across an amplifier or midway between two amplifiers in a concatenated chain. In figure 3.3 (a) is the residual frequency shift for a range of collision centres between two amplifiers in a concatenated chain, each $50km$ apart. Line (b) shows the residual frequency shift for the same chain of amplifiers but with a dispersion map of the same periodicity, made up of alternate $25km$ steps of fibre, $D_1 = 1.5ps/(nm.km)$ and $D_2 = 0.5ps/(nm.km)$. Collision centre is measured as the distance from the last amplifier.

This shows how some dispersion maps can improve the residual frequency shift due to soliton collisions. Which dispersion maps are best at reducing residual frequency

shift will be addressed in the following chapters. In the course of researching this topic, a large number of combinations of parameters have been tried and several phenomena observed. With this experience, a few features of figure 3.3 can be explained. The phase of the variation in frequency shift in the uniform case does not match that of the amplifier spacing. This is because the most asymmetric collisions are not *centred* on the amplifiers but occur just before them. That is, the most asymmetric energy exchange is achieved when some of the re-separation occurs before amplification. Obviously, for there to be significant asymmetry, a collision has to still be under-way during amplification, so the amount of off-set between collision-centre associated with maximum frequency shift and amplifier position also depends on the length over which collisions occur. Discontinuities in the variation in frequency shift coincide with the discontinuities in the dispersion map, making the curve a composite of two sinusoids like the one in the uniform case.

In practical terms, the relationship between the maximum value of residual frequency shift and collision distance, L_c shows which frequency separations are viable in a WDM system. Figure 3.4 shows that in (a) the uniform dispersion case and (b) where $L_1/L_a = 1/2$ the maximum residual frequency shift is large for values of $L_c/L_{pert} < 2$.

From data similar to that in figure 3.4, Mollenauer et al pointed out that when $L_c/L_{pert} > 2$ the residual frequency shift was negligible and concluded that there was a 'safe' region of operation for WDM where,

$$\frac{L_c}{L_{pert}} = \frac{2\tau}{D\Delta\lambda L_{pert}} \geq 2, \tag{3.32}$$

or, in other words,

$$\Delta\lambda_{max} = \frac{\tau}{DL_{pert}}. \tag{3.33}$$

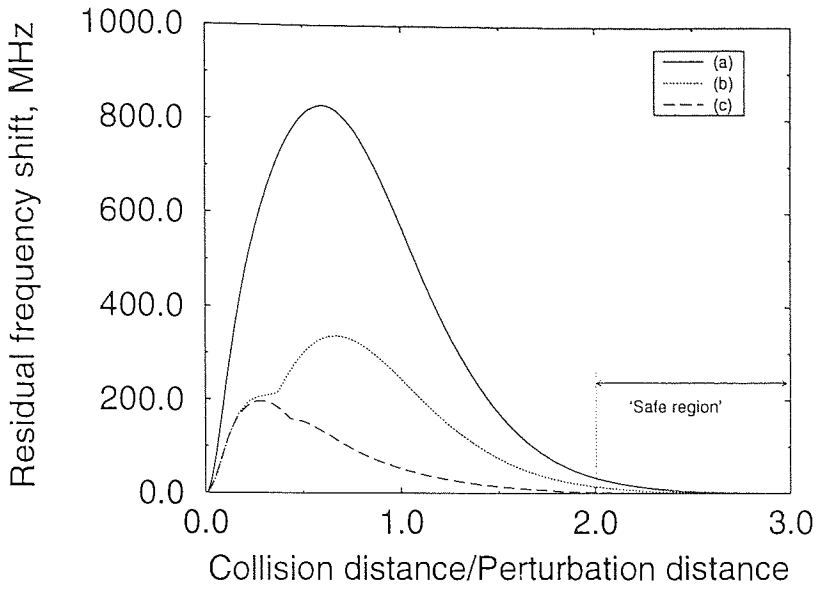

Figure 3.4: Maximum frequency shift against collision length for two solitons, $1.6nm$ apart in fibre with $\alpha = 0.2dB/km$ and $D_{av} = 0.5ps/(nm.km)$. (a) Uniform dispersion, (b) $D_1 - D_2 = 1.0ps/(nm.km)$ and $L_1/L_a = 1/2$, and (c) $D_1 - D_2 = 0.57ps/(nm.km)$ and $L_1/L_a = 17.08km$.

This sets an upper limit to the bandwidth used by a WDM system - for $\tau = 20ps$, $D = 0.5ps/(nm.km)$ and $L_{pert} = 50km$, $\Delta\lambda_{max} = 0.8nm$. One might also conclude that there is a similar region for $L_c/L_{pert} < 0.05$, but this is only allows a narrow set of possible parameters. Lowering the average dispersion or increasing the pulse width would allow a larger wavelength 'window'. However, this is still a fraction of the bandwidth of the erbium-doped fibre amplifier (EDFA). The third line, (c) was for values of D_1, D_2 and L_1/L_a which Forysiak et al [19] showed led to much lower maximum frequency shifts and pushed back the limits on channel separation. How this prescription was arrived at is described below.

A lower limit to separation of channels was predicted [84] to be given by the requirement that pulses not overlap initially. That is,

$$N \leq \frac{T}{\tau}, \tag{3.34}$$

where N is the number of channels, T is the bit period per channel and τ is the pulse width (FWHM). Hence, for a $10Gb/s$ data-rate per channel with $20ps$ pulses, this would limit us to a maximum of 5 channels.

Wai et al demonstrated, in 1996, that it would be collisions at the detector causing frequency shifts which would restrict the minimum channel spacing to four spectral widths (assuming that pulses from every channel arrive at the same time) and that the flatness of gain would restrict the usable bandwidth [88]. In the case of filtered transmission, Golovchenko et al found that the minimum spacing was limited by the free spectral range of the Fabry-Perot filters used [89].

More detailed analysis of the effects of dispersion compensation [18, 19] showed that the residual frequency shift predicted by [84] could be minimised further using stepped profiles which approximated to the exponential decrease in soliton energy between amplifiers.

Chi and Lin [16] attempted to approximate to the exponential decay in soliton power with propagation with a sequence of fibres of equal length. They succeeded in increasing the stability of the solitons propagating in the link, although their work did not consider pulse stability over a sequence of such links. Forysiak et al [17] proposed that the length of component fibres in a step-wise exponential approximation be chosen by minimising the perturbations which occur between amplifiers. This was achieved by minimising the integral of the difference between the step-profile and the exponential profile. Hasegawa, Kumar and Kodama [18] chose their step-lengths by making the steps equal in soliton units, with the intention of minimising collision-induced frequency shift. The Forysiak prescription is the best of the three described here in terms of reducing dispersive radiation from a single soliton *and* residual frequency shift due to collisions between solitons of different wavelengths (as proven experimentally by

Cardinal et al [90]). An even better prescription for approximating to the exponential profile exists however, as described below.

The dispersions of the steps in such a stepped approximation are then given by,

$$\Delta_m = \frac{\Lambda^2}{L_m - L_{m-1}} \int_{L_{m-1}}^{L_m} \exp(-\alpha z) dz, \tag{3.35}$$

where

$$\Lambda^2 = \frac{\alpha L_{pert}}{[1 - \exp(-\alpha L_{pert})]}, \tag{3.36}$$

the average soliton factor, L_m is the distance from the last amplifier to the end of the mth step, and α is the fibre loss.

Combining and minimising eq'n 3.35 and eq'n 3.28 (as developed in [84]) for stepwise dispersion profiles with M sections, such that the fibre dispersion averages to unity [19] gives,

$$\int_0^{L_a} \Delta(z) dz = \sum_{m=1}^{M} \Delta_m (L_m - L_{m-1}) = L_a. \tag{3.37}$$

The components, g_n, are then given by,

$$g_n = \Lambda^2 e^{in\phi_c} \sum_{m=1}^{M} \left(\frac{e^{-(\alpha L_{m-1} + in\phi_{m-1})} - e^{-(\alpha L_m + in\phi_m)}}{\alpha L_a + i2\pi n \Delta_m} \right) \tag{3.38}$$

where,

$$\phi_m = \frac{2\pi}{L_a} \int_0^{L_m} \Delta(z) dz, \tag{3.39}$$

and,

$$\phi_c = \frac{2\pi}{L_a} \int_0^{z_c} \Delta(z) dz, \tag{3.40}$$

where z_c is the position of the collision centre with respect to the amplifiers.

By minimising the components, g_n in eq'n 3.38, Forysiak et al [19] found a two-step

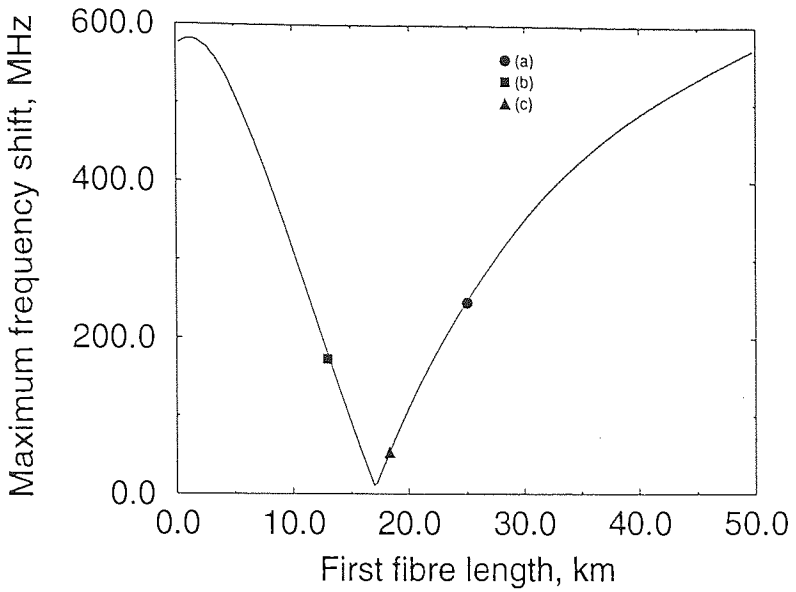

Figure 3.5: Maximum residual frequency shift versus the length of the first fibre step, L_1, in a two-step profile for $L = 50km$, $\alpha = 0.2dB/km$ and $\Delta\lambda = 1.6nm$. Also marked are three previously recommended 2-step dispersion schemes, (a) steps of equal length [16], (b) steps of equal size in soliton units [18] and (c) minimised difference between exponential and stepped profile [17]. After [19].

dispersion profile (fig. 3.5) which gave less maximum residual frequency shift than the three-step approximation with equal steps in soliton units. In doing so, it was shown that a two-step profile could reduce collision-induced frequency shifts to a magnitude comparable with a tapered exponential profile.

In the following chapters, this analysis will be expanded to find new minima in residual frequency shifts. It will then be shown how these minima effect timing jitter of pseudo-random data after transmission.

Chapter 4

Two-Step Profiles - Lossless Analysis of WDM Collisions

4.1 Introduction

It must be remembered that the purpose of any soliton control method is to reduce one or more effects until they are significantly less important than other detrimental effects, or to achieve a given performance level (in terms of bit-error rate, for example). It has been noted [19] that a two-step dispersion profile which mimics the exponential decay of energy between amplifiers reduces collision-induced frequency shift enough that the losses due to splicing more fibre-steps into each link become significant. Any further improvement should therefore be made with a two-step profile.

The expression for collision induced frequency shift derived by Mollenauer et al [84] is not easily analysed, even though it does ignore the effects of four-wave mixing (FWM). In this chapter, in order to get an impression of the effects of dispersion alone and to simplify matters we look at the lossless case. Although it is impossible to manufacture lossless fibre, the conclusions obtained from this analysis are directly applicable

to lossy communication links within the same constraints as the average soliton model where the amplifier spacing is not the same as the periodicity of the dispersion map. Where the amplifier spacing and dispersion map periodicity are identical, the analysis can also be easily adapted. It will then be possible to identify the features of the collision dynamics which are due to the dispersion map and those which are due to loss.

It is then possible to check the limits of the validity of the theory by comparing the results of numerical solutions of the the NLSE. Other problems arise as we move to deeper dispersion maps and a workable approach is decided upon.

4.2 Analytic Theory

Setting the loss, $\alpha = 0$, the expression for the frequency shift in the two-step case becomes,

$$\delta(\frac{\delta f}{2}) = 0.2274 \frac{L_{pert}}{z_0 \tau} \sum_{n=1}^{\infty} Im(g_n) \frac{n^3 x^4}{\sinh^2(nx)} \tag{4.1}$$

as before (in eq'n 3.28), but now the components, g_n, are then given by,

$$\begin{aligned} g_n &= \Lambda^2 e^{(in\phi_c)} \left[\frac{e^{-in(2\pi/L_a)\Delta_1 L_1}}{i2\pi n\Delta_2} - \frac{e^{-in(2\pi/L_a)\Delta_1 L_1}}{i2\pi n\Delta_1} \right] && (4.2) \\ &= \Lambda^2 e^{(in\phi_c)} \left[\frac{(\Delta_1 - \Delta_2) e^{in(2\pi/L_a)L_1\Delta_1}}{i2\pi n\Delta_1\Delta_2} \right] && (4.3) \\ &= \frac{\Delta_2 - \Delta_1}{\pi n\Delta_1\Delta_2} \sin\left(\frac{n\phi_1}{2}\right) \exp\left(in\left(\phi_c - \phi_1/2\right)\right). && (4.4) \end{aligned}$$

where,

$$\phi_c = \frac{2\pi}{L_a} \int_0^{z_c} \Delta(z) dz, \tag{4.5}$$

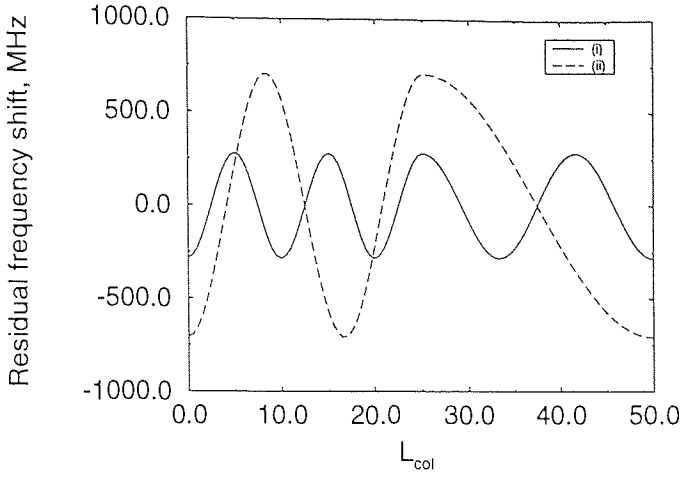

Figure 4.1: Residual frequency shift as a function of collision centre. (i) $\Delta_1 = 5$. (ii) $\Delta_1 = 3$. Other variables; $\alpha = 0$, $D_{av} = 0.5ps/nm/km$, $L_1/L_a = 0.5$.

and,

$$\phi_1 = \frac{2\pi L_1 \Delta_1}{L_a}, \tag{4.6}$$

and $\Delta_{1,2}$ are the local normalised dispersions in the two parts of the profile.

This has a few obvious and easily separated features. The two oscillatory terms are independent of one another. The first, ϕ_c, controls the periodicity of frequency shift with collision centre as in figure 4.1. As the dispersion map deepens the number of cycles in each amplifier spacing increases. Later, it will be shown how this correlates to the number of collisions in any two-soliton interaction.

The second, ϕ_1 produces zeroes in $sin(n\phi_{1/2})$ at values of

$$\Delta_1 L_1/L_a = m, \tag{4.7}$$

where m is an integer, and subsequently there are potential zeroes in residual frequency shift for these values. This can be seen for any value of L_1/L_a by plotting maximum residual frequency shift against Δ_1 as in figure 4.2. When $\Delta_1 = 0$ ($\Delta_2 = 2$) and $\Delta_1 = 2$ ($\Delta_2 = 0$), one might expect g_n to tend to infinity because of the presence of Δ_1 and

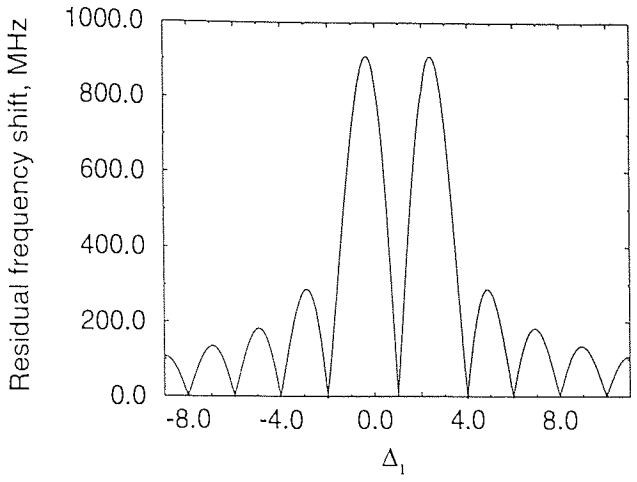

Figure 4.2: Maximum residual frequency shift as a function of first step normalised dispersion. Variables; $\alpha = 0$, $D_{av} = 0.5ps/nm/km$, $L_1/L_a = 1/2$.

Δ_2 in the denominator of eq'n 4.4. However, the equation tends to a finite value, continuous with the rest of the function, as these values are approached. In uniform dispersion, where $\Delta_1 = 1$, there is zero frequency shift because of the $\Delta_1 - \Delta_2$ term in g_n. Physically, this is because the collision in the lossless, uniform dispersion case is always perfectly symmetric in terms of the energy involved in the interaction before and after the collision centre.

Note that a figure such as 4.1 plotted for $\Delta_1 = \cdots, -6.0, -4.0, -2.0, 1.0, 4.0, 6.0, \cdots$ will simply be a line of zero across all possible collision centres, as these values have zero maximum frequency shift.

In order to generalise to any value of L_1/L_a, we can plot maximum frequency shift against the normalised accumulated dispersion in the first segment of fibre, as in figure 4.3 for a range of values of L_1/L_a. Close to $L_1/L_a = 0$ and 1, the values of individual dispersions are very large and, in order to maintain confidence in the values estimated by solving the analytic equation (eq'n 4.1), a large number of components of the sum have to be calculated with great precision. Hence, for speed and accuracy, only the values of $0.05 < L_1/L_a < 0.95$ have been plotted.

Note the line of zero frequency shift associated with uniform dispersion, running

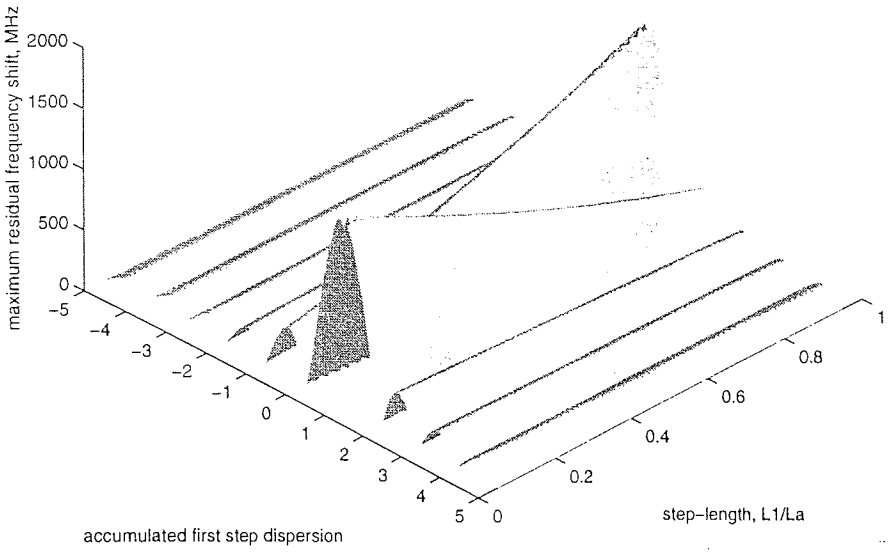

Figure 4.3: Maximum residual frequency shift as a function of normalised first step accumulated dispersion, $\Delta_1 L_1/L_a$ and normalised length of the first step, L_1/L_a. Variables; $\alpha = 0$, $D_{av} = 0.5ps/nm/km$.

between the largest ridges, from where $L_1/L_a = 0$ and accumulated dispersion $= 0$ to where $L_1/L_a = 1$ and accumulated dispersion $= 1$.

Another normalised unit to measure dispersion map depth is

$$A_1 = (\Delta_1 - 1)L_1/L_a \tag{4.8}$$

which has the added benefit of being proportional to the square-root of the energy enhancement factor in [80] for constant pulse width, τ. This is the normalised *excess* first-step dispersion. The zero values of residual frequency shift then occur when,

$$A_1 = m - \frac{L_1}{L_a}. \tag{4.9}$$

The differences between a surface plot of this (figure 4.4) and that for $\Delta_1 L_1/L_a$ are small and A_1 can also be used to predict minima in residual frequency shift. Another

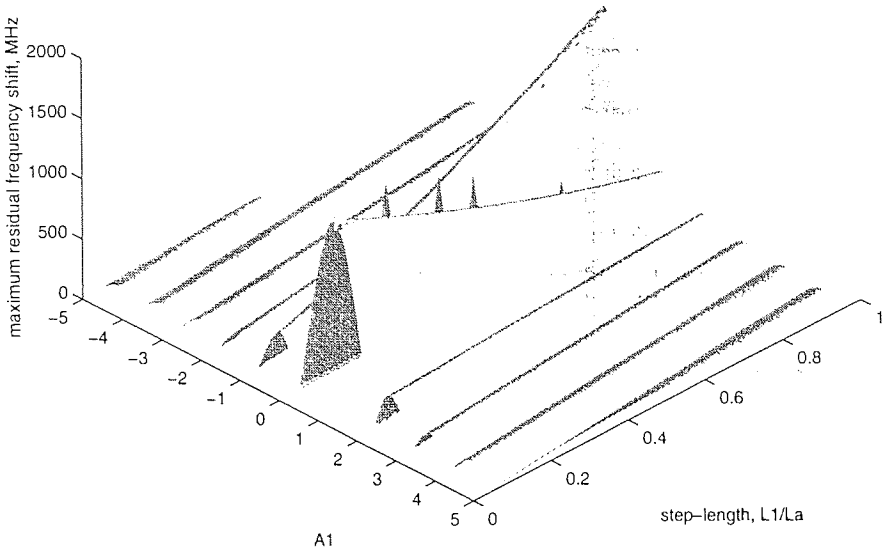

Figure 4.4: Maximum residual frequency shift as a function of accumulated normalised excess first step accumulated dispersion, A_1 and normalised length of the first step, L_1/L_a. Variables; $\alpha = 0$, $D_{av} = 0.5ps/nm/km$. The spikes are spurious results near where $\Delta_{1,2} = 0$ and the summation requires more and more accurate terms.

benefit in using A_1 is that a uniform map (i.e. one where there is only one value of dispersion) corresponds to $A_1 = 0$ for all values of L_1/L_a.

4.3 Testing the Limits of the Adiabatic Theory by Numerical Simulation

4.3.1 Methods

In order to test the limits of the adiabatic theory, we can run a series of numerical simulations of two-soliton collisions. The numerical solution of the NLS equation used is described in Appendix A.

A typical collision is shown in figure 4.5. In order that the results of the simulation are consistent and unambiguous, several criteria have to be upheld. The pulses must

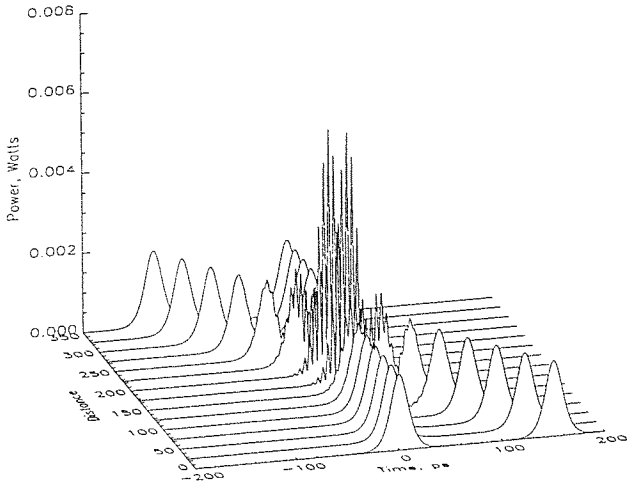

Figure 4.5: Collision between solitons of different centre frequencies. Variables; $\alpha = 0$, $D = 0.5ps/nm/km$, $\tau = 20ps$, frequency separation $\Delta f = 0.2THz$.

be well separated temporally, both at the start of their propagation and at the end. Otherwise, only a partial collision may be observed, giving an incorrect (and usually overly large) value for the residual frequency shift. The solitons must also be spectrally resolvable, so that the frequency shift can be measured accurately.

The frequency separation chosen for simulations in this thesis is $0.2THz$. This is twice the minimum industrial standard [14], hence a practical value. Figure 4.6 shows the spectra of the two solitons shown colliding in figure 4.5. The pulses are $20ps$ FWHM wide and have a bandwidth of $17.5GHz$.

One of the assumptions in formulating the analytic theory [84] is that the pulses are not significantly distorted during propagation. In uniform dispersion, with low loss or no loss at all, this is not an unreasonable assumption. However, as the dispersion map gets deeper, the pulses evolve more dramatically over each dispersion period [80, 91]. Figure 4.7 shows how a soliton in a lossless dispersion map of depth $A_1 = 5$ evolves over one period of the dispersion map. In alternate signs of dispersion the pulse is chirped one way or the other and the pulse 'breathes'.

The theory is also formulated assuming that the pulses are solitons obeying the

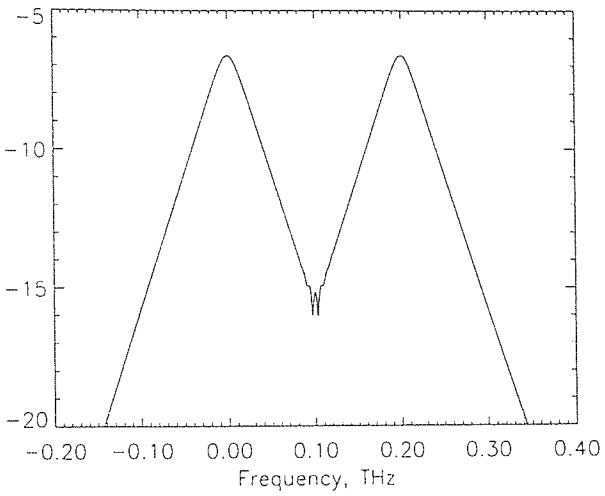

Figure 4.6: Spectra of solitons colliding in figure 4.5. Variables; $\alpha = 0$, $D = 0.5ps/nm/km$.

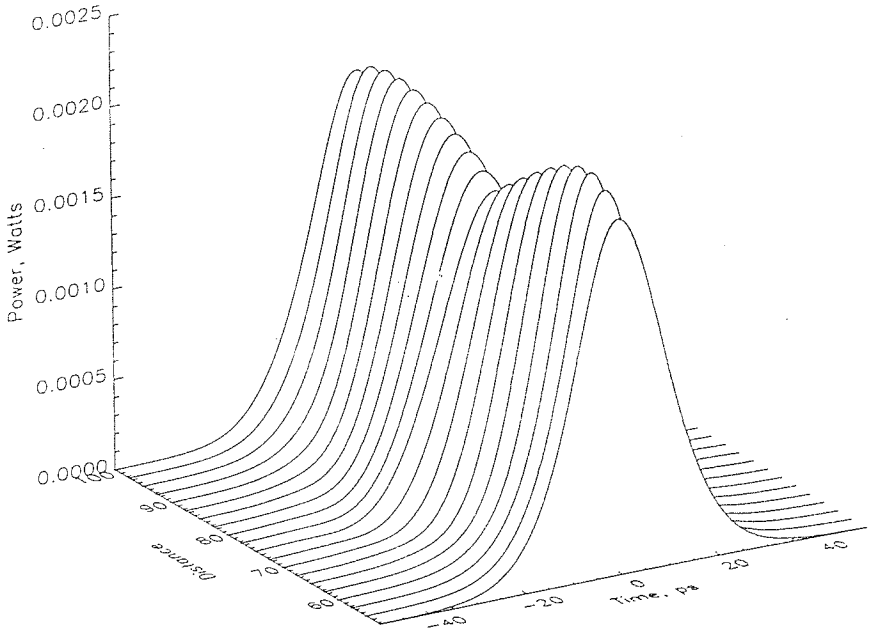

Figure 4.7: Evolution of a soliton over one dispersion period. Variables; $\alpha = 0$, $D_{ave} = 0.5ps/nm/km$, $A_1 = 5$.

soliton energy relationship (eq'n 2.29). As shown by Smith et al [80], the soliton energy relationship is modified by the depth of a dispersion map. The relationship then becomes,

$$E_{sol} = E_0 \left[1 + 0.7 \left(\frac{(\ddot{\beta}_1 - \ddot{\beta}_{av}) l_1 - (\ddot{\beta}_2 - \ddot{\beta}_{av}) l_2}{\tau^2} \right)^2 \right] \quad (4.10)$$

$$= E_0 \left[1 + 0.28 \left(\frac{D_{12} L_a}{\tau^2} \right)^2 \right] \quad (4.11)$$

where D_{12} is the difference between the dispersions of the component fibres in $ps/(nm.km)$. The relationship between D and β is given by equation 2.28 and the wavelength is assumed to be $1.55\mu m$. It will be shown that this expression only holds closely in the lossless case and over a limited range of dispersion depths. In the range of values studied in this section, this equation is sufficiently accurate however.

If eq'n 4.10 is not used, the soliton is not periodically stable, and the residual frequency shift measured will vary with collision centre relative to propagation distance as well as relative to dispersion map period.

4.3.2 Lossless Results

The maximum residual frequency shift is plotted in figure 4.8 for $L_1/L_a = 1/2$ for a range of values of A_1 from -20 to 20 and compared with numerical simulations of the expected worst case (maximum residual shift). Initial conditions (i.e. pulse separation) for the worst possible frequency shift were calculated from simple geometry such that the collision centre occured at an amplifier. As can be seen, the numerical simulations where the enhancement factor has not been incorporated do not agree as well as those where the factor is included for $|A_1| > 1.5$. This is due to their pulses not having enough power for solitons to be maintained. The pulses are therefore broadened when

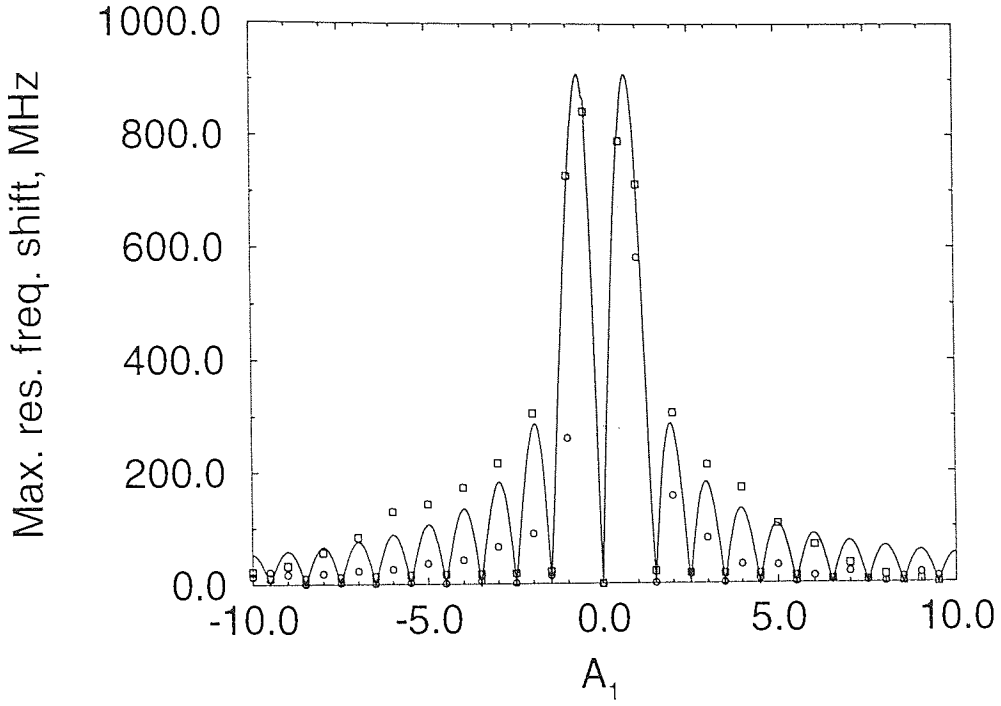

Figure 4.8: Maximum residual frequency shift as a function of accumulated normalised first step dispersion. Variables; $\alpha = 0$, $D_{av} = 0.5ps/nm/km$, $L_1/L_a = 1/2$. The solid line is calculated using the adiabatic theory, the circles are the numerical simulations of un-enhanced solitons and the squares are the numerics of enhanced solitons.

they interact and the frequency shifts are smaller. The longer their propagation before the collision, the lower the residual frequency shift, i.e. these numerical values are for collisions occuring after one particular propagation distance but for non-uniform maps, the shifts will always be less than those predicted by the adiabatic theory. This is the phenomenon exploited in [92] but the scheme proposed is complicated and pulses with sub-soliton powers are best avoided in practice as the SNR will be degraded at the receiver.

The numerical simulations where the enhancement factor is incorporated also stray from the analytic values after $|A_1| > 1.5$. This time, however, the values of maximum residual frequency shift are greater than those predicted by the analytic theory in the range $1.5 < |A_1| < 5.0$ and less than the analytic predictions for $|A_1| > 5.0$.

4.3.3 Interpretation of Results

The analytic theory has been formulated assuming that the pulses are not significantly distorted as they propagate but as the dispersion map used gets deeper, the enhancement factor,

$$a = \frac{E_{sol}}{E_0}, \tag{4.12}$$

increases, as does the amount of breathing which can be quantified by the factor b, given by

$$b = \sqrt{1 + \left(\frac{D_1 L}{\pi L_a D_{ave}}\right)^2}. \tag{4.13}$$

The factors a and b are very useful expressions, derived in [91] by assuming a gaussian form of solution for the NLS in dispersion managed systems,

$$Q(z,t) = a(z) f[t/b(z)] \exp[i\lambda(z) + i\mu(z)t^2] \tag{4.14}$$

(their notation). After inserting this into the Lagrangian form of the NLS, it is possible to derive the form and relationship between a and b. As can be seen, a is the amplitude of the gaussian and b the width.

The frequency shift is proportional to a^2 but the variable x in eq'n 3.22 and eq'n 3.23 increases proportionally with b. The quadratic increase of a dominates for small values of A_1 but the linear increase of b in the simplified relationship,

$$\partial\Omega = a^2 L_{pert} \frac{(bx)^4}{\sinh^2(bx)} \tag{4.15}$$

becomes dominant for larger A_1 - leading to an exponential decrease in maximum residual frequency shift.

The origin of the oscillations and their periodicity can be understood by considering the details of the soliton collisions in periodic dispersion maps. For example, figure 4.9 shows the residual frequency shift calculated as a function of collision centre (analytic) and initial pulse separation (numerical) for the parameters of figure 4.8 and $A_1 = 2.0$ ($\Delta_1 = 5, \Delta_2 = -3$). Good agreement is seen between the two figures with the numerical simulations accurately reflecting the analytic prediction, but with only one cycle in the corresponding period because each point in figure 4.9(b) corresponds to five degenerate points in figure 4.9(a), as identified by the crosses, for one particular initial separation of $526ps$. Note that each degenerate point is of the same phase when the collision occurs in anomalous fibre, and opposite phase when it occurs in normal fibre.

The physical meaning of these degenerate collision centres is clarified in figure 4.10 which plots the zig-zag motion of one soliton in the time frame of the other, for the case discussed above. Each pulse centre crossing seen in figure 4.10 at $571km$, $582km$, $612km$, $648km$, and $652km$ corresponds to one of the five marked, degenerate points marked in figure 4.9(a).

Figure 4.11 shows the relative motion of the solitons at the next maximum of figure 4.8, for $A_1 = 3.0$, and the same initial pulse separation. The geometry of the overall collision is very similar, to the one above, but with two additional pulse crossings, due to the increased amplitude of the zig-zags.

In general, as $|A_1|$ increases, the amplitude of the zig-zags increases, as does the total number of crossings (for symmetric maps it is approximately $2|A_1|$). Consequently, the component crossings become faster, more evenly distributed throughout the gain/loss cycle, and their sum effect is closer to zero. Thus, each of the oscillations in figures 4.4 and 4.8 corresponds to an increased number of fast crossings (determined by the large local dispersions) within each slower overall interaction (determined by the low

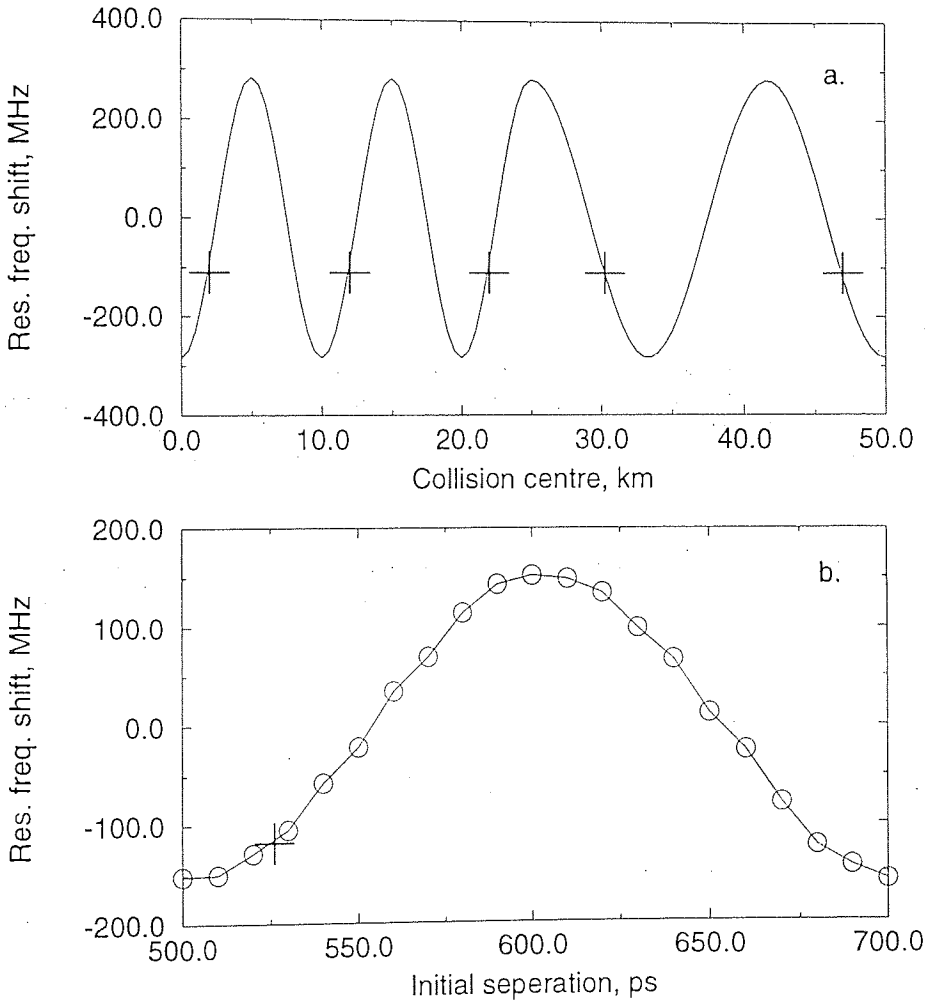

Figure 4.9: (a) Residual frequency shift against collision centre (analytic theory). (b) Residual frequency shift against initial pulse separation (numeric simulation). Both over the same corresponding period. Variables; $\alpha = 0$, $D_{av} = 0.5ps/nm/km$, $A_1 = 2.0$ and $L_1/L_a = 1/2$, $\tau = 20ps$.

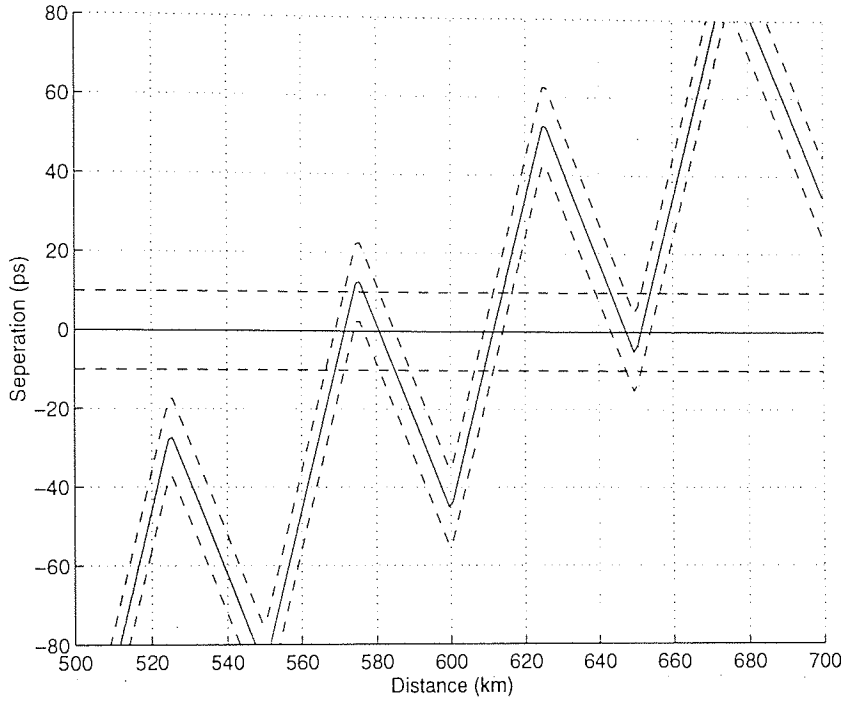

Figure 4.10: Collision mechanism for $\alpha = 0$, $D_{av} = 0.5ps/nm/km$, $A_1 = 2.0$ and $L_1/L_a = 1/2$. Solid lines show the position of the pulse centres, dotted lines show the position of the FWHM points of the pulses.

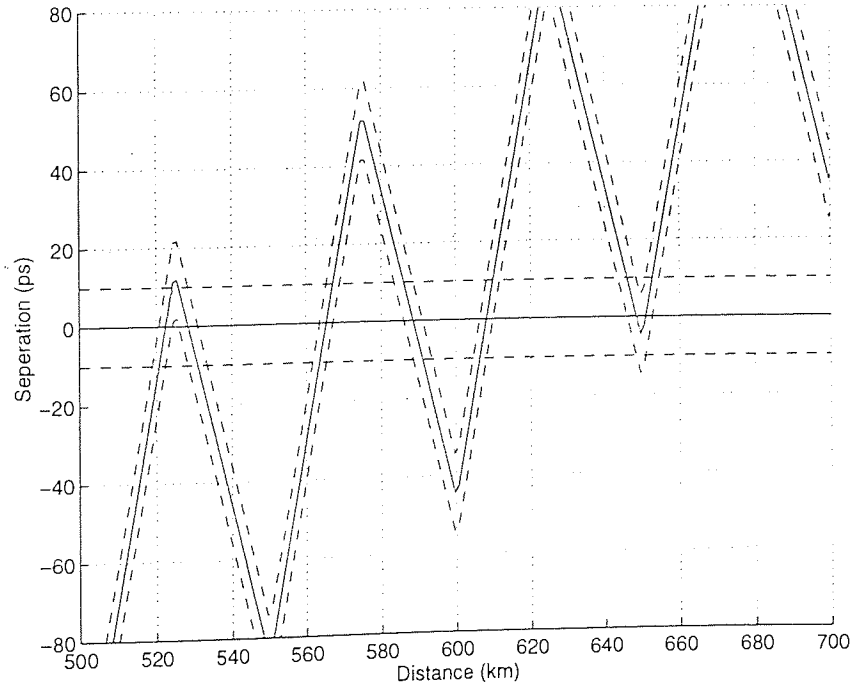

Figure 4.11: Collision mechanism for $\alpha = 0$, $D_{av} = 0.5ps/nm/km$, $A_1 = 3.0$ and $L_1/L_a = 1/2$.

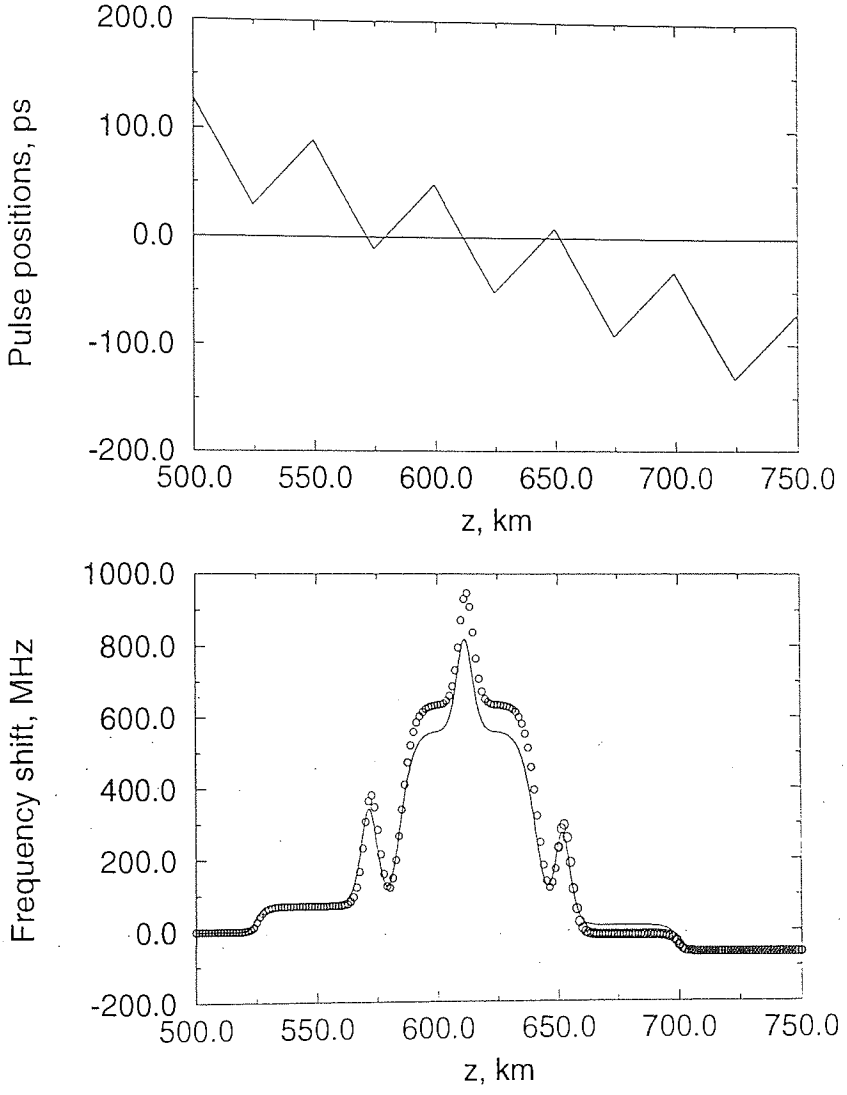

Figure 4.12: Collision mechanism and evolution of frequency shift for $\alpha = 0$, $D_{av} = 0.5ps/nm/km$, $A_1 = 2.0$ and $L_1/L_a = 1/2$. Solid line in the frequency shift diagram from the adiabatic theory, dots found by numerical simulation.

average dispersion).

Further clarification is achieved by plotting the frequency shift of one soliton during a single interaction as in fig 4.12. The net effect of any complete collision is seen to be close to zero but partial collisions cause relatively large frequency shifts. It is also possible to see how the adiabatic theory strays from agreement with numerical simulation, as explained in section 4.3.2.

At this value of A_1, the interactions are stronger than predicted by the adiabatic theory, due to the enhanced power of the solitons. However, the residual frequency shift

is not considerably greater in the numerical simulations as the differences between the positive and negative shifts almost cancel out.

Note that there is also a residual temporal shift given by integrating across the frequency shift. Experience has shown that this is always very small compared to the temporal shifts that build up afterwards but is also reduced by the deeper dispersion maps.

4.4 Conclusions

The adiabatic theory developed in chapter 3 has been shown to accurately predict the collision-induced frequency shift due to two-soliton collisions over a range of dispersion map depths. The limitations of the theory have been explained - primarily that predictions will be increasingly over-estimated with increasing dispersion map depth. The adiabatic theory can be used to give a good idea of the collision-induced shifts for $|\Delta_1| < 7$, for the parameters studied ($D_{ave} = 0.5ps/(nm.km)$ and $\tau = 20ps$).

Both the theory and numerical simulations show that there are dispersion maps for which there is no residual frequency shift due to soliton collisions. As the dispersion maps get deeper, interactions between solitons of different wavelengths are composed of more and more small collisions. At the minima, the component collisions cause residual frequency shifts which are opposite in sign but equal in magnitude in either half of the interaction, leaving a net residual frequency shift of zero.

Chapter 5

Analysis and Numerical Investigation of Soliton Collisions with Loss

5.1 Introduction

The previous chapter addressed the limitations of the adiabatic theory when loss is disregarded. This allowed us to determine what effects were due to the dispersion profile alone.

However, lossless fibre is not achievable. It will be shown that the effect of loss is only significant over a small range of values of possible dispersion maps. Again, the adiabatic theory will be shown to be accurate over a significant range of depths of profile (up to map depths of $|A_1| \approx 5$).

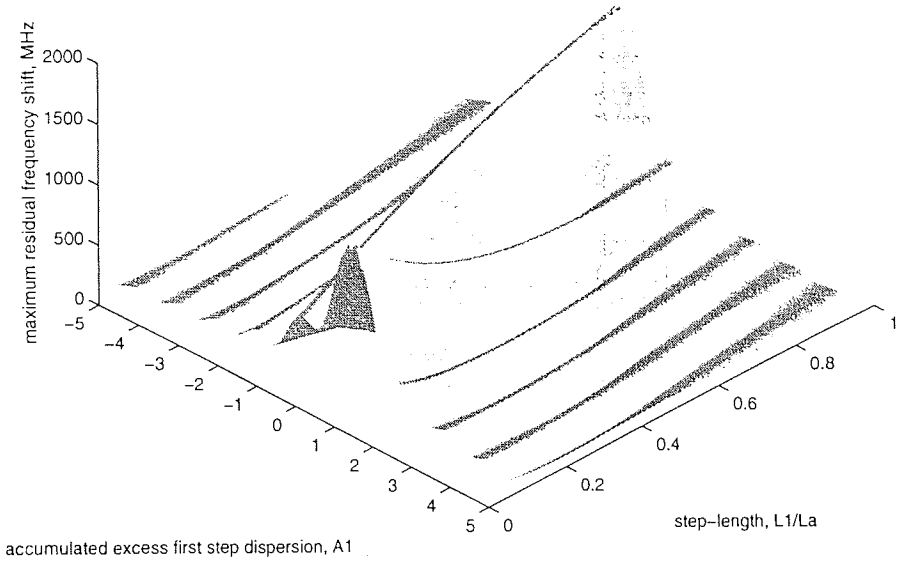

Figure 5.1: Residual frequency shifts against A_1, the accumulated normalised dispersion of the first step of the dispersion profile and L_1/L_a for $\alpha = 0.2dB/km$, $D_{av} = 0.5ps/nm/km$.

5.2 The Effect of Loss on the Adiabatic Theory

Figure 5.1 is figure 4.4 re-drawn incorporating loss, with amplifiers located once every dispersion-map period ($L_{amp} = L_{pert}$). It can be seen that the realistic value of α used ($0.2dB/km$) has little effect on the overall surface plot and the incidence of minima. The minima can now be picked out in a contour plot such as figure 5.2. One easily noticeable effect is that the line of minima which corresponded to uniform dispersion in the lossless case has shifted to closely follow the exponential rule of equation 3.35 recommended in [90, 93, 19]. This rule is the curved line running from top to bottom through the figure. This and all the other 'valleys' of minima are no longer zero at any point and no longer follow a straight line.

Three of these minima were highlighted by [94]; one closely corresponding to the exponential taper and the next two profiles where anomalous dispersion is compensated by approximately the same length of normal dispersion. In figure 5.2 it is also possible

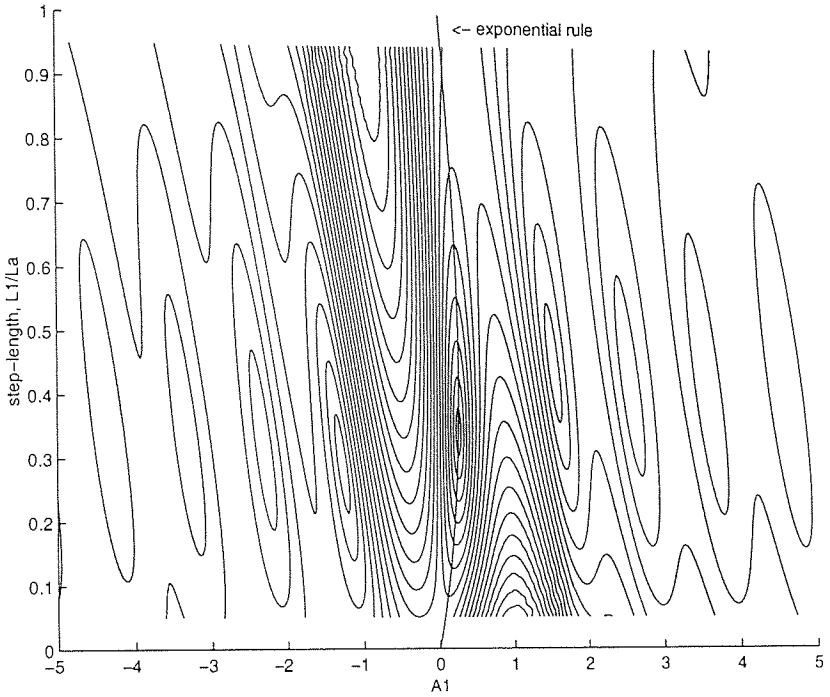

Figure 5.2: Maximum residual frequency shifts against $A_1 = (\Delta_1 - 1)L_1/L_a$, the dispersion depth and L_1/L_a for $\alpha = 0.2dB/km$, $D_{av} = 0.5ps/nm/km$.

to see that these are only part of a family of minima with both A_1 positive and negative.

From figure 5.3 and table 5.1 it can be seen that normal dispersion fibre followed by anomalous dispersion between amplifiers (i.e., where Δ_1 is less than Δ_2) can be as effective in reducing collision-induced frequency shifts as when A_1 is positive.

Figure 5.4 compares the maximum residual frequency shifts for a series of loss characteristics in the fibre. The addition of realistic loss ($0.2dB/km$) makes very

Description	A_1	L_1/L_a	L_1 (km)	Maximum Residual Shift (MHz)
$\sim$ exponential rule	0.2643	0.342	17.078	7.73
$2nd + ve$	1.5321	0.444	22.214	0.92
$3rd + ve$	2.575	0.412	20.62	0.39
$4th + ve$	3.592	0.399	19.95	0.22
$5th + ve$	4.601	0.392	19.59	0.16
$1st - ve$	-1.274	0.291	14.56	0.87
$2nd - ve$	-2.311	0.322	16.09	0.36
$3rd - ve$	-3.327	0.335	16.74	0.19
$4th - ve$	-4.336	0.342	17.09	0.12

Table 5.1: Positions and values of minima in maximum residual frequency shift for $\alpha = 0.2dB/km$, $D_{av} = 0.5ps/nm/km$.

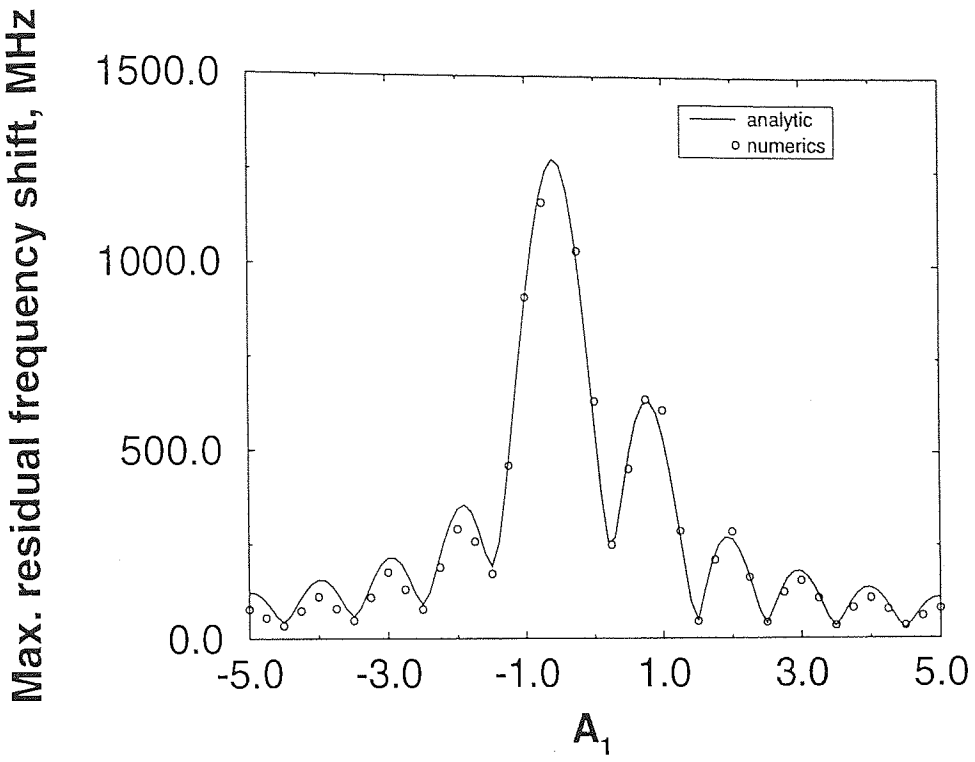

Figure 5.3: Maximum residual frequency shifts against A_1, the normalised accumulated dispersion for $L_1/L_a = 1/2$, $\alpha = 0.2dB/km$, $D_{av} = 0.5ps/nm/km$.

little difference above $A_1 = 2.5$, dispersion becoming the dominant influence. When $\alpha = 0.6dB/km$, perhaps the highest value of loss one might expect to find in single-mode fibre, there is very little variation from the 'inverse law' envelope and there is a very large penalty for slightly negative A_1. That is, there is a general trend for maximum residual frequency shift to reduce as the inverse of A_1 and as α increases, deviation from this rule becomes less and less noticeable.

The universal nature of the constant, A_1 can be seen in figure 5.5. Increasing the amplifier spacing increases the maximum residual frequency shift but does not change the incidence of minima with A_1.

As observed by other researchers [95], loss can lead to a change in the amount of power enhancement needed for stable propagation. When the periodicity of the amplification and loss is the same as the periodicity of the dispersion map, and the amplifiers are located at the transition from one type of fibre to another, as they are here, the power enhancement always decreases. No rule has been formulated for

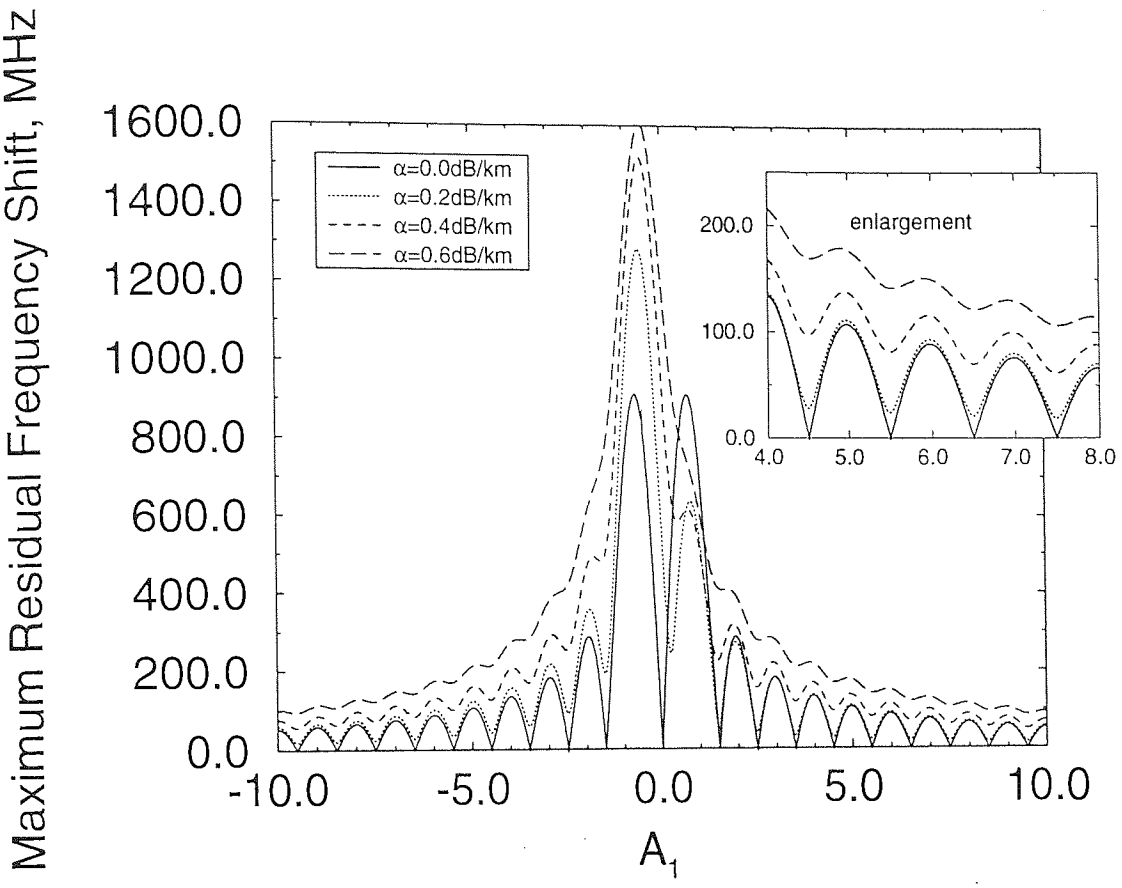

Figure 5.4: Maximum residual frequency shifts against A_1, the normalised accumulated dispersion for $L_1/L_a = 1/2$ and $D_{av} = 0.5ps/nm/km$ for a range of values of α.

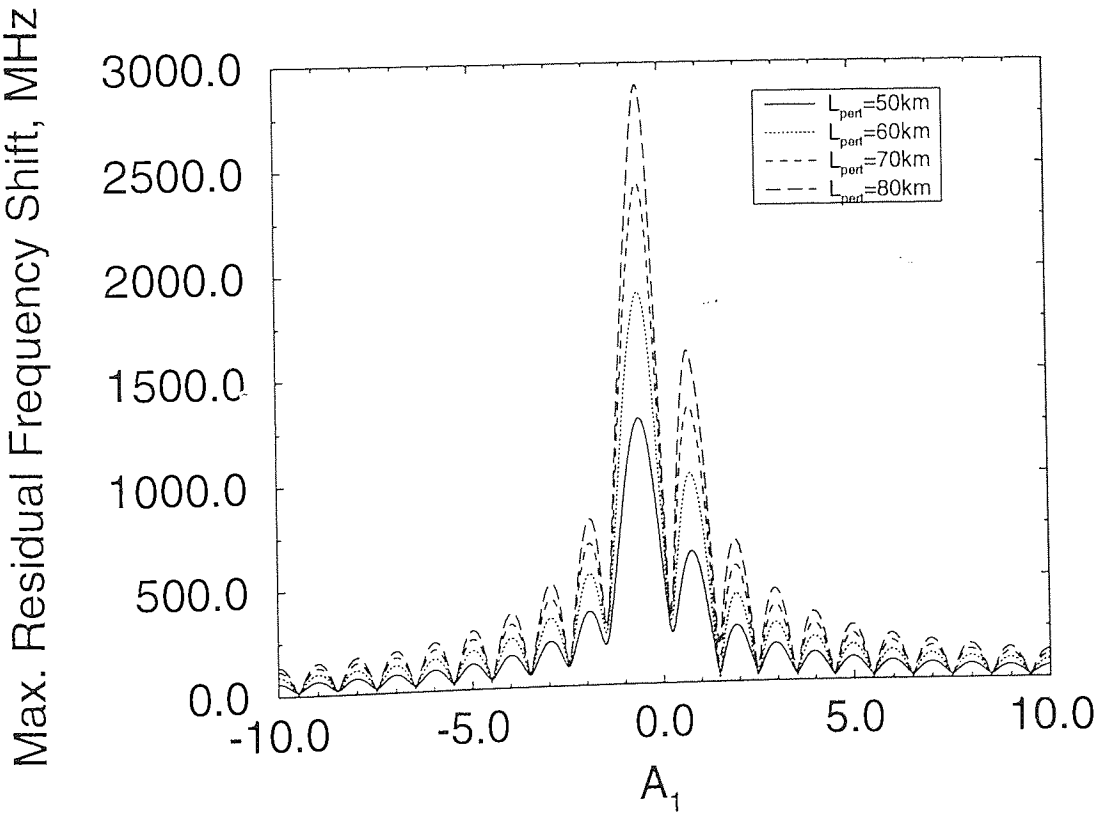

Figure 5.5: Maximum residual frequency shifts against A_1, the normalised accumulated dispersion for $L_1/L_a = 1/2$, $\alpha = 0.2dB/km$ and $D_{av} = 0.5ps/nm/km$ for a range of values of L_{pert}.

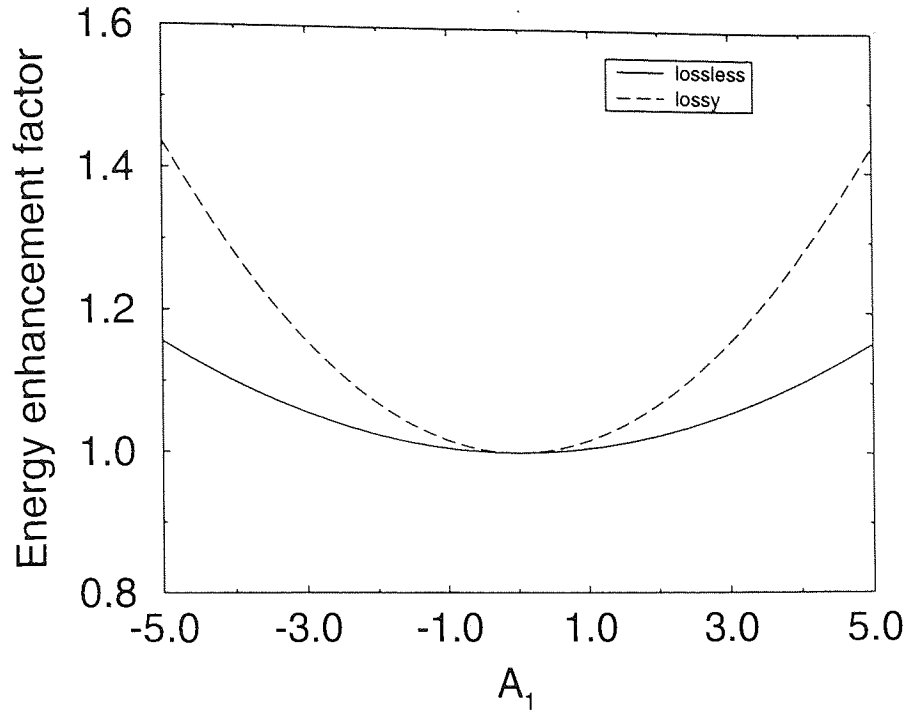

Figure 5.6: Enhancement factor against dispersion map depth for $L_a = 1/2$ and $\alpha = 0.2dB/km$.

predicting the amount of enhancement needed when loss is present but in general the amount of enhancement decreases with the total amount of loss between amplifiers, i.e. as the amplifier spacing or rate of loss in the fibres increases.

The power levels used in these simulations were arrived at by trying a range of input powers and iterating towards the most stable value for a single soliton in the deepest dispersion map used ($A_1 = 5.0$). The form of equation 4.10 remains valid and was used with a reduced value for the enhancement proportionality constant. It was found that for these simulations, with loss $\alpha = 0.2dB/km$ and amplifier spacing $L_a = 50km$, the proportionality constant was reduced in equation 4.11 from 0.28 to 0.10 leading to the enhancement factor dependency illustrated in figure 5.6

The good agreement between numerical simulation and adiabatic theory in figure 5.3 can be explained by this adjustment in the enhancement factor. In the lossless case (figure 4.8), between $|A_1| = 1.5$ and $|A_1| = 5.0$, the numerically simulated results are greater than the analytic predictions. In the lossy case, however, the enhancement

factor is reduced and so is the amount of collision-induced frequency shift, bringing it closer to the adiabatic prediction.

5.3 WDM Data Propagation in Two-Step Dispersion Profiles

5.3.1 Introduction - the Problems

In light of the discrepancies between numerical simulations and the adiabatic theory, it might be asked whether the adiabatic analysis tells us anything of any interest in design of a practical WDM system. In addition, what about the effects of multiple collisions in real data propagation? Single collisions never occur in isolation - a random number of complete and incomplete collisions are going to occur over any transmission distance.

Complicating the picture further are the effects of third-order (and higher-order) dispersion, Gordon-Haus jitter and pseudo-phase-matched four-wave mixing. These will be addressed in the following chapters and shown to be either compensatable or insignificant in real systems.

Some analysis has been made of three soliton collisions [96, 97]. This is complex enough without trying to generalise to the sum effect of the hundreds of collisions and partial collisions in multi-channel propagation which we are interested in.

Figure 5.7 shows three examples of sequences of solitons in one data channel. The first, *a.* is a series of 'ones', or 'clock pulses' for reference. Secondly, *b.* is a pseudo-random data-stream. No attempt is made to restrict the number of consecutive ones or zeros. Lastly, *c.* is an example of a coding system which ensures that there are no consecutive zeros. In this instance, this is simply the sequence in *b.* interleaved with a

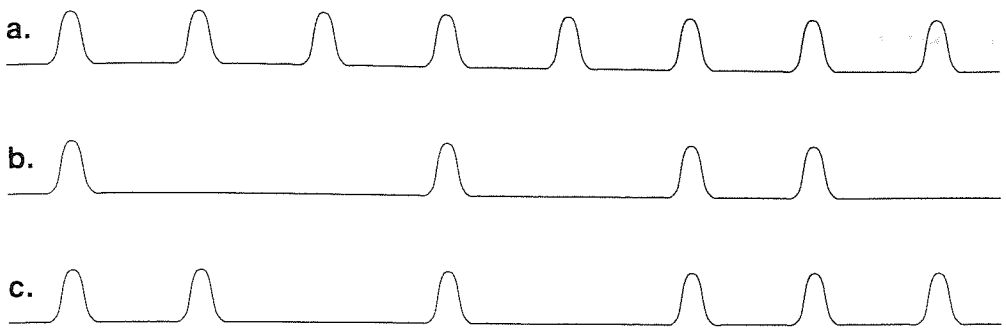

Figure 5.7: Examples of possible bit-streams; *a.*, clock pulses, *b.*, pseudo-random data and *c.*, no consecutive zeros.

clock-stream.

Analytic Method of Estimating Timing Jitter Levels

It is possible to make an estimate of the amount of collision-induced timing jitter in a dispersion managed system by amalgamating the theory used previously with the analysis of data-dependent timing jitter made by Jenkins et al [98].

The variance in timing shift ($\langle \Delta t^2 \rangle_p$) for the pth channel is given by summing over the effects on that channel caused by collisions with each of the other N channels, i.e.,

$$\langle \Delta t^2 \rangle_p \approx \sum_{q=1, q \neq p}^{N} \left(\frac{T}{\Lambda_{pq}} \right)^2 \left(\frac{L}{Z_c^{pq}} \right)^3 \frac{\langle \Delta \lambda^2 \rangle_{pq}}{6}, \tag{5.1}$$

where T is the bit period, Λ_{pq} is the wavelength separation between channels p and q, L is the system length, Z_c^{pq} is the distance travelled between collisions,

$$Z_c^{pq} = \frac{T}{\bar{D}_{pq} \Lambda_{pq}}, \tag{5.2}$$

($\bar{D}_{pq}$ is the average dispersion between channel p and channel q), and $\langle \Delta \lambda^2 \rangle_{pq}$ is the variance in wavelength between channels p and q.

An estimate of $\langle \Delta \lambda^2 \rangle_{pq}$ can be made by calculating the maximum residual fre-

quency shift by the methods described earlier and assuming that the variation of $\Delta\lambda$ is sinusoidal with collision centre. Hence,

$$\langle \Delta\lambda^2 \rangle_{pq} = \frac{(\Delta\lambda_{max}^{pq})^2}{\sqrt{2}}. \tag{5.3}$$

This method can be used to indicate possible optima in terms of dispersion depth and channel allocation but the number of assumptions and approximations made mean that its accuracy is limited, particularly in deeper dispersion maps where the adiabatic theory has been shown to give over-estimates of collision-induced frequency shift and interaction distances become significant compared to propagation distance. In all instances, numerical simulations should be used to confirm predictions made.

Numerical Method of Calculating Accumulated Timing Jitter or Q-factor

The number of consecutive zeroes (ρ) in a the data-stream directly influences the amount of collision induced frequency shift [98], with the possibility for large shifts growing with ρ. All the data simulations in this thesis were performed using a pseudo-random bit sequence as the worst possible scenario. The NLS code uses a temporal window which 'wraps round' with periodic boundary conditions. This means that if a pulse 'walks off' out of the temporal window allocated, it will reappear at the opposite end of the window. As such, if the window is filled with a pseudo-random bit-stream comprising 16 bits, this will propagate as an infinitely repeated $16-bit$ sequence. Each simulation in this thesis is comprised of at least six runs with different pseudo-random, $16-bit$ sequences in each channel. One other consequence of this is that the maximum meaningful number of consecutive zeroes is 15.

The decision to use six runs of $16-bits$ per channel was made in order to have

approximately 100 'ones' and 'zeros' in each evaluation of Q or timing jitter. It was found, by iteration, that a reliable value for Q or timing jitter could be obtained with more than approximately 60 'ones' and 'zeros'. $16 - bit$ sequences were chosen to give a balance between the need for a reasonable number of permutations of consecutive 'ones' and 'zeros', the size of the window needed and the time taken to perform the simulations.

In addition, in the presence of third-order dispersion, either the pulse width or the pulse amplitude must be modified to stay in agreement with equation 2.29. Simulations were performed by either keeping the energy level in each channel the same and varying the pulse widths or keeping the pulse width constant and varying the pulse energies. If the average dispersion characteristics of a transmission system are as shown in figure 5.8 then the soliton energy conditions (eq'n 2.29) for λ_1 and λ_2 can be set equal to one another giving the pulse width or the equation can be re-arranged in terms of pulse width to give,

$$\tau_0 = \frac{2|\beta_2|A_{eff}c}{n_2\omega_0}\frac{1.76}{E_s}, \tag{5.4}$$

and solved to give the required energy in each channel for a given pulse width, τ_0.

If the soliton conditions have been calculated for λ_1, with dispersion D_1 and pulse width τ_1 then the pulse width at λ_2 is given by,

$$\tau_2 = \frac{D_2\tau_1}{D_1}. \tag{5.5}$$

Figure 5.9 shows a typical eye-diagram composed of 96 ones (solitons) and zeros after propagation. The parameters used to calculate Q-factor and timing jitter are marked. The detector parameters chosen were an optical filter bandwidth of $20GHz$, to separate the channels and an electrical bandwidth of $10GHz$, to reflect the response

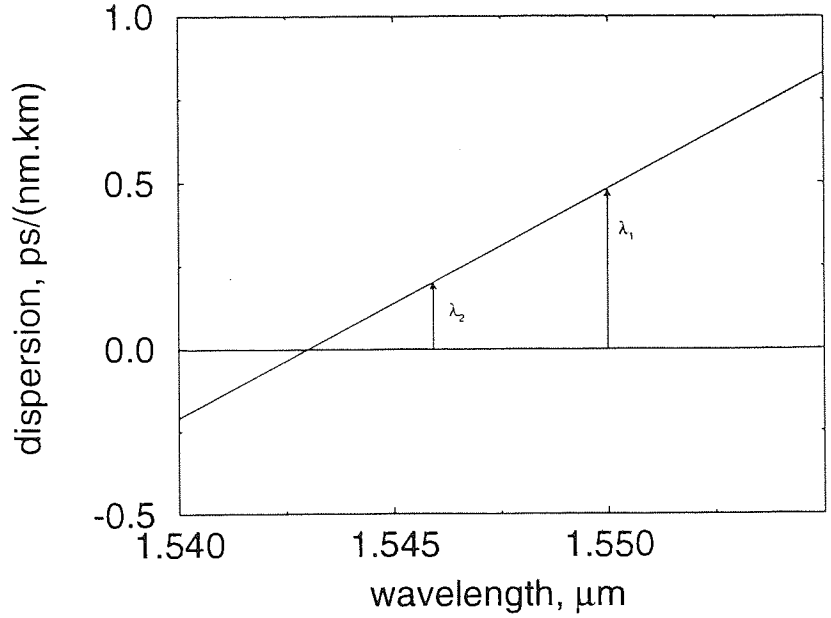

Figure 5.8: Typical average dispersion characteristics showing the different (second-order) dispersions for two wavelengths.

of a typical photo-diode. These values were used in all calculations in this thesis.

Q-factor is calculated as,

$$\frac{\sigma_1 + \sigma_0}{\mu_1 - \mu_0}, \tag{5.6}$$

where $\sigma_{1,0}$ and $\mu_{1,0}$ are the variances and mean values of the power levels of the 'ones' and 'zeroes' respectively at the middle of the pulses' expected time window. This effectively gives a measure of eye-closure.

In principle, timing jitter is calculating by taking the variance of the points sampled on one side of the pulse within the power window, P_w, at the power level, P_m, where P_w is infinitesimally small and P_m is the level of the centre of the eye. In this thesis P_w was chosen to give enough points for a reasonable variance (about 50) and P_m was chosen as either the half-maximum or the steepest part of the slope (almost the same when there is no amplitude noise).

Both numerical methods mimic the method used by a sampling oscilloscope in the laboratory in calculating Qs and jitters.

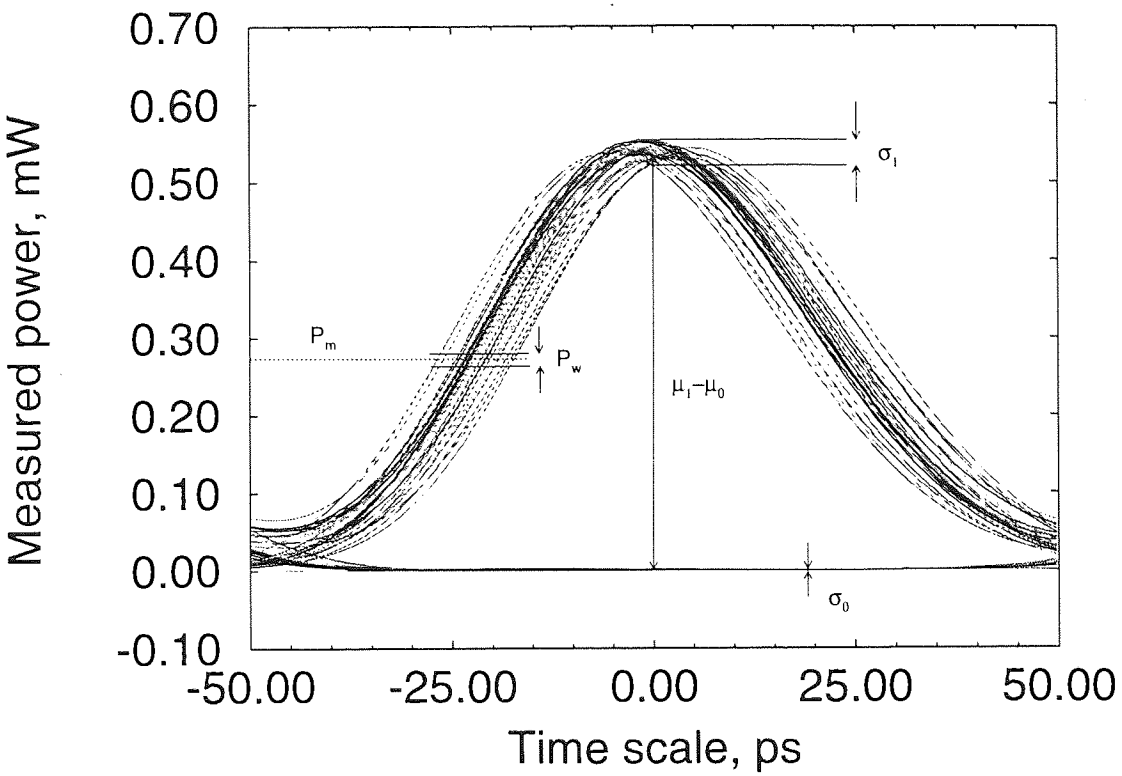

Figure 5.9: Typical numerically simulated eye-diagram. This was for $10Gbit/s$, two-channel propagation after $1000km$.

Also, note that values of Q and jitter do not decline smoothly with propagation. Since all the channels in these simulations have the same data-rate, if a single soliton collision occurs at a point of detection then it is very likely that a significant number of other collisions will also occur there. Where there are collisions, the solitons involved will be temporally displaced from their expected arrival times and the Q values and jitter will suffer.

Another problem in showing how data degrades with propagation is the validity of the measure used. Figure 5.10 shows how, as often happens at high data-rates, the detector cannot distinguish between neighbouring pulses (due to the response time of the photo-diode and the pulses moving out of their allocated time-slots) whilst the amplitude at the time-window centre is not significantly changed. The result of this is that a Q measurement still gives an 'acceptable' value although the data content is lost.

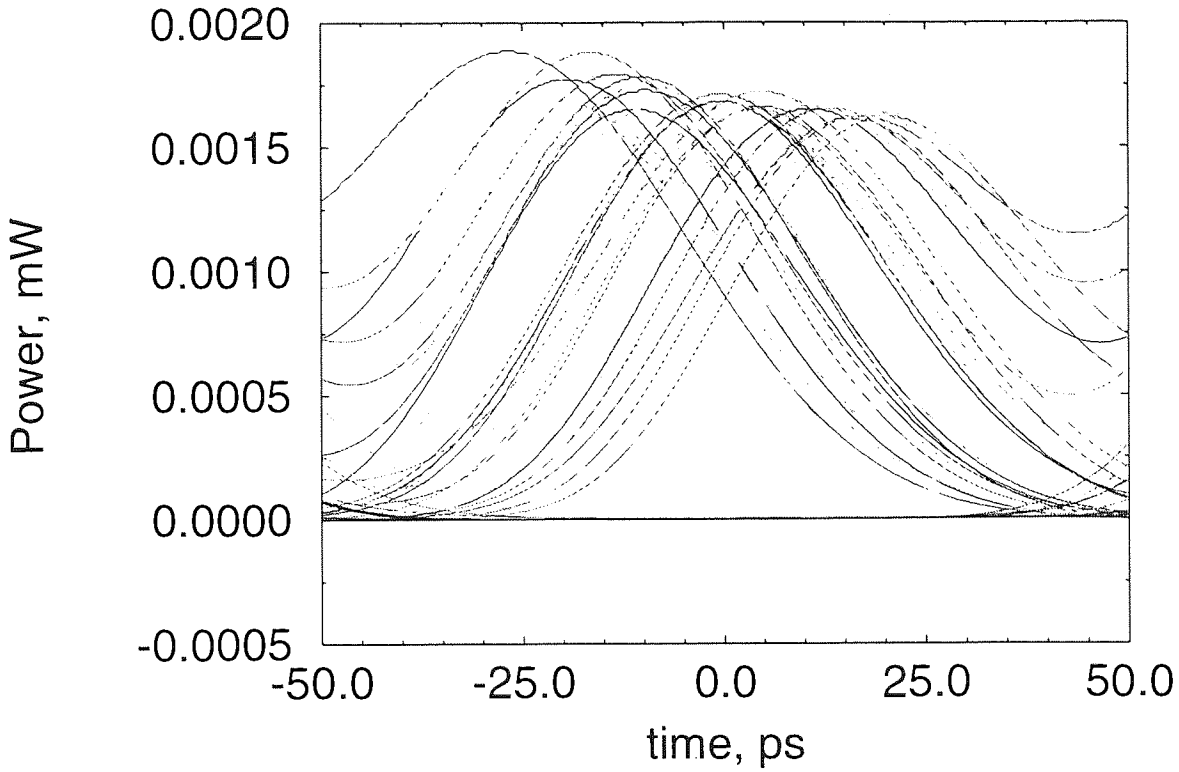

Figure 5.10: Typical numerically simulated eye-diagram after data has been lost. This was for $10Gbit/s$, two-channel propagation after $4000km$.

Also, this definition of Q (or 'amplitude Q') assumes a gaussian distribution of amplitude noise. Collision induced frequency shift leads, primarily, to timing jitter and does not effect the amplitude of the pulses.

For these reasons, jitter measurements are used most often as a measure of the quality of the signal received.

5.3.2 Two and Four-Channel Propagation With No Third-Order Dispersion

In order to isolate the effects of third-order dispersion and inter-channel interaction from pulse interaction within a single channel, $10Gbit/s$ pseudo-random data was transmitted over $4000km$ and the increase in jitter measured. Over values of A_1 from 0.0 (uniform) to 10.0 and z beyond $4000km$ with an average dispersion of $0.5ps/nm/km$,

the data was not found to degrade significantly. Timing jitter remained below $1ps$. This range of values of A_1 was chosen because, beyond $|A_1| = 10.0$, stable pulses would have required a more gaussian profile and more attention to matching the 'breathing' cycle of the dispersion map.

Hence, any significant degradation in Q value or jitter can be attributed to the effects of soliton collisions and, later, to complications arising from third-order dispersion.

In each of the following simulations, the pulses are initially interleaved in order to minimise residual frequency shifts due to partial collisions. In the two channel cases, this means that pulses are spaced $50ps$ apart. In the four channel cases, they are $25ps$ apart. Again, each simulation uses a 'half-step' of fibre at the beginning of of propagation.

Simulation of Two-Channel Propagation

The simplest case of WDM data transmission is that of two channels. At any one time, assuming the pulses have not been badly perturbed already, only two solitons can be in a collision at one time (although, in deeper maps, more than two solitons can be involved in an interaction at any time).

Figure 5.11 shows how jitter levels rise with distance propagated across a range of dispersion maps of $-5.0 < A_1 < 5.0$. The jitter limit for data in a $10Gbit/s$ channel is $8.2ps$ (from [42]). In uniform fibre, this limit is reached before $3000km$. Where the maximum residual frequency shift is highest (A_1 slightly negative), the limit is reached within $2000km$.

Comparison with the single-collision plot of maximum residual frequency shift (figure 5.3) shows a good correlation between residual frequency shift and the accumulation

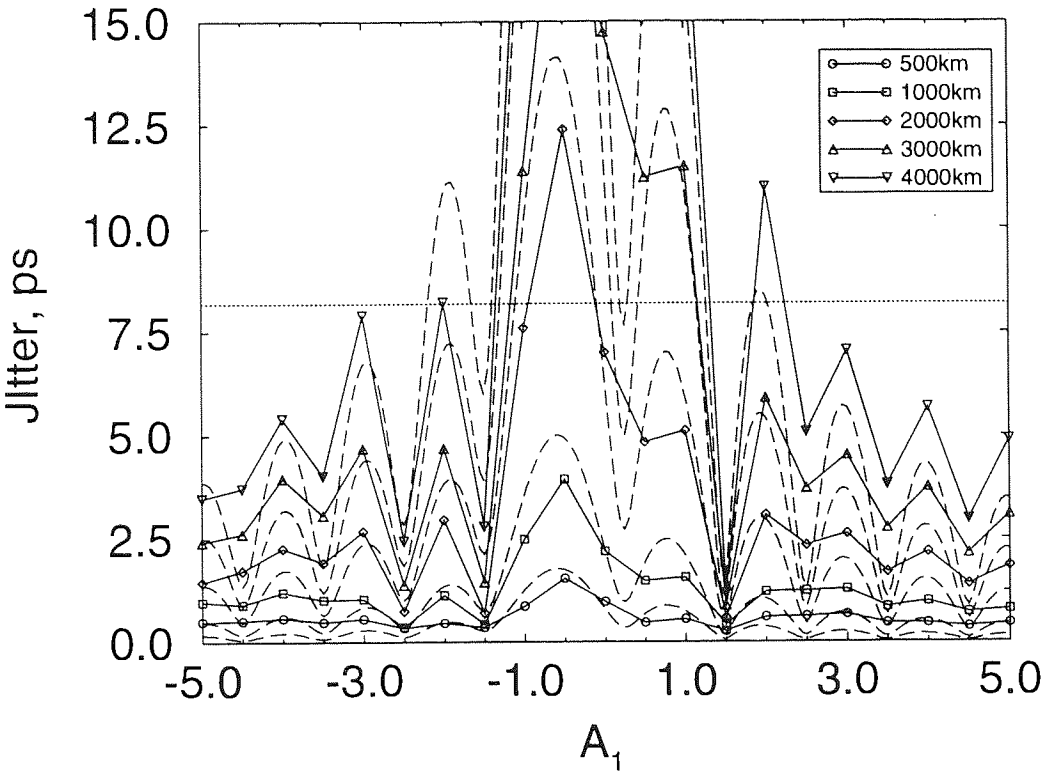

Figure 5.11: Evolution of timing jitter for two $10Gbit/s$ WDM channels over a range of values for A_1. The three dashed lines are the analytic predictions for $500km$, $2000km$ and $4000km$.

of jitter. In interpreting this data, the number of solitons interacting at any time, the timing and frequency shifts during an interaction as well as the maximum residual frequency shift have to be taken into consideration.

For $-1.5 < A_1 < 1.5$, timing jitter increases dramatically with distance. This corresponds to both large timing shifts during interactions and large residual frequency shifts. Also, with $L_{coll} > 5km$, locally, the chances of data detection taking place while a collision is underway are quite high. Hence, the timing jitter for uniform and shallow dispersion maps rises very quickly - disproportionately compared to the expected residual frequency shift. Also of note is how poor the quality of data propagated in the nearest to 'exponential rule' profile (first positive minimum) is compared to the deeper profiles. This would suggest that, although better than the uniform case, this sort of profile is not highly profitable for improving WDM transmission in comparison with

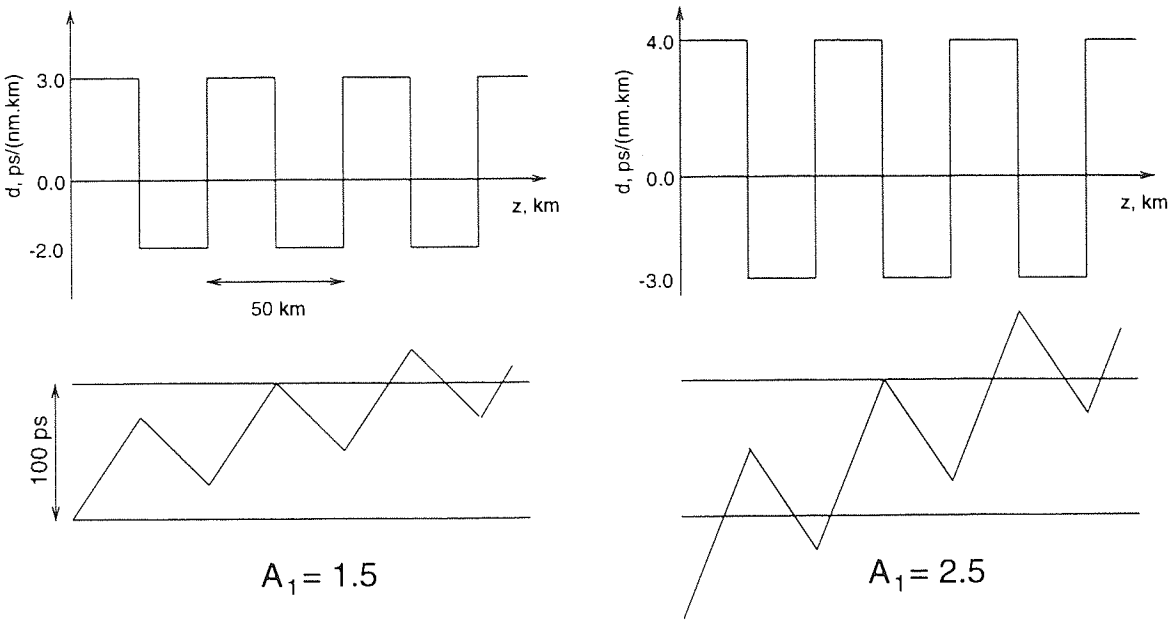

Figure 5.12: Collision mechanism for $A_1 = 1.5$ and 2.5 and two $10Gbit/s$ per channels.

deeper profiles.

Three excellent minima can be observed at $A_1 = -2.5, -1.5$, and 1.5. These may offer the optimum design parameters, particularly $A_1 = 1.5$. These maps correspond to collision mechanisms where there are only a few collisions in any interaction, much reduced residual frequency shifts from the smaller values of A_1 and also smaller temporal shifts during interactions. Perhaps most significantly, at $10Gbit/s$, solitons will only interact with one soliton of the other channel at a time within $-2.0 < A_1 < 2.0$. In deeper dispersion maps, a more complex interaction will take place, involving 4, 6. etc. solitons. The collision mechanism for $A_1 = 1.5, 2.5$ is shown in figure 5.12.

The component collisions in deeper dispersions cause much smaller shifts in the temporal position of the pulses. The result is that jitter rises very slowly in the deepest maps, as the frequency shifts translate into Gordon-Haus-like timing shifts. As the maps get deeper, there is also a slight 'smearing out' of the oscillations in jitter accumulation. This effect is due to the low residual frequency shift effect, compared to the (also small) effects of partial collisions. This means that design of the dispersion

map becomes less critical - that is, they do not have to be tailored to exactly match a minimum in figure 5.3.

At any detection point interactions will be incomplete and some solitons may be over-lapping solitons in different channels (partial collisions), which means that there will be some random temporal shifts in soliton position. This leads to small fluctuations in the accumulation of jitter. It is possible to minimise the number of partial collisions at the detector by making the length of the system such that the pulses return to being interleaved at the detector, as they were at transmission (the reverse is exploited in [99]) but this is a tight constraint on system design and depends on propagation distances in each channel remaining fixed.

Simulation of Four-Channel Propagation

With four channels being transmitted simultaneously, there are not only more collisions happening to each soliton but there is also the chance of more complicated three- and four-soliton collisions. In most regimes, we would expect the interaction of neighbouring frequencies to be strongest since these will have the longest collision and interaction lengths. Hence, the central frequencies (with two nearest neighbours) are expected to be worse effected than those at extreme frequencies (with only one neighbour).

Figure 5.13 shows the jitter levels after $2000km$ of propagation across a range of $-5.0 < A_1 < 5.0$. Data in some of the shallowest maps has already been lost. Comparison with the analytic prediction helps to explain why the points at $A_1 = 0.5$ are more greatly scattered than the others. This corresponds to a steep change in the expected shift so partial collisions will have more effect than in the other cases. The expected split between 'outer' (1 and 4) and 'inner' (2 and 3) channels is not observed. However, the effect of residual frequency shift is still seen reflected in the accumulated

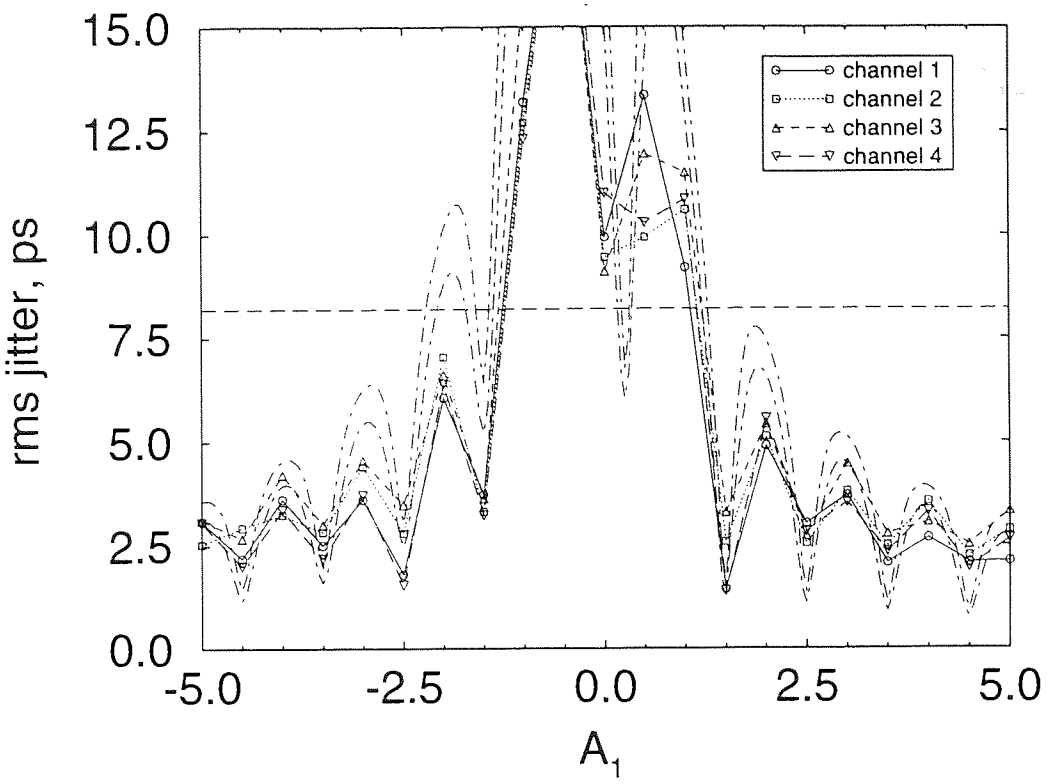

Figure 5.13: Timing jitter for four $10Gbit/s$ WDM channels over a range of values for A_1 after $2000km$ of propagation. Dot-dashed lines are the analytic prediction.

jitter. Figure 5.14 shows how jitter accumulates with propagation across the same range of values of A_1. This time, only the channel with the worst value for jitter at any distance is presented to clarify the diagram (most often, this is one of the central channels, 2 or 3). As with two-channel propagation, the greatest effect is observed for shallow profiles.

The phenomenon of 'smearing out' is less noticeable after $2000km$ with four-channel propagation. The poor quality of data propagated in the approximately 'exponential rule' profile is observed again, now even worse than the uniform case. The sharp minimum at $A_1 = 1.5$ is no longer observed. With four channels, the effect of partial collisions becomes noticeable at lower values of A_1 because it is more likely that a collision will be occuring when a measurement is made and multiple collisions are also possible. The channel separation between the outermost channels is now three times the neighbouring channel separation, so solitons in the outer channels will interact with

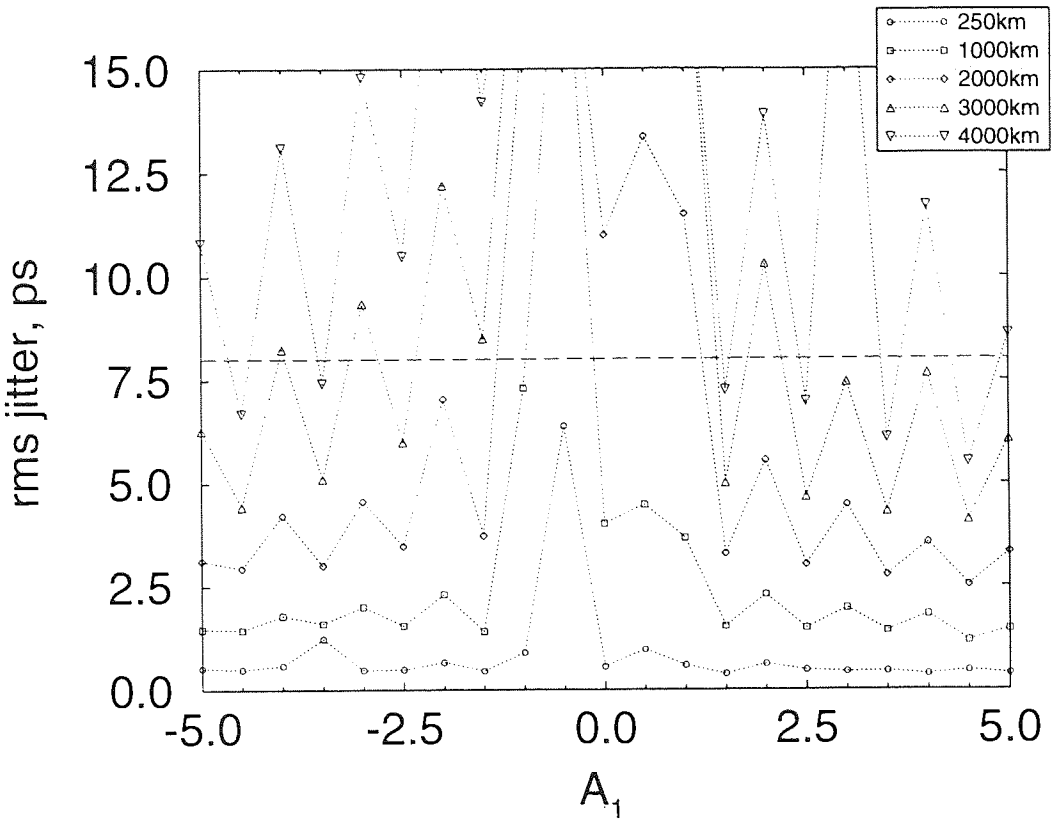

Figure 5.14: Evolution of timing jitter for four $10Gbit/s$ WDM channels over a range of values for A_1.

more than one soliton at a time in the other outer channel once $-0.66 > A_1 > 0.66$. Hence, it is not possible to distinguish different regions of interaction mechanism.

Conclusions

Dispersion management has been shown to be beneficial in the propagation of data in a WDM system. Dispersion maps of depth, $A_1 > 1.5$, where minima have been predicted in residual frequency shift have been predicted have been seen to be the most beneficial (better than any uniform or shallow profiles). Detailed deep map design has been seen to be fairly unimportant in data propagation for two-channel propagation, but more critical in four-channel propagation.

Four-channel propagation showed the same pattern of data degradation with dispersion profile as two channels but the degradation was much faster and varied faster with map profile. Since practical systems are most likely to have more than two chan-

nels if WDM is to be used, and because four-channel propagation has been shown to be most design-sensitive, the rest of the simulations in this thesis have been performed with four channels.

The rapid increase of residual-induced timing jitter with the number of channels would be expected to continue as more and more channels are added. This means that for projected systems of 16 or 32 channels, this will be a severe problem.

5.4 The Addition of Gordon-Haus Jitter

The effects of collision-induced frequency shift and the frequency-shift due to stochastic noise [11, 42] are very similar, both leading to solitons walking out of their expected time slots. The effects are independent and should have no effect on one another, however it is anticipated that the two effects will add quadratically.

To check this, the four-channel pseudo-random data propagation with no third-order dispersion was repeated with stochastic noise in the amplifiers (figure 5.15). An idealised value for noise figure of 1.0 was used.

The effect of collision-induced frequency shift can be seen to be much stronger than that of Gordon-Haus jitter for a single channel with this average dispersion ($0.5ps/(nm.km)$) and dispersion map depth. The accumulated jitter for a single channel is also shown in figure 5.15, both as predicted using the formulae developed by Gordon and Haus [11] and developed by Marcuse [42] and as indicated by data simulation. With third-order dispersion or a lower average dispersion, the difference would be more significant. The two effects do not exacerbate one another.

It is worth noting that in an NRZ system of this length, using conventional fibre, polarisation mode dispersion (PMD) would have built up to $\approx 30ps$ and hence would

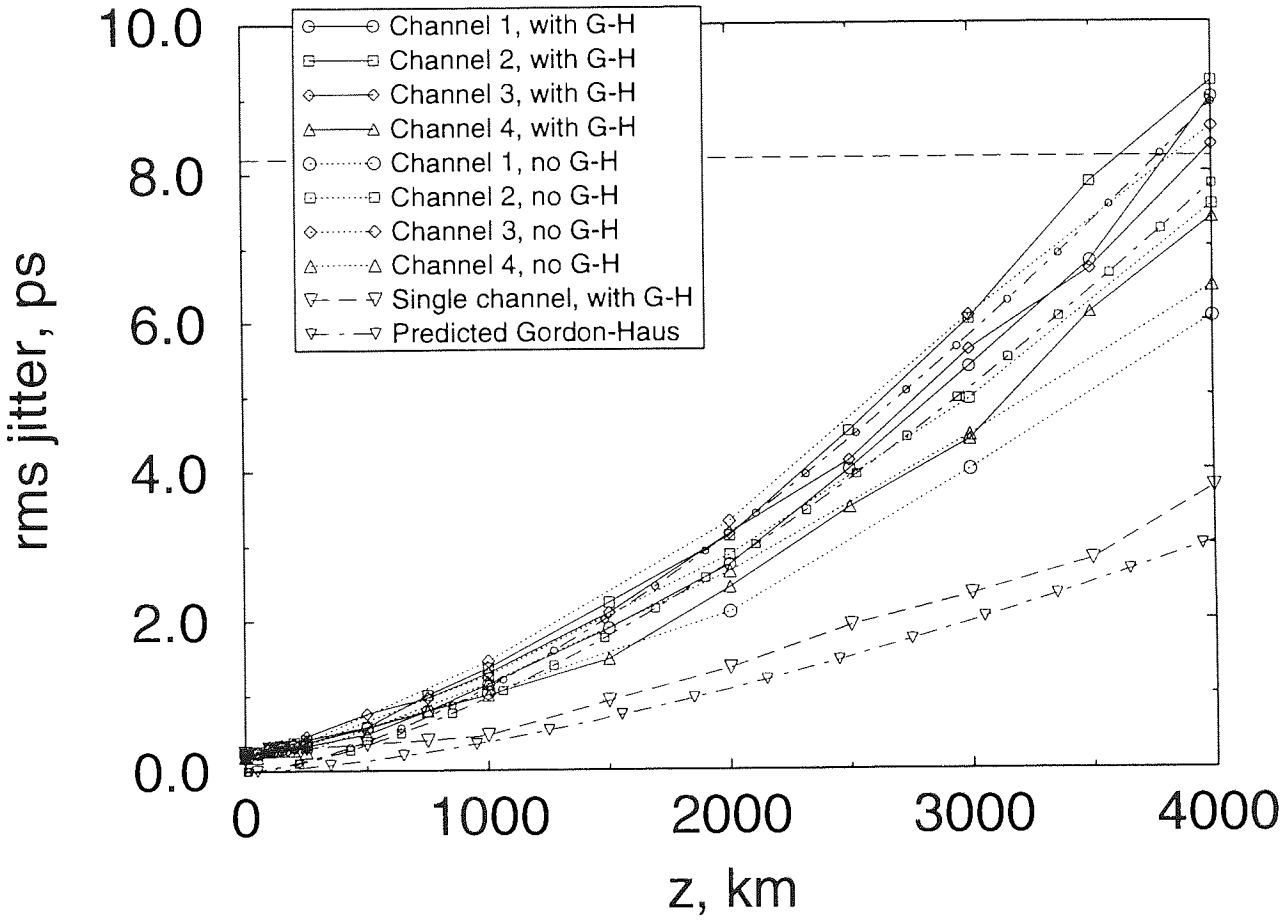

Figure 5.15: Evolution of timing jitter in four $10Gbit/s$ WDM channels with (solid lines) and without (dotted lines) simulated amplified spontaneous emission (ASE), leading to Gordon-Haus jitter. $A_1 = 5.0$ for channel 1 in both cases, channel spacing $200GHz$. Dot-dashed lines are the analytic predictions for outer and inner channels with no Gordon-Haus jitter. Inverted triangles are predicted and data-simulated Gordon-Haus jitter for a single channel.

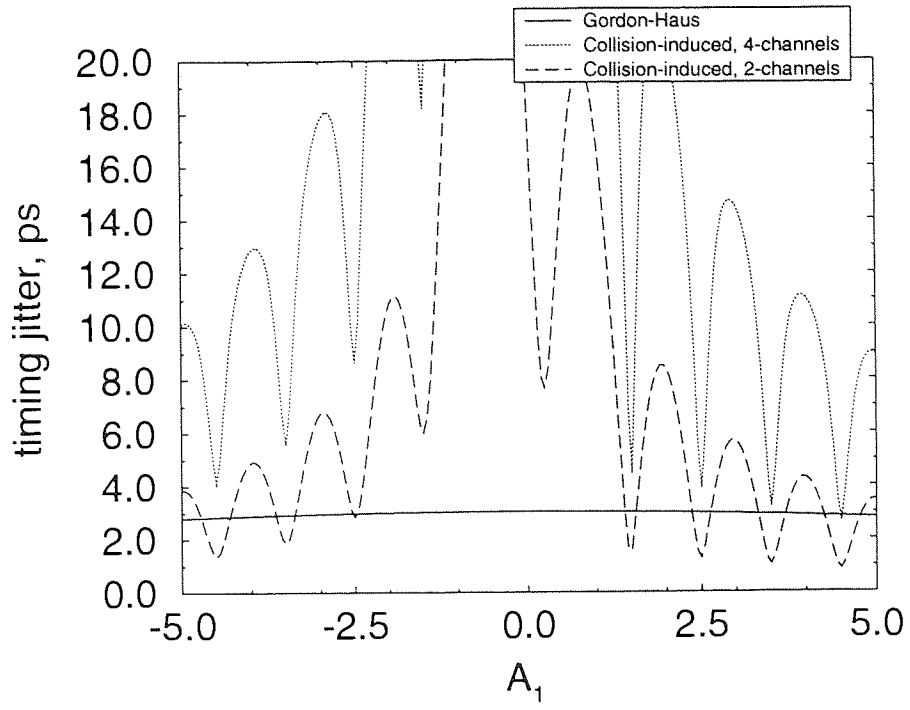

Figure 5.16: Estimates of the collision-induced timing jitter after $4000km$ of propagation for the worst effected channel in a two or four-channel $10Gbit/s$ WDM system (dashed and dotted lines) without stochastic noise in the amplifiers and in a single channel with simulated amplified spontaneous emission (ASE), leading to Gordon-Haus jitter. Channel spacing $200GHz$, $D_{ave} = 0.5ps/(nm.km)$.

be much more significant than either of these phenomena. However, soliton-trapping is still expected to occur in these dispersion-managed cases [52], although limited by the strength of the random birefringence as mentioned in chapter 2.

A comparison of the variation in jitter due to the two effects is made in figure 5.16. It can be seen that at an average dispersion of $0.5ps/(nm.km)$, that collision-induced jitter is the dominant effect over the entire range of dispersion maps studied in this thesis for four channels and is only significant over a small range of dispersions for two channels.

Dispersion management has already been shown to improve the amount of Gordon-Haus jitter [79] in a soliton system because the enhancement factor increases the SNR. Within this range of dispersion values, the suppression of Gordon-Haus jitter is not significant, however. As described in [98] design recommendations can be made based

on limitations set by Gordon-Haus jitter, signal-to-noise ratio and residual frequency shift. As illustrated in figure 2.13, the design window is opened out by the energy enhancement which accompanies deepening dispersion. A low average dispersion is hence desirable from every point of view. Jenkins et al [98] also concluded that several low-data-rate WDM channels are better than a few high-data-rate channels.

Chapter 6

Third-Order Dispersion

6.1 Introduction

As described earlier, typical optical fibre does not have the same value of dispersion across the erbium-doped fibre amplifier window. Dispersion-flattened fibre has been manufactured (e.g. [100], with a third-order dispersion of $-0.0007ps/(nm^2.km)$ over $15nm$) and shown to be useful in propagating WDM solitons. However, like all special fibres, this is rather difficult and expensive to manufacture and have relatively high loss. In these simulations, it has been assumed that third-order dispersion will have a fairly typical value of $0.07ps/(nm^2.km)$.

Collision-induced jitter increases with propagation distance at a rate proportional to second-order dispersion. Hence, it is desirable to use as low a value of average dispersion as possible without the soliton energy being so low as to be infeasible in terms of SNR. When allocating WDM channels in the presence of third order dispersion, however, only one channel can be at the optimally small dispersion and all the other channels must be at larger values of dispersion. These channels should all suffer greater degradation in jitter with propagation.

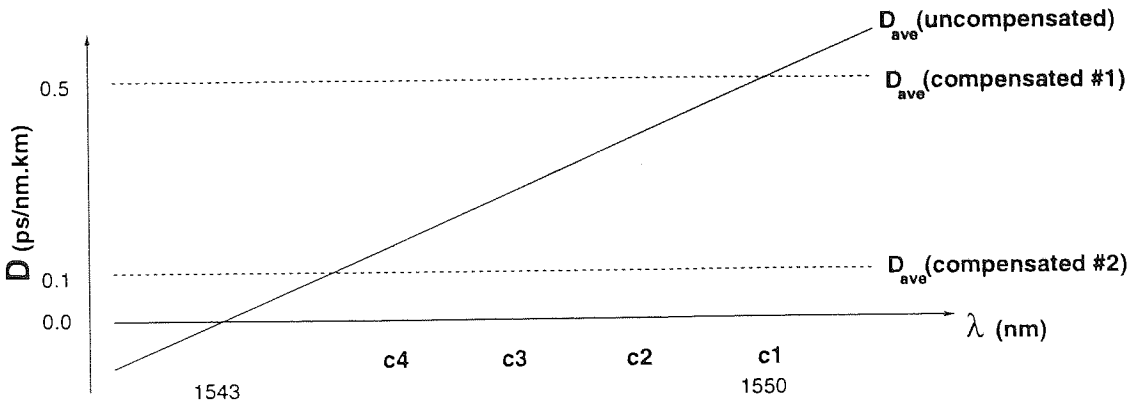

Figure 6.1: Third-order dispersion compensation dispersion profiles. $\lambda_1 = 1.550\mu m$ is the wavelength of channel one.

Three approaches will be taken to this problem in this thesis which are illustrated in figure 6.1. First, the soliton energy will be scaled with average dispersion. Using this method, the longest wavelengths will be anticipated to propagate intact for the least distance. Second, the pulse width will be scaled with average dispersion. Frequency shifts should then be reduced for the wider pulses, although pulse interaction within individual channels will increase with dispersion as the amount neighbouring pulses overlap increases. Lastly, negative-slope dispersion fibre will be used to compensate for positive third-order dispersion in the other fibre used, leaving no net slope. Negative-slope dispersion fibre has already been manufactured and marketed [101]. Two compensating fibres will be tried to give average dispersion values of $0.5ps/(nm.km)$ (compensation #1) and $0.1ps/(nm.km)$ (compensation #2).

6.2 Scaled Amplitude Propagation

As described in the last chapter, the amplitude of pulses are scaled with second-order dispersion, so that the soliton energy equation (2.30) is still obeyed. With a positive value of third-order dispersion, pulse energies will be higher the longer the wavelength. It is anticipated that the longer wavelengths will suffer larger frequency shifts due to

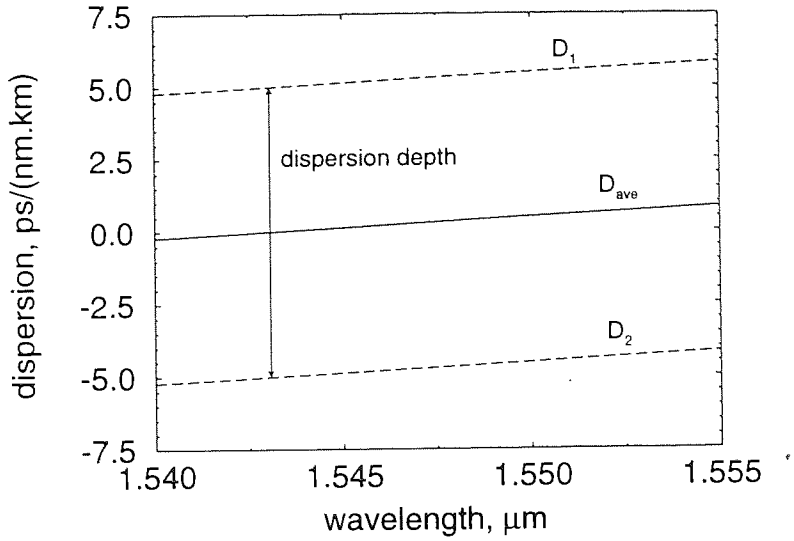

Figure 6.2: Dispersion characteristics of component fibres with the same third-order value.

the larger energies involved in any interaction. Also, timing jitter will grow faster because of the larger average dispersion.

Since the third-order dispersion is the same in both fibres, the depth of dispersion profile will be the same for all channels - only the average second-order dispersion will vary as shown in figure 6.2. The average value of dispersion then determines how quickly frequency-shifted pulses walk out of their expected time slots, so those with highest average dispersion should suffer the greatest degradation in timing jitter. Another problem in making this scheme realisable is that most commercial EDFAs attempt to have flat gain across the window when differential gain would be required.

Figure 6.3 shows how jitter increases with propagation distance for three dispersion regimes; uniform, two steps approximated to exponential decrease and $A_1 = 5.0$. In both the exponential approximation and the deepest profile, only channel 1 is at the exact value of A_1 intended, the others depend on the relationship between D_{ave} (which increases with wavelength) and D_{12} (which is fixed). Table 6.1 shows the parameters for each channel in more detail. Although $A_1 = 5.0$ is not one of the values associated with a minimum in residual frequency shift, all four channels in this regime remain

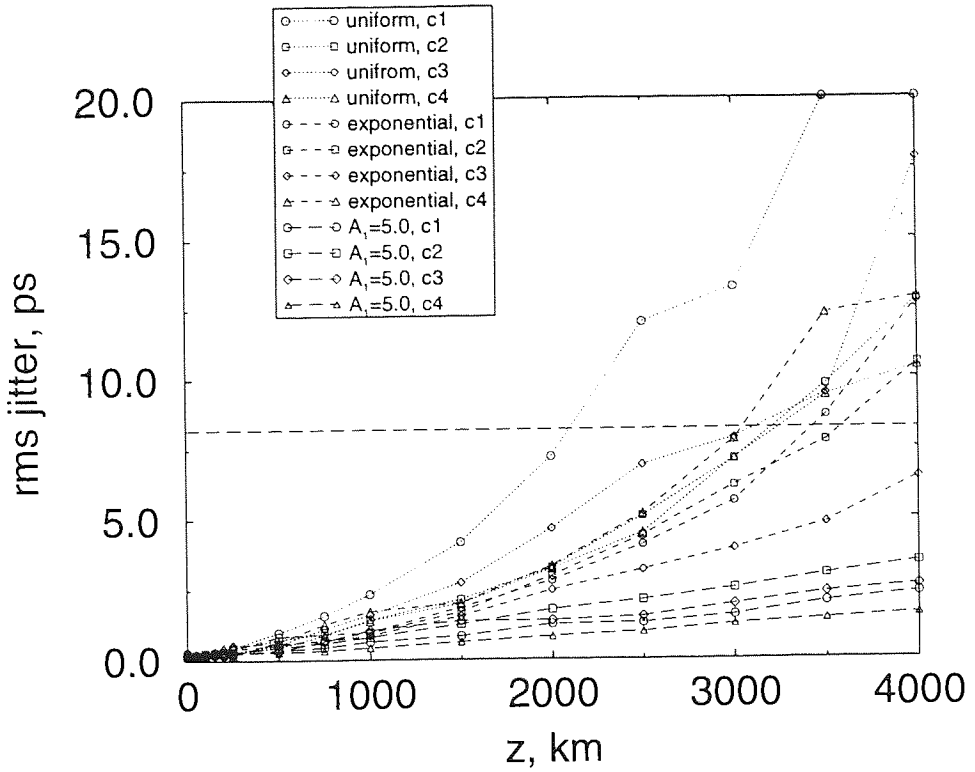

Figure 6.3: Evolution of timing jitter of four $10Gbit/s$ WDM channels for three dispersion profiles. Amplitude scaled with third-order dispersion.

Channel	$\lambda\mu m$	D_{ave} (ps/nm.km)	A_1 - exponential profile	A_1 - deep profile
1	1.550	0.500	0.264	5.00
2	1.548	0.388	0.340	4.89
3	1.547	0.276	0.478	4.78
4	1.545	0.164	0.805	4.66

Table 6.1: Parameters for each channel used in simulations with amplitude scaled with dispersion.

intact over $4000km$ whereas none of the channels in uniform dispersion and only one in the exponential approximation would be error-free after this distance.

In the uniform case, the channel with longest wavelength (channel 1) degrades quickest, as expected. However, the relationship between the wavelength and rate of increase of jitter in the other channels is not quite so clear. After $4000km$, channel 3 has a higher jitter level than channel 2. This may be due to random fluctuations as a result of partial collisions.

This explains why, although the average dispersion decreases with decreasing wave-

length, the jitter characteristics do not improve across the exponential cases. Instead, all the channels behave in much the same way, one factor (average dispersion) improving behaviour while another makes things worse (residual frequency shift).

In the deeper case, although the exact value of A_1 was not expected to be too critical, the best channel is channel 4 where the residual frequency shift and average dispersion are most optimal. Channels 2 and 3 have higher jitter levels than channels 1 and 4, because they undergo more inter-channel interaction, where frequency shifts are higher.

6.3 Scaled Pulse-Width Propagation

The soliton energy equation 2.30 can also be adhered to by changing the pulse width as dispersion increases and keeping the energy of the pulses fixed. Since the amount of frequency shift is dependent on the energy involved in the interaction, this should not be significantly increased for any of the wavelengths. However, the higher second-order dispersions should still lead to more walk-off at longer wavelengths.

Figure 6.4 shows how jitter evolves with distance for the same channels as in section 6.2 but with scaled pulse-widths and only the uniform and $A_1 = 5.0$ profiles.

Again, when $A_1 = 5.0$, all channels propagate better than in the uniform case. In general, however, behaviour is worse than in the amplitude-scaled cases. Channel 1 was expected to behave in much the same way in both regimes, having the same energy and pulse width, but is also worse. This is because the pulses in the other channels have the same energy as those in channel 1 and, as explained in chapter 4, section 4.3.2, the amount of residual frequency shift is directly related to the pulse energy whilst the relationship with pulse width is more complex (similar to the relationship

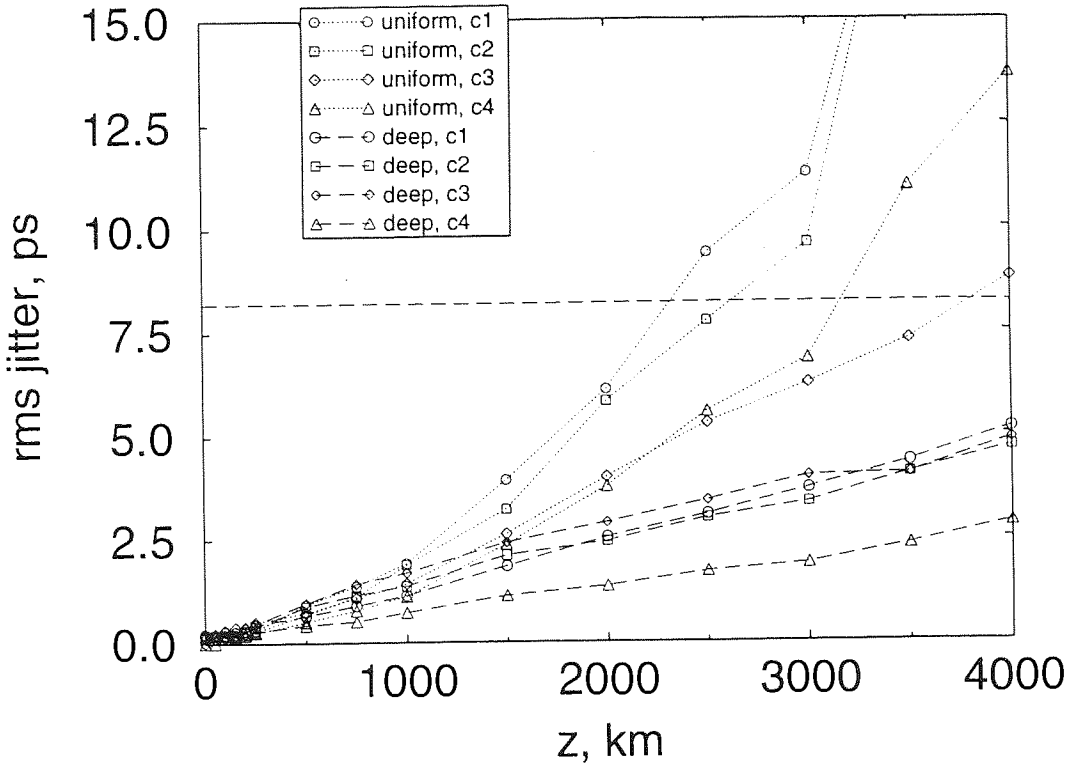

Figure 6.4: Evolution of timing jitter of four $10Gbit/s$ WDM channels for uniform and $A_1 = 5.0$ dispersion profiles. Pulse width scaled with third-order dispersion.

with pulse-breathing). Scaling the widths to create lower pulse energies would make the situation better but would be limited by soliton-soliton interaction as the wider pulses overlap with more of their neighbours.

6.4 Third-Order Fibre Dispersion Compensation

In order to return to the same average dispersion at all wavelengths, one of the fibres used can be chosen to have a negative value of third-order dispersion. Now the different channels propagate in different depths of profile but with the same average dispersion. Again, this means that different channels will have different values of A_1 and that the 'uniform' case will only be uniform at one wavelength. Table 6.2 shows the variation in A_1 for the parameters used in these simulations.

Figure 6.5 shows the dispersion vs wavelength characteristics of the four fibres

Channel	$\lambda\mu m$	A_1 - 'uniform' profile	A_1 - deep profile
1	1.550	0.0	5.00
2	1.548	-0.11	4.89
3	1.547	-0.22	4.78
4	1.545	-0.34	4.66

Table 6.2: Parameters for each channel used in simulations with third-order dispersion compensation.

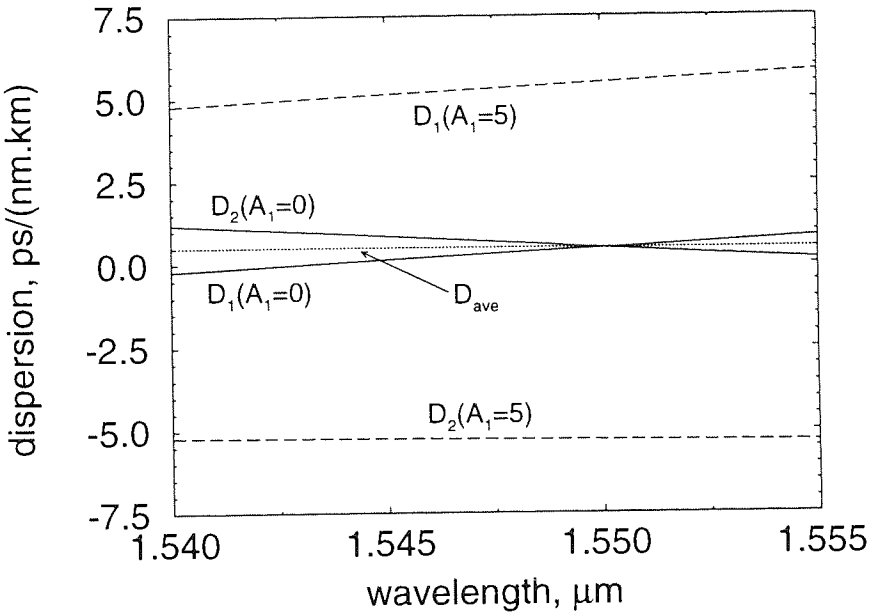

Figure 6.5: First third-order dispersion compensation scheme ($D_{ave} = 0.5ps/(nm.km)$) for uniform and $A_1 = 5.0$ dispersion profiles. $\lambda_1 = 1.550\mu m$ is the wavelength of channel one.

modelled. The same wavelengths have been used as in previous simulations. Since the maps have $L_1/L_a = 1/2$, the negative third-order dispersion used is of the same magnitude but opposite sign.

The results of these simulations are shown in figure 6.6. Again a dramatic improvement in timing jitter is seen between the 'uniform' case and the deep dispersion case. In the 'uniform' case, channel 4 suffers the most rapid degradation because it has the most negative value of A_1. All channels in the 'uniform' case have reached unacceptable jitter levels by $1500km$. All but one of the deep profile cases is error free after $4000km$ however.

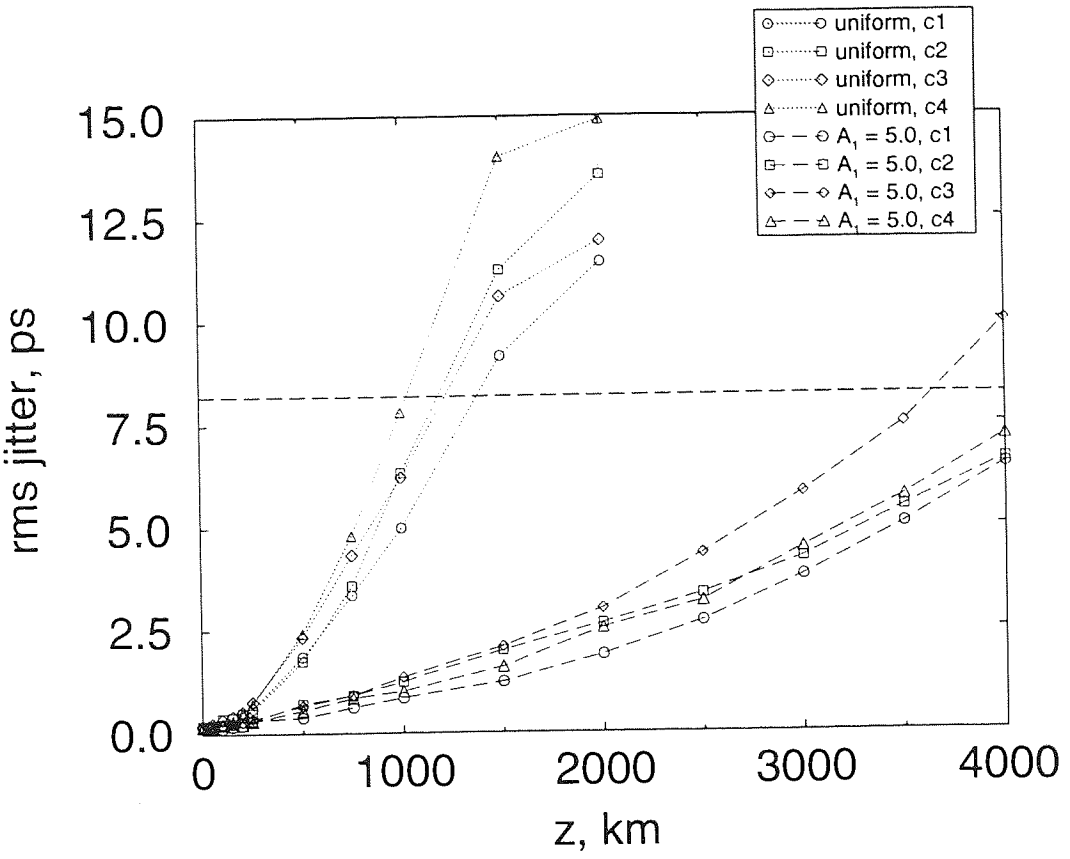

Figure 6.6: Evolution of timing jitter of four $10Gbit/s$ WDM channels for third-order compensated 'uniform' and $A_1 = 5.0$ dispersion profiles.

These results are obviously much worse than the uncompensated results. This is to be expected as the dispersions, and hence soliton powers, are higher in most of the channels.

The jitter in the deep profile case in figure 6.6 is worse for all channels than it was for the deep profile case in figure 6.3. This is partly because the average dispersion in all channels is $0.5ps/(nm.km)$, causing a faster walk-off in channels $2-4$. However, the dominant effect is that of the strength of interaction due to the energy of the pulses involved. All the pulses in these simulations have the same energy as those in channel 1 (the largest) in the uncompensated case.

Repeating these simulations with third-order compensated to set the average at $0.1ps/(nm.km)$, it can be seen that the timing jitter is dramatically reduced, below that of any other regime. Figure 6.7 shows how jitter evolves with distance for the four

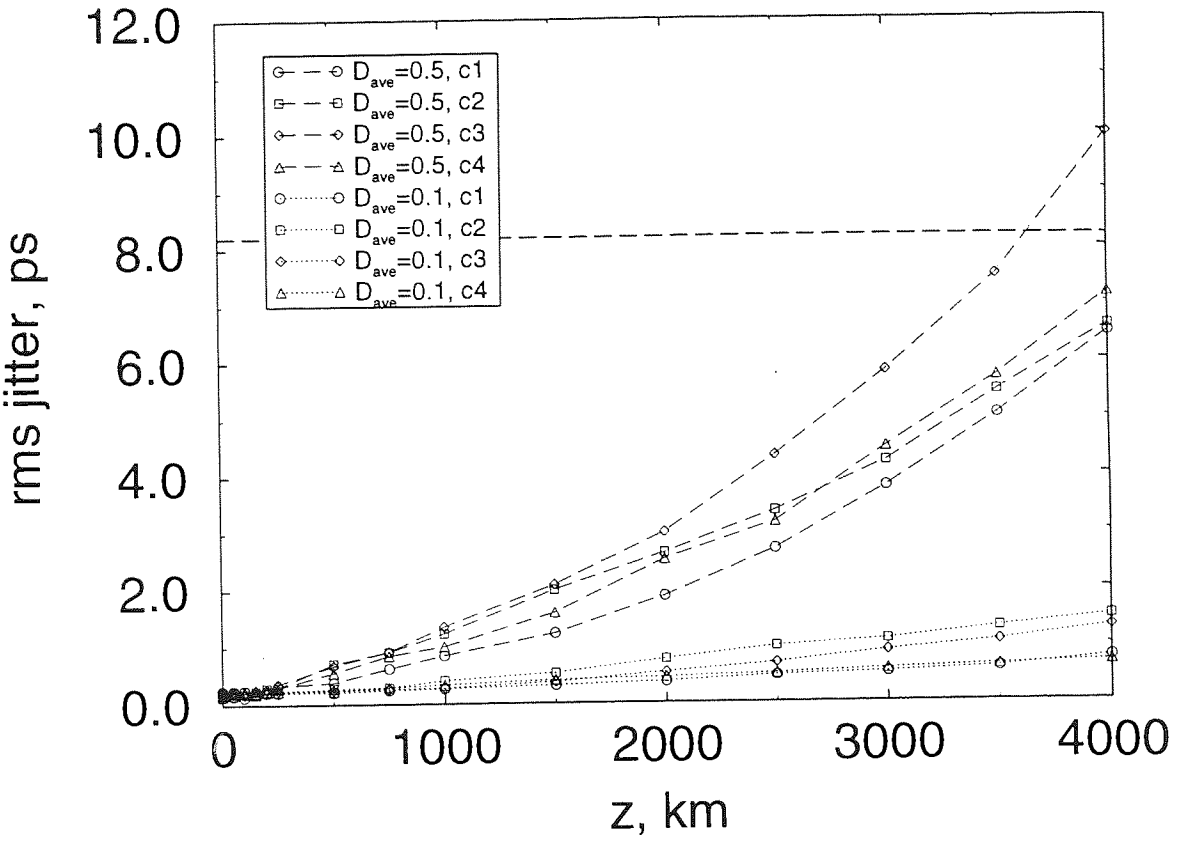

Figure 6.7: Evolution of timing jitter of four $10Gbit/s$ WDM channels for third-order compensated to $D_{ave} = 0.1$ and $D_{ave} = 0.5$ in dispersion profile, $A_1 = 5.0$.

channels compensated to $D_{ave} = 0.1ps/(nm.km)$ and $D_{ave} = 0.5ps/(nm.km)$.

With $D_{ave} = 0.1ps/(nm.km)$, the increased effect of collision-induced shifts on the middle channels is more noticeable than in previous cases. These channels have two channels at frequencies close to their own and one further away, whereas the outer channels have only one close frequency channel, one further away and another even further away. The theory developed in Chapter 3 showed a rapid decrease in residual frequency shift with increasing channel separation.

6.5 Conclusions

At first glance, it appears that data propagated better in the presence of third-order dispersion than in zero third-order dispersion. Figure 6.8 shows how the worst jitter fig-

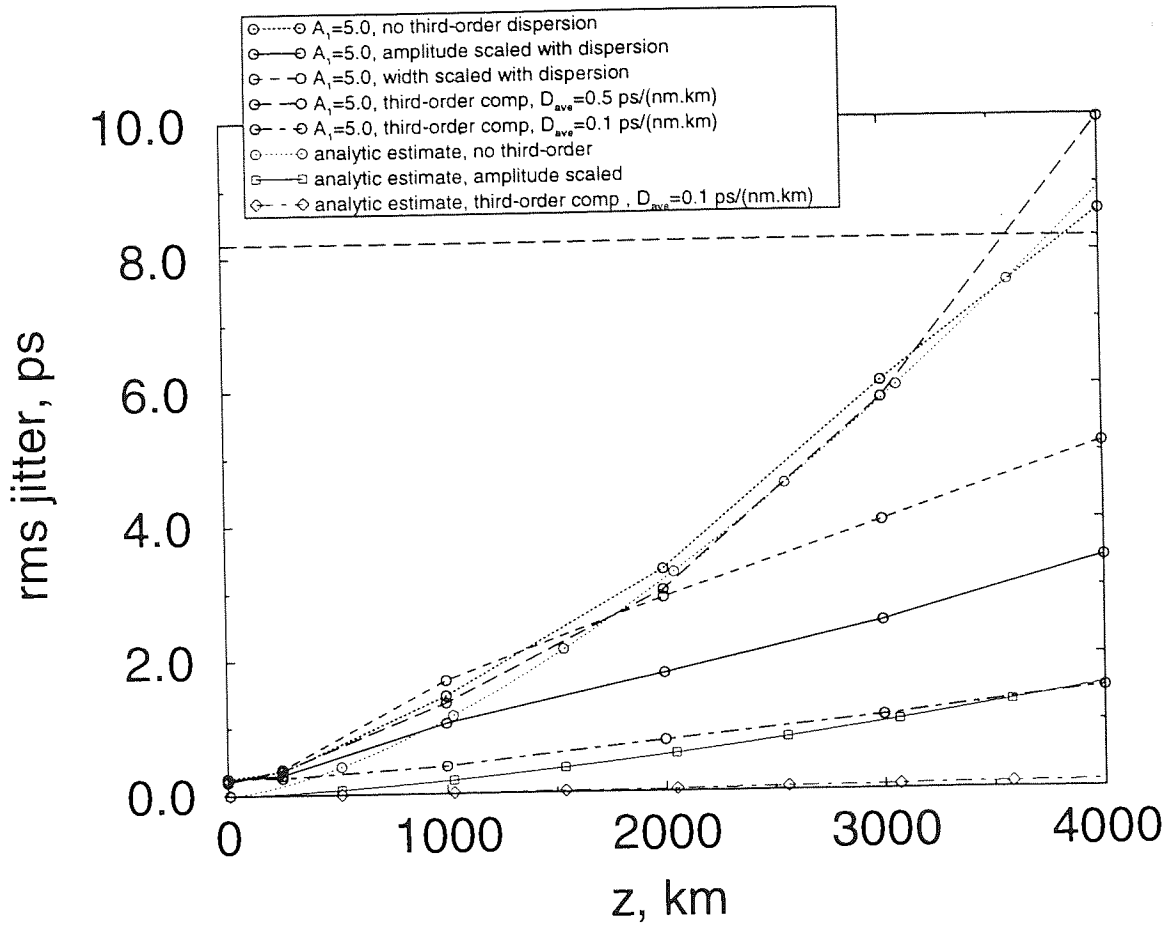

Figure 6.8: Evolution of timing jitter of the worst of four $10Gbit/s$ WDM channels in different third-order dispersion regimes and with different compensation methods. $A_1 = 5.0$ for channel 1 in each case. Analytic estimates also given.

ure in flat dispersion, amplitude-scaled, width scaled and two third-order compensated regimes evolves with distance.

The dominant variable in these simulations is the energy of the pulses and, more importantly, the energy of pulses in the *other channels*. This explains why the channels with the same wavelength and propagating in the same depth of dispersion map do not have the same rate of evolution of jitter when the other channels vary in average dispersion or dispersion depth.

It is most significant to note that the least amount of jitter builds up when third-order dispersion compensation is used to achieve a very low average dispersion across the bandwidth exploited. This is the real strength of such compensation - being able to

achieve low dispersion, with all its benefits of reduced Gordon-Haus jitter, enhancement factor and reduced collision-induced jitter, for all channels transmitted.

Over small bandwidths, such as those in these simulations, third-order dispersion does not create a huge difference in dispersion between the outer channels or a large single-channel value of dispersion which would make soliton propagation infeasible due to large pulse energies or collision induced jitter. With 16, 32 or 64 channels, which will be utilised in future WDM systems and require large bandwidths, typical fibre will have a large variation of dispersion and large ($> 1ps/(nm.km)$) single-channel values of dispersion. In these systems, third-order compensation will be absolutely necessary to bring pulse energies back to feasible levels and to avoid catastrophic amounts of collision induced jitter.

The main benefit of third-order compensation over any bandwidth, however, is the ability to tailor the single-channel dispersion in all channels to as small a value as possible, reducing Gordon-Haus and collision-induced jitter.

The analytic estimate for propagation in a dispersion map comprised of fibre with no third-order dispersion, very accurately reflects the build-up of jitter found by data simulation. As the average dispersion decreases, the accuracy of the estimate decreases until, at $D_{ave} = 0.1ps/(nm.km)$, the initial data-simulation jitter figure, due to the accuracy of the measurement technique used, is larger than the amount of jitter accumulated in the analytic estimate after $4000km$.

Chapter 7

Conclusions

The magnitude and effect of residual frequency shift due to inter-channel collisions in soliton WDM systems have been mapped over a large range of possible values. Adiabatic theory [84], formulated to model dispersion profiles in close approximation to the ideal exponential decrease with loss, has been shown to be valid in realistic systems with dispersion profiles up to a depth of $A_1 = 5.0$.

Two general trends have been observed. Residual frequency shift is reduced approximately inversely with depth of profile. Numerical simulations show that this fall-off is even more rapid than predicted by the adiabatic theory. This is because of the pulse-breathing in deeper dispersion maps which reduces the amount of interaction. Second, there are periodic minima in residual frequency shift with increasing depth of dispersion map. These are due to resonances between the periodicity of the map and the collision mechanism. That is, the minima occur when the length of a soliton interaction (from the first overlap to the last) coincides with an integer number of map periods.

Simulation of WDM soliton data propagation showed a strong relationship between residual frequency shift and the degradation of timing jitter. The reduction in timing

jitter with increasing depth of dispersion is much faster than the reduction of residual frequency shift, however. In the shallowest profiles, large frequency shifts occur, early in the propagation of the data, letting jitter build up over the rest of the propagation distance, whereas in the deeper profiles complete interactions take longer and are comprised of several small frequency shifts (or 'kicks') and jitter accumulates more slowly. That is, the propagation distance between the first overlap of two pulses and the last (interaction distance) increases with dispersion depth. A system designed with a depth of $A_1 = 5.0$ will have significantly better jitter characteristics than one designed with uniform or approximately exponential profile. This means that either longer transmission distances or amplifier spacing can be achieved.

An important consideration after loss and dispersion, is third-order dispersion. Simulation of WDM soliton systems with third-order dispersion and methods showed the strong importance of reducing the energy of the pulses being propagated in reducing the amount they interacted. There is a limit to how much the pulse energy can be reduced set by the acceptable signal-to-noise ratio (SNR), as the pulse energy scales with average dispersion. In order to isolate the effects of residual frequency shifts, most of the simulations were performed with no spontaneous emission from the amplifiers. Addition of stochastic noise was shown not to exacerbate residual frequency shift induced jitter and to be quite insignificant in comparison with most cases considered.

In general, deep dispersion maps with an average dispersion less than $0.5ps/(nm.km)$ were found to be beneficial in WDM soliton propagation. Third-order compensation was found to only be beneficial in reducing the average dispersion value across the window used. Over large bandwidths, third-order dispersion compensation is essential in keeping the average dispersion levels down.

Further work looking at deeper maps, simulating more asymmetric maps and maps

with periodicity which is not the same as that of the loss of the system would be the natural next step. It is not yet certain whether the adiabatic theory used here would still be valid for such systems. Others are already working on analysis of soliton behaviour in much deeper maps than have been considered here [102, 103] and it is hoped that a coherent theory across all regimes may be found, although it may be quite complex. It was thought that there would be a limit to how deep dispersion maps could be made before propagation became unstable but very deep maps (equivalent to $A_1 \gg 10.0$) have already been shown to have periodically stable [104] soliton solutions. Other limitations will have to be looked for in terms of data-rate, pulse-size, bandwidth and number of channels.

It is certain, with the current growth in demand for bandwidth, that WDM will become a common feature of optical networks. Current commercial equipment, using NRZ pulses, has reached a total data capacity of $100Gbit/s$ [105] whilst laboratory experiments with RZ pulses have achieved over $500Gbit/s$ over $1600km$ [13]. Total commercial data capacities of several Tbit/s now seem feasible over local area networks and trans-oceanic links, with all-optical regeneration of WDM channels, could reach the order of a Tbit/s. The results of this thesis show that solitons with dispersion management are a viable method of achieving this expansion.

Bibliography

[1] N. Robinson. Optical transmission system design: From the beginning toward the future. In *Proceedings of Optical Fibre Communications (OFC '97) - Dallas, USA*, volume - Tutorials, pages 43–60. OSA, 97.

[2] R. K. Dodd, J. C. Eilbeck, J. D. Gibbon, and H. C. Morris. *Solitons and Nonlinear Wave Equations.* Academic Press, 82.

[3] D. J. Korteweg and G. de Vries. On the change of form of long waves advancing in a rectangular canal, and on a new type of long stationary waves. *Phil. Mag.*, 20:382–386, 1895.

[4] N. J. Zabusky and M. D. Kruskal. Interaction of solitons in a collisionless plasma and the recurrence of initial states. *Phys. Rev. Lett.*, 15:240–243, 65.

[5] A. Hasegawa and F. Tappert. Transmission of stationary nonlinear optical pulses in dispersive dielectric fibers. I Anomalous dispersion. *Applied Physics Letters*, 23(3):142–144, 73.

[6] L. F. Mollenauer, R. H. Stolen, and J. P. Gordon. Experimental observation of picosecond pulse narrowing and solitons in optical fibers. *Phys. Rev. Lett.*, 45(13):1095–1098, 80.

[7] E. Desurvire, J. R. Simpson, and P. C. Becker. High-gain erbium-doped traveling-wave fiber amplifier. *Opt. Lett.*, 12(11):888–890, 87.

[8] R. J. Mears, L. Reekie, I. M. Jauncey, and D. N. Payne. Low-noise erbium-doped fibre amplifier operating at $1.54\mu m$. *Electron. Lett.*, 23(19):1026–1028, 87.

[9] A. Hasegawa and Y. Kodama. Guiding-center soliton in optical fibers. *Opt. Lett.*, 15(24):1443–1445, 90.

[10] K. J. Blow and N. J. Doran. Average soliton dynamics and the operation of soliton systems with lumped amplifiers. *IEEE Photon. Technol. Lett.*, 3(4):369–371, 91.

[11] J. P. Gordon and H. A. Haus. Random walk of coherently amplified solitons in optical fibre transmission. *Opt. Lett.*, 11(10):665–667, 86.

[12] E. Desurvire. *Erbium-Doped Fibre Amplifiers: Principles and Applications.* John Wiley & Sons, 94.

[13] H. Taga, T. Miyakawa, K. Murashige, N. Edagawa, M. Suzuki, H. Tanaka, K. Goto, and S. Yamamoto. A half $Tbit/s(50 \times 10.66Gbit/s)$, over $1600km$ transmission experiment using widely gain-flattened EDFA chain. In *23rd European Conference on Optical Communications (ECOC '97), Edinburgh, UK*, volume 5, pages 13–16. OSA, 97.

[14] M. Têtu. Absolute frequency control of semiconductor lasers for WDM applications. In *Proceedings of Optical Fibre Communications (OFC '97), Dallas, USA*, volume - Tutorials, pages 169–220. OSA, 97.

[15] F. M. Knox, W. Forysiak, and N. J. Doran. $10 - Gbit/s$ soliton communications systems over standard fiber at $1.55\mu m$ and the use of dispersion compensation. *Opt. Lett.*, 11(10):665–667, 95.

[16] S. Chi and M. C. Lin. Concatenated soliton fibre link. *Electron. Lett.*, 27(3):237–238, 91.

[17] W. Forysiak, F. M. Knox, and N. J. Doran. Average soliton propagation in periodically amplified systems with stepwise dispersion-profiled fiber. *Opt. Lett.*, 19(3), 94.

[18] A. Hasegawa, S. Kumar, and Y. Kodama. Reduction of collision-induced time jitters in dispersion managed soliton transmission systems. *Opt. Lett.*, 21(1):39–41, 96.

[19] W. Forysiak, J. F. L. Devaney, N. J. Smith, and N. J. Doran. Dispersion management for WDM soliton transmission. *Opt. Lett.*, 22(9):600–602, 97.

[20] V. S. Grigoryan, T. Yu, E. A. Golovchenko, C. R. Menyuk, and A. N. Pilipetskii. Dispersion-managed soliton dynamics. *Opt. Lett.*, 22(21):1609–1611, 97.

[21] E. G. Shapiro and S. K. Turitsyn. Theory of guiding-center breathing soliton propagation in optical communication systems with strong dispersion management. *Opt. Lett.*, 22(20):1544–1546, 97.

[22] O. Leclerc, E. Desurvire, and O. Audouin. Robustness of $80Gbit/s$ ($4 \times 20Gbit/s$) regenerated WDM soliton transoceanic transmission to practical system implementation. *Optical Fiber Technology*, 3:117–119, 97.

[23] D. Le Guen, F. Favre, M. L. Moulinard, M. Henry, G. Michaud, L. Macé, F. Devaux, B. Charbonnier, and T. Georges. 200Gbit/s 100km-span soliton WDM transmission over 1000km of standard fiber with dispersion compensation and pre-chirping. In *Proceedings of Optical Fibre Communications (OFC '97), Dallas, USA*, volume - post-deadlines, pages PD17–1 – PD17–3. OSA, 97.

[24] K. J. Blow and N. J. Doran. *Anisotropic and Nonlinear Waveguides - Soliton Phenomena in Optical Fibres*, chapter - Soliton Phenomena in Optical Fibres, pages 159–183. Elsevier Science Publishers B. V., 92.

[25] L. F. Mollenauer, R. H. Stolen, and M. N. Islam. Experimental demonstration of soliton propagation in long fibers: Loss compensated by Raman gain. *Opt. Lett.*, 10(5):229–231, 85.

[26] L. F. Mollenauer and K. Smith. Demonstration of soliton transmission over more than $4000km$ in fiber with loss periodically compensated by Raman gain. *Opt. Lett.*, 13(8):675–677, 88.

[27] A. Hasegawa and Y. Kodama. Amplification and reshaping of optical solitons in a glass fiber - I. *Opt. Lett.*, 21(1):39–41, 82.

[28] Y. Kodama and A. Hasegawa. Amplification and reshaping of optical solitons in glass fiber - II. *Opt. Lett.*, 7(7):339–341, 82.

[29] K. J. Blow and N. J. Doran. Bandwidth limits of nonlinear (soliton) optical communication systems. *Electron. Lett.*, 19(11):429–430, 83.

[30] J. P. Gordon. Interaction forces among solitons in optical fibers. *Opt. Lett.*, 8(11):596–598, 83.

[31] C. Desem and P. L. Chu. Soliton interaction in the presence of loss and periodic amplification in optical fibers. *Opt. Lett.*, 12(5):349–351, 87.

[32] Y. Kodama and K. Nozaki. Soliton interaction in optical fibers. *Opt. Lett.*, 12(12):1038–1040, 87.

[33] L. F. Mollenauer, J. P. Gordon, and M. N. Islam. Soliton propagation in long fibers with periodically compensated loss. *IEEE J. Quantum Electron.*, 22(1):157–173, 86.

[34] L. F. Mollenauer, S. G. Evangelides, and H. A. Haus. Long-distance soliton propagation using lumped amplifiers and dispersion shifted fiber. *IEEE J. Lightwave Technol.*, 9(2):194–197, 91.

[35] Y. K. Park, T. V. Nguyen, O. Mizuhura, C. D. Chen, L. D. Tzeng, P. D. Yeates, F. Heismann, Y. C. Chen, D. G. Ehrenberg, and J. C. Feggeler. Field demonstration of $10 - Gb/s$ line-rate transmission on an installed transoceanic submarine lightwave cable. *IEEE Photon. Technol. Lett.*, 8(3):425–427, 96.

[36] M. Matsuda, A. Naka, and S. Saito. $10Gbit/s$, $6000km$ NRZ and $4400km$ RZ signal transmission experiments at zero-dispersion wavelength. *Electron. Lett.*, 32(3):229–231, 96.

[37] L. F. Mollenauer, E. Lichtman, M. J. Neubelt, and G. T. Harvey. Demonstration, using sliding-frequency guiding filters, of error-free soliton transmission over more than $20Mm$ at $10Gbit/s$, single channel and over more than $13Mm$ at $20Gbit/s$ in a two-channel WDM. *Electron. Lett.*, 29(10):910–911, 93.

[38] N. S. Bergano, C. R. Davidson, M. A. Mills, P. C. Corbett, S. G. Evangelides, B. Pederson, R. Menges, J. L. Zyskind, J. W. Sulhoff, A. K. Srivastava, C. Wolf, and J. Judkins. Long-haul wdm transmission using optimum channel modulation: A $160Gb/s$ $(32 \times 5Gb/s)$ $9,300km$ demonstration. In *Proceedings of Optical Fibre Communications (OFC '97) - Dallas, USA*, volume - post-deadlines, pages PD16/1–PD16/4, 97.

[39] M. Nakazawa, K. Suzuki, H. Kubota, A. Sahara, and E. Yamada. 100 Gbit/s WDM (20 Gbit/s x 5 channels) soliton transmission over 10,000km using in-line synchronous modulation and optical filtering. In *Proceedings of Optical Fibre Communications (OFC '97) - Dallas, USA*, volume - post-deadlines, pages PD21-1 – PD21-4. OSA, 97.

[40] N. J. Smith. *Solitons in Optical Communications and Fibre Lasers.* PhD thesis, University of Strathclyde, 94.

[41] S. M. J. Kelly. Characteristic sideband instability of periodically amplified average soliton. *Electron. Lett.*, 28(8):806–807, 92.

[42] D. Marcuse. An alternative derivation of the Gordon-Haus effect. *IEEE J. Lightwave Technol.*, 10(2):273–278, 92.

[43] E. Desurvire. *Erbium-Doped Fibre Amplifiers: Principles and Applications*, pages 76–77. John Wiley & Sons, 94.

[44] J. V. Wright and S. F. Carter. Constraints on the design of long-haul soliton systems. In *Nonlinear Guided Waves and their Applications*, pages 6–9. OSA, 91.

[45] F. M. Mitschke and L. F. Mollenauer. Experimental observation of interaction forces between solitons in optical fibers. *Opt. Lett.*, 12(5):355–357, 87.

[46] M. Suzuki, N. Edagawa, H. Taga, H. Tanaka, S. Yamamoto, and S. Akiba. $10Gb/s$, over $12200km$ soliton data transmission with alternating-amplitude solitons. *IEEE Photon. Technol. Lett.*, 6(6):757–759, 94.

[47] M. Suzuki, N. Edagawa, H. Taga, H. Tanaka, S. Yamamoto, and S. Akiba. Feasibility demonstration of $20Gbit/s$ single channel soliton transmission over $11500km$ using alternating-amplitude solitons. *Electron. Lett.*, 30(13):1083–1084, 94.

[48] G. P. Agrawal. *Nonlinear Fiber Optics.* Academic Press, 89.

[49] R. H. Stolen, J. Botineau, and A. Ashkin. Intensity discrimination of optical pulses with birefringent fibers. *Opt. Lett.*, 7(10):512–514, 82.

[50] C. R. Menyuk. Stability of solitons in birefringent optical fibers. i: Equal propagation amplitudes. *Opt. Lett.*, 12(8):614–616, 87.

[51] L. F. Mollenauer, K. Smith, and J. P. Gordon. Resistance of solitons to the effects of polarization dispersion in optical fibers. *Opt. Lett.*, 14(21):1219–1221, 89.

[52] X. Zhang, M. Karlsson, P. Andrekson, and K. Bertilsson. Impact of polarisation-mode dispersion in dispersion-managed soliton systems. *Electron. Lett.*, 34(11):1122–1124, 98.

[53] D. Marcuse. Simulations to demonstrate reduction of the Gordon-Haus effect. *Opt. Lett.*, 17(1):34–36, 92.

[54] Y. Kodama and A. Hasegawa. Generation of asymptotically stable solitons and suppression of the Gordon-Haus effect. *Opt. Lett.*, 17(1):31–34, 92.

[55] A. Mecozzi, J. D. Moores, H. A. Haus, and Y. Lai. Modulation and filtering control of soliton transmission. *J. Optical Society of America, B*, 9(8):1350–1357, 92.

[56] L. F. Mollenauer, M. J. Neubelt, M. Haner, E. Lichtman, S. G. Evangelides, and B. M. Nyman. Demonstration of error-free soliton transmission at $2.5Gbit/s$ over more than $14000km$. *Electron. Lett.*, 27(22):2055–2066, 91.

[57] L. F. Mollenauer, J. P. Gordon, and S. G. Evangelides. The sliding-frequency guiding filter - an improved form of soliton control. *Opt. Lett.*, 17(22):1575–1577, 92.

[58] M. Nakazawa, E. Yamada, H. Kubota, and K. Suzuki. $10Gbit/s$ soliton data transmission over one million miles. *Electron. Lett.*, 27(14):1270–1272, 91.

[59] Y. Kodama, M. Romagnoli, and S. Wabnitz. Soliton stability and interactions in fibre lasers. *Electron. Lett.*, 28(21):1981–1983, 92.

[60] W. Forysiak and N. J. Doran. Conjugate solitons in amplified optical fibre transmission systems. *Electron. Lett.*, 30(2):154–155, 94.

[61] T. Widdowson, D. J. Malyon, A. D. Ellis, K. Smith, and K. J. Blow. Soliton shepherding: All-optical active soliton control over global distances. *Electron. Lett.*, 30(12):990–991, 94.

[62] A. Hasegawa and Y. Kodama. *Solitons in Optical Communications.* Clarendon Press, 95.

[63] N. J. Smith, N. J. Doran, K. J. Blow, and W. J. Firth. Gordon-Haus jitter suppression using a single phase modulator. *Electron. Lett.*, 30(12):987–988, 94.

[64] O. Leclerc, E. Desurvire, and O. Audouin. Synchronous WDM soliton regeneration: Towards $80 - 160 Gbit/s$ transoceanic systems. *Optical Fiber Technology*, 3:97–116, 97.

[65] N. J. Doran and D. Wood. Nonlinear optical loop mirror. *Opt. Lett.*, 13(1):56–58, 88.

[66] N. J. Smith and N. J. Doran. Picosecond soliton transmission using concatenated nonlinear optical loop-mirror intensity filters. *J. Optical Society of America, B*, 12(6):1117–1125, 95.

[67] D. Atkinson, W. H. Loh, V. V. Afanasjev, A. B. Grudinin, A. J. Seeds, and D. N. Payne. Increased amplifier spacing in a soliton system with quantum-well saturable absorbers and spectral filtering. *Opt. Lett.*, 19(19):1514–1516, 94.

[68] D. S. Govan, N. J. Smith, F. M. Knox, and N. J. Doran. Stable propagation of solitons with increased energy through the combined action of dispersion management and periodic saturable absorption. *J. Optical Society of America, B*, 14(11):2960–2966, 97.

[69] F. M. Knox, P. Harper, P. N. Kean, N. J. Doran, and I. Bennion. Low jitter, long distance pulse transmission near the net fibre dispersion zero wavelength. *Electron. Lett.*, 31(17):1467–1468, 95.

[70] A. H. Gnauck, R. M. Jopson, and R. M. Derosier. $10-Gb/s$ $360-km$ transmission over dispersive fiber using midsystem spectral inversion. *IEEE Photon. Technol. Lett.*, 5(6):663–666, 93.

[71] R. I. Laming, D. J. Richardson, D. Taverner, and D. N. Payne. Transmission of $6ps$ linear pulses over $50km$ of standard fiber using midpoint spectral inversion to eliminate dispersion. *IEEE J. Quantum Electron.*, 3(9):2114–2119, 94.

[72] M. C. Tatham, G. Sherlock, and L. D. Westbrook. Compensation fibre chromatic dispersion by optical phase conjugation in a semiconductor laser amplifier. *Electron. Lett.*, 29(21):1851–1852, 93.

[73] R. J. Essiambre and G. P. Agrawal. Ultrahigh-bit-rate soliton communication systems using dispersion-decreasing fibers and parametric amplifiers. *Opt. Lett.*, 21(2):116–118, 96.

[74] C. G. Goedde, W. L. Kath, and P. Kumar. Controlling soliton perturbations with phase-sensitive amplification. *IEEE Photon. Technol. Lett.*, 9(7):1020–1022, 97.

[75] A. Shipulin, G. Onishchukov, and B. A. Malomed. Soliton jitter suppresion by a copropagating support structure. In *Nonlinear Guided Waves and their Applications - Cambridge, UK*. OSA, 96.

[76] J. K. Lucek and K. Smith. All-optical signal regenerator. *Opt. Lett.*, 18(15):1226–1228, 93.

[77] A. Niculae and W. L. Kath. Timing-jitter reduction in a fiber laser mode locked by an input bit stream. *Opt. Lett.*, 22(13):979–981, 97.

[78] D. J. Richardson, R. P. Chamberlin, L. Dong, and D. N. Payne. High quality soliton loss-compensation in $38km$ dispersion-decreasing fibre. *Electron. Lett.*, 31(19):1681–1682, 95.

[79] N. J. Smith, W. Forysiak, and N. J. Doran. Reduced Gordon-Haus jitter due to enhanced power solitons in strongly dispersion managed systems. *Electron. Lett.*, 32(22):2085–2086, 96.

[80] N. J. Smith, N. J. Doran, F. M. Knox, and W. Forysiak. Energy scaling characteristic of solitons in strongly dispersion managed fibres. *Opt. Lett.*, 96.

[81] M. K. Chin and X. Y. Tang. Quasi-stable transmission in dispersion managed fiber links with lumped amplifiers. *IEEE Photon. Technol. Lett.*, 9(4):538–540, 97.

[82] N. J. Doran. The soliton communication system. In *IEE Colloquium on Nonlinear Effects in Fibre Communications London, UK*, 90.

[83] A. F. Mitchell, J. V. Wright, S. F. Carter, A. D. Ellis, A. Lord, J. Lyle, and J. M. Scott. The future of optically amplified submarine systems. In *Proceedings of Suboptic '93 (2nd International Conference on Optical Fiber Submarine Telecommunication Systems)*, pages 49–54, 93.

[84] L. F. Mollenauer, S. G. Evangelides, and J. P. Gordon. Wavelength division multiplexing with solitons in ultra-long distance transmission using lumped amplifiers. *IEEE J. Lightwave Technol.*, 9(3):362–367, 91.

[85] M. J. Ablowitz, G. Biondini, S. Chakravarty, R. B. Jenkins, and J. R. Sauer. Four-wave mixing in wavelength-division-multiplexed soliton systems: Damping and amplification. *Opt. Lett.*, 21(20):1646–1648, 96.

[86] T. Georges and B. Charbonnier. Reduction of the dispersive wave in periodically amplified links with initially chirped solitons. *IEEE Photon. Technol. Lett.*, 9(1):127–129, 97.

[87] P. V. Mamyshev and L. F. Mollenauer. Pseudo-phase-matched four-wave mixing in soliton wavelength-division mulitiplexing transmission. *Opt. Lett.*, 21(6):396–398, 96.

[88] P. K. A. Wai, C. R. Menyuk, and B. Raghavan. Wavelength division multiplexing in an unfiltered soliton communication system. *IEEE J. Lightwave Technol.*, 14(6):1449–1454, 96.

[89] E. A. Golovchenko, A. N. Pilipetskii, and C. R. Menyuk. Minimum channel spacing in filtered soliton wavelength-division-multiplexing transmission. *Opt. Lett.*, 21(3):195–197, 96.

[90] S. Cardinal, E. Desurvire, J. P. Hamaide, and O. Audouin. Wavelength-multiplexed transoceanic soliton systems: Comparison of step-wise exponential dispersion-management techniques. *Electron. Lett.*, 33(1):77–78, 97.

[91] I. R. Gabitov, E. G. Shapiro, and S. K. Turitsyn. Optical pulse dynamics in fiber links with dispersion compensation. *Optics Comm.*, 134:317–329, 97.

[92] S. Kumar and A. Hasegawa. Reduction of initial collision effects by adiabatic expansion in soliton wavelength-division multiplexed systems. *Opt. Lett.*, 21(23):1903–1905, 96.

[93] S. Kumar, Y. Kodama, and A. Hasegawa. Optimal dispersion management schemes for WDM soliton systems. *Electron. Lett.*, 33:459–461, 97.

[94] H. Sugahara, H. Kato, and Y. Kodama. Maximum reductions of collision induced frequency shift in soliton-WDM systems with dispersion compensation. *Electron. Lett.*, 33(12):1065–1067, 97.

[95] X. Y. Tang, M. K. Chin, and H. S. Tan. Quasi-stable soliton transmission in a long-distance fibre link with periodic dispersion management and lumped amplifiers. *Optics Comm.*, 136:379–384, 97.

[96] S. G. Evangelides and J. P. Gordon. Energy transfer and frequency shifts from three soliton collisions in a multiplexed transmission line with periodic amplification. *IEEE J. Lightwave Technol.*, 14(7):1639–1643, 96.

[97] M. J. Ablowitz, G. Biondini, S. Chakravarty, R. B. Jenkins, and J. R. Sauer. Four-wave mixing in wavelength-division-multiplexed soliton systems: Ideal fibers. *J. Optical Society of America, B*, 14(7):1788–1794, 97.

[98] R. B. Jenkins, J. R. Sauer, S. Chakravarty, and M. J. Ablowitz. Data-dependant timing jitter in wavelength-division-multiplexing solition systems. *Opt. Lett.*, 20(19):1964–1966, 95.

[99] O. Leclerc, E. Desurvire, and O. Audouin. Assessment of 80 Gbit/s (4x20Gbit/s) regenerated WDM soliton transoceanic transmission. *Electron. Lett.*, 32(12):1118–1119, 96.

[100] N. Edagawa, I. Morita, M. Suzuki, S. Yamamoto, K. Tanaka, and S. Akiba. Long distance soliton WDM transmission using a dispersion-flattened fiber. In *Proceedings of Optical Fibre Communications (OFC '97) - Dallas, USA*, volume post-deadlines, pages PD19 1–4. OSA, 97.

[101] Negative-slope dispersion fibre. Lucent Technology Data Sheet.

[102] A. Niculae, W. Forysiak, and N. J. Doran. Solitons in strong dispersion managed wdm systems. In *Nonlinear Guided Waves and their Applications - Victoria, Canada*, pages 184 – 186. OSA, 98.

[103] J. H. B. Nijhof, N. J. Doran, W. Forysiak, and F. M. Knox. Stable soliton-like propagation in dispersion managed systems with net anomolous, zero and normal dispersion. *Electron. Lett.*, 33(20):1726–1727, 97.

[104] J. H. B. Nijhof. Personal Communication, 97.

[105] See CIENA score a perfect 100 at OFC '98. CIENA publicity material.

[106] T. R. Taha and M. J. Ablowitz. Analytical and numerical aspects of certain nonlinear evolution equations. II. numerical, nonlinear Schrödinger equation. *J. Comp. Phys.*, 55(2):203–230, 84.

[107] H. Ghafouri-Shiraz, P. Shum, and M. Nagata. A novel method for analysis of soliton propagation in optical fibers. *IEEE J. Quantum Electron.*, 31(1):190–200, 95.

[108] J. Van Roey, J. van der Donk, and P. E. Lagasse. Beam-propagation method: Analysis and assessment. *J. Opt. Soc. Am.*, 71(7):803–810, 81.

[109] F. Forghieri. Modeling of wavelength multiplexed lightwave systems. In *Proceedings of Optical Fibre Communications (OFC '97) - Dallas, USA*, volume - Tutorial Sessions, pages 3–40. OSA, 97.

Appendix A

Numerical Simulation Method

The numerical method used in this thesis and in the majority of research into optical communication systems is the split-step Fourier method, in turn using a fast-Fourier-transform (FFT) algorithm. Other methods have been proposed which are either slower [106] or are as yet viewed as being difficult to implement over the full set of possible systems we may wish to model [107].

The split-step method is so-called because the NLSE is split into two parts with one differential operator, $\hat{D}$, accounting for the linear terms and another differential operator, $\hat{N}$, accounting for fibre nonlinearities and pulse propagation. That is, in normalised units,

$$-i\frac{\partial u}{\partial z} = [\hat{D}(u) + \hat{N}(u)]u, \tag{A.1}$$

where,

$$\hat{D} = \frac{1}{2}\frac{\partial^2}{\partial t^2} + \frac{i\Gamma}{2}, \tag{A.2}$$

$$\hat{N} = |u|^2, \tag{A.3}$$

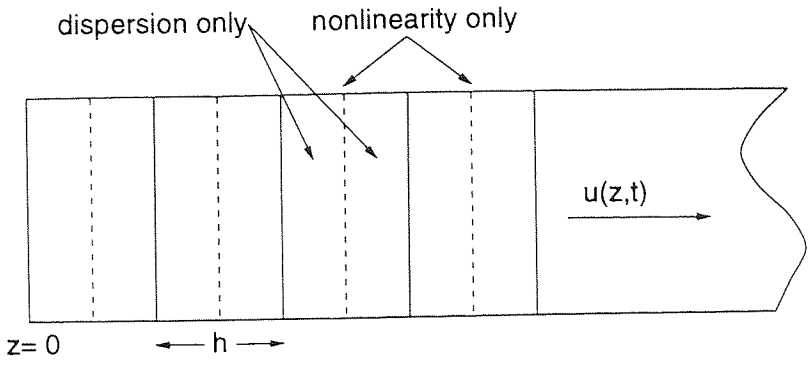

Figure A.1: Split-step Fourier method.

where $\Gamma = \alpha t_0^2/2|\beta_2|$.

A full derivation of the split-step method from this point is given by Agrawal [48] but the essence of the method is as follows. The NLSE in equation A.1 is solved approximately by solving separately for each operator over any segment of fibre of length, h, by,

$$u(z+h,t) \approx \exp\left(\frac{h}{2}\hat{D}\right) \exp\left(\int_z^{z+h} \hat{N}(z')dz'\right) \exp\left(\frac{h}{2}\hat{D}\right) u(z,t). \qquad \text{(A.4)}$$

The fibre is split up into a number of segments small enough to keep the rounding errors within the desired limits, as illustrated in figure A.1. The optical field is propagated the distance $h/2$ with dispersion only. The integral is performed using an FFT algorithm. Then the field is multiplied by a nonlinear term representing the effect of the nonlinearities over distance h. The field is then propagated over $h/2$ again. These three processes are repeated until the entire fibre length has been covered.

In utilising the split-step method, a decision has to be made on which step-size to use as well as the spectral and temporal resolution used.

It is possible to repeat simulations with a range of step-sizes until a maximum step-size below which results are consistent, and preserve the conserved quantities which are expected (e.g. pulse energy in the lossless case). Alternatively, guidelines (e.g. [108])

can be built into any simulation program in order to set the step-size, but it is always wise to check the validity of the answers given. Such step-size calculations often include a measurement of the bandwidth of pulse energies. In a single-channel system, this gives a good indication of how non-linear the pulses are likely to be. Without consideration of individual channel bandwidths, this will always give overly small step-sizes in WDM simulations which unnecessarily slow the computation down. Conversely, one particular problem with over-long step-size in simulating WDM systems is the production of spurious FWM products which, in turn, produces cross-talk and degradation of the signal [109]. Sidebands are also formed in single-channel propagation of solitons, phase matched to the step-length if that step-length is too long [40].

Spectral and temporal resolution are best chosen to be able to see expected phenomena such as side-band formation and the FFT requires the same number of points across both the frequency and time windows.

Accuracy is also limited by how comprehensive the version of the NLSE incorporated and, again, no version of the NLSE has unlimited applicability. Further limitations include the resolution of 'fine detail' in pulse shape, spectrum and temporal evolution, which are limited to $\approx 3-4$ time or frequency divisions or temporal step-sizes respectively. Raman and Brillouin scattering also have to be added to the model as a perturbation and have to be either included at all times (possibly slowing processing times unnecessarily) or whenever their effects are anticipated to be significant. For example, soliton self-frequency shift would be expected to occur in pulses of $< 1ps$ FWHM but will not be predicted by numerical solution of the NLSE unless Raman terms are included.

Modelling the effects of other system components such as amplifiers, filters, wavelength multiplexers, etc. can be done simply. For example, a noiseless amplifier can be

modelled by multiplying the vector of energies across the time window by the square root of the desired gain.

The core of the code used in the numerical simulations in this thesis was developed at BT Laboratories, Martlesham Heath, Ipswich. The code has been developed, improved and re-structured by many at BT and Aston University. The code is written in Sun FORTRAN (an enhanced version of FORTRAN-77) and run on Sun IPC, SPARC and ULTRA stations.

A typical two-soliton collision simulation could be completed on a Sun SPARC10 in approximately 10 minutes. In order that pulses could be reasonably well separated before and after the collision, a temporal window $1600ps$ wide was used most of the time. At all times the number of points across the field was kept to the maximum allowed by the program structure (4096), although this was probably quite a lot more than needed to avoid spurious results. The program estimates the step size required to avoid spurious side-band formation, etc. [109] by calculating a linear and non-linear variable. The algorithm used to decide the step size calculates a measure of both how linear and non-linear the situation is. Non-linearity is measured in terms of the non-linearity coefficient of the fibre (in $rad/(W.km)$), the total intensity of the light and how concentrated it is (how tall and narrow the pulses are). The linearity is measured from the energy in the fibre and the loss of the fibre.

The maximum and minimum step sizes can also be set manually in the input file. Before performing the simulations reported in this thesis, a series of trial simulations were run. The minimum step size was given a series of values and the residual frequency shift for each was calculated. As the minimum step size decreased, the value for the residual frequency shift varied asymptotically towards a single value. Hence, in order to avoid spurious results, when the step-size algorithm would consider the level of

linearity and non-linearity to be insignificant, the maximum step-size was always set to $600m$. The program typically drove the step-size down to less than $100m$ when four channels were being propagated in deep dispersion maps. Periodically, checks were run by setting the minimum step-size to different values. By doing so, FWM could be monitored to look for spurious side-bands.

Frequency shifts were calculated by integrating across as much of the spectrum of the pulse, after filtering, as possible. This was partly because the shifts being measured were smaller than the frequency resolution of the numerical model, of the order of $1Ghz$, (and any reasonably fast model) and partly because the frequency shifts were in the average central frequency and not the peak frequency.

It was also found that, for approximately transform limited pulses, with a FWHM of $20ps$, a frequency separation of $200GHz$ was needed to get an accurate estimate of the frequency shifts. This separation was needed because the frequency shift is found by integrating across the entire spectrum of the pulse to find the 'centre of mass'. $200GHz$ of spectrum was required for the required accuracy. This is twice the current minimum industrial standard, and hence practical value.